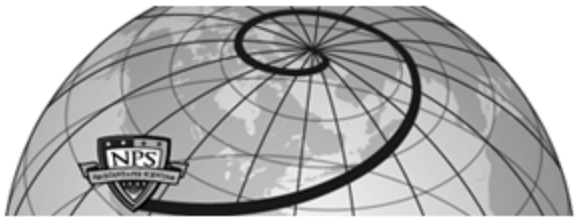

NAVAL POSTGRADUATE SCHOOL

MONTEREY, CALIFORNIA

THESIS

EVALUATION OF LIDAR FOR AUTOMATING RECOGNITION OF ROADS AND TRAILS BENEATH FOREST CANOPY

by

Steven Louis Muha

September 2011

Thesis Advisor:	R. C. Olsen
Second Reader:	Cajun James

Approved for public release; distribution is unlimited

THIS PAGE INTENTIONALLY LEFT BLANK

REPORT DOCUMENTATION PAGE			Form Approved OMB No. 0704–0188

1. AGENCY USE ONLY *(Leave blank)*	2. REPORT DATE September 2011	3. REPORT TYPE AND DATES COVERED Master's Thesis

4. TITLE AND SUBTITLE Evaluation of LIDAR for Automating Recognition of Roads and Trails Beneath Forest Canopy	5. FUNDING NUMBERS
6. AUTHOR(S) Steven Louis Muha	
7. PERFORMING ORGANIZATION NAME(S) AND ADDRESS(ES) Naval Postgraduate School Monterey, CA 93943–5000	8. PERFORMING ORGANIZATION REPORT NUMBER
9. SPONSORING /MONITORING AGENCY NAME(S) AND ADDRESS(ES) N/A	10. SPONSORING/MONITORING AGENCY REPORT NUMBER

11. SUPPLEMENTARY NOTES The views expressed in this thesis are those of the author and do not reflect the official policy or position of the Department of Defense or the U.S. Government. IRB Protocol number _____N/A_____.

12a. DISTRIBUTION / AVAILABILITY STATEMENT Approved for public release; distribution is unlimited	12b. DISTRIBUTION CODE

13. ABSTRACT (maximum 200 words)

This thesis discusses the utility of evaluating Light Detection and Ranging (LiDAR) to automate the recognition of roads and trails beneath forest canopy on Digital Elevation Models (DEMs) for use in military and forestry applications. Data were analyzed from three separate locations, including low elevation mixed conifer Indian Creek Watershed in Trinity County, CA; High elevation mixed conifer Cold Creek Trailhead area in South Lake Tahoe, CA; and lowland mesic forests in Kahuku training area, Oahu, HI. LiDAR data were evaluated to extract a DEM from ground points and to build a point cloud object layer between the estimated ground and an Above Ground Level (AGL) defined limit of 1.8 meters. By comparison of this point cloud data with the terrain model, small corridors above the forest floor extracted using linear feature detection were recognized as potential roads or trails. The object layer was of limited value, due partly to point collection density issues, and understory density in the different forest types. When evaluated using statistical classification techniques, results produced were inconsistent in segregating trails and roads from non-trail regions. It was determined that automated classification of these regions utilizing this method was ineffective and remains unacceptable without further research.

.

14. SUBJECT TERMS LiDAR, automated, road and trail detection, linear feature, classification, forestry	15. NUMBER OF PAGES 113
	16. PRICE CODE

17. SECURITY CLASSIFICATION OF REPORT	18. SECURITY CLASSIFICATION OF THIS PAGE	19. SECURITY CLASSIFICATION OF ABSTRACT	20. LIMITATION OF ABSTRACT
Unclassified	Unclassified	Unclassified	UU

NSN 7540–01–280–5500

Standard Form 298 (Rev. 2–89)
Prescribed by ANSI Std. 239–18

THIS PAGE INTENTIONALLY LEFT BLANK

Approved for public release; distribution is unlimited

EVALUATION OF LIDAR FOR AUTOMATING RECOGNITION OF ROADS AND TRAILS BENEATH FOREST CANOPY

Steven Louis Muha
Captain, United States Marine Corps
B.S., Humboldt State University, 1998

Submitted in partial fulfillment of the
requirements for the degree of

MASTER OF SCIENCE IN SPACE SYSTEMS OPERATIONS

from the

NAVAL POSTGRADUATE SCHOOL
September 2011

Author: Steven Louis Muha

Approved by: R. C. Olsen
Thesis Advisor

Cajun James
Second Reader

Rudy Panholzer
Chair, Space Systems Academic Group

THIS PAGE INTENTIONALLY LEFT BLANK

ABSTRACT

This thesis discusses the utility of evaluating Light Detection and Ranging (LiDAR) to automate the recognition of roads and trails beneath forest canopy on Digital Elevation Models (DEMs) for use in military and forestry applications. Data were analyzed from three separate locations, including low elevation mixed conifer Indian Creek Watershed in Trinity County, CA; High elevation mixed conifer Cold Creek Trailhead area in South Lake Tahoe, CA; and lowland mesic forests in Kahuku training area, Oahu, HI. LiDAR data were evaluated to extract a DEM from ground points and to build a point cloud object layer between the estimated ground and an Above Ground Level (AGL) defined limit of 1.8 meters. By comparison of this point cloud data with the terrain model, small corridors above the forest floor extracted using linear feature detection were recognized as potential roads or trails. The object layer was of limited value, due partly to point collection density issues, and understory density in the different forest types. When evaluated using statistical classification techniques, results produced were inconsistent in segregating trails and roads from non-trail regions. It was determined that automated classification of these regions utilizing this method was ineffective and remains unacceptable without further research.

THIS PAGE INTENTIONALLY LEFT BLANK

TABLE OF CONTENTS

I. INTRODUCTION....1
A. PURPOSE OF RESEARCH....1
B. OBJECTIVE....1
II. BACKGROUND....3
A. LIDAR FUNDAMENTALS....3
B. HISTORY AND TECHNOLOGY....5
1. Airborne and Spaceborne LiDAR....6
a. Scanning assembly....8
b. GPS/IMU assemblies....10
c. Control and data recording unit....10
2. Terrestrial LiDAR....10
C. LIDAR APPLICATIONS....11
1. Selected Forestry and Natural Resource Management Applications....11
a. Forest Inventory, Mapping and Watershed Management....11
b. Stand Characterization....15
c. Forest Operations....18
2. Selected Archaeology Applications....20
3. Selected Government Research and Military Applications....23
a. Terrain Mapping and Vegetation Survey....23
b. Bathymetry and Coastal Mapping....25
c. Tactical River Crossings....26
4. Selected Space–Based Applications....27
a. LiDAR In-Space Technology Experiment (LITE) and Shuttle Laser Altimeter (SLA)....28
b. Geoscience Laser Altimeter System (GLAS)....29
c. ICESat–2 and Slope Imaging Multi-polarization Photon Counting LiDAR (SIMPL)....29
D. AUTOMATIC EXTRACTION OF FEATURES USING LIDAR....31
III. PROJECT DESCRIPTION....37
A. AUTOMATING TRAIL DETECTION BENEATH FOREST CANOPY....37
B. DATA AND SITE DESCRIPTION....39
1. Indian Creek Watershed....39
2. Lake Tahoe Basin....41
3. Kahuku Training Area....43
C. PROCESSING SOFTWARE....44
1. Quick Terrain Modeler, Version 7.1.4....44
2. Environment for Visualizing Images (ENVI) + Interactive Data Language (IDL), Version 4.8....45
IV. OBSERVATIONS AND ANALYSIS....47

A. DATA PREPARATION 47
1. Quick Terrain Modeler 47
a. Data Import 47
b. DEM Creation 52
c. AGL Analyst 57
d. Image File Creation and Export 59
2. ENVI 62
a. Topographic Modeling 62
b. Image Preparation and Layer Stacking 65
c. Minimum Noise Fraction (MNF) Transform 66
B. DATA SPECTRAL ANALYSIS 67
1. Indian Creek 67
a. Region of Interest Selection 67
b. n–Dimensional Visualizer Analysis 68
c. Maximum Likelihood Classification 69
2. Lake Tahoe, Cold Creek 72
a. Region of Interest Selection 72
b. n–Dimensional Visualizer Analysis 72
c. Maximum Likelihood Classification 73
3. Kahuku 75
a. Region of Interest Selection 75
b. n–Dimensional Visualizer Analysis 76
c. Maximum Likelihood Classification 76

V. SUMMARY 79

VI. CONCLUSION 83

LIST OF REFERENCES 85

INITIAL DISTRIBUTION LIST 91

LIST OF FIGURES

Figure 1. Measuring principle of pulse and CW lasers showing amplitudes of transmitted ($A_{t)}$ and received (A_r) signals. (From Wehr & Lohr, 1999) 3

Figure 2. Rangefinding scanning and aircraft orientation (From McGaughey, Andersen, & Reutebuch, 2006).....4

Figure 3. CALIPSO LiDAR collection, June 2006 from sea level to 30km (From National Aeronautics and Space Administration [NASA], 2011) 6

Figure 4. Illustration of LiDAR waveform and discrete recording characteristics (From Diaz, 2011).....7

Figure 5. Leica ALS70 LiDAR airborne system components including laser, scanner, range counting electronics, position/attitude measurement subsystem, flight planning and execution software (From Leica ALS70 brochure) 9

Figure 6. DEM formed from LiDAR survey under multistoried forest canopy (From Reutebuch, Andersen, & Carson, 2003) 11

Figure 7. Display shows (a) Location of individual trees plotted over aerial photography and (b) LiDAR point clouds of individual trees selected out for study based on intensity values. Conifers are on top displayed in white, broadleaved species below displayed in yellow (From Kim et al., 2009) 13

Figure 8. Description of specific method advocated by TreeMetrics software company for utilizing terrestrial LiDAR in timber measurement and optimization (From TreeMetrics, Ltd., 2011). 14

Figure 9. Total cost of a double sampling LiDAR cruise and a fixed plot ground cruise for three coefficients of determination and a range of relative plot costs for a 100,000 acre tract (From Tilley et al., 2004).....15

Figure 10. LiDAR derived forest canopy fuel weight map (30 m resolution) (From Andersen, McGaughey, & Reutebuch, 2005) 16

Figure 11. Comparison of predicted tree density to field measured tree density for all polts measured in the study for two height classes. The red icons are for trees greater than 20 m tall and the blue icons are for trees between 5m and 20 m tall. Locations are he Ahtanum Multiple Use Area (AMUA), Colville National Forest (CNF), and Training Plots (TP) (From Richardson & Moskal, 2011). 17

Figure 12. LiDAR–derived roads in the Little Creek watershed (From White et al., 2010) 19

Figure 13. Contour lines overlayed on LiDAR-derived DEM with slope class coloring revealing the greater detail available than from working with Topographic map alone (After Krogstad & Schiess, 2004).....20

Figure 14. Prehistoric, fortified enclosure known as Welshbury Hill in the Forest of Dean, Gloucestershire, UK. Left image from digital imagery, center image is a LiDAR DTM, and right image is an extracted DEM (After Devereux et al., 2005) 21

Figure 15. Rendering from airbone LiDAR point cloud surrounding Mayan pyramid (From Diaz, 2011).....22
Figure 16. 3D LiDAR model of a Dinosaur track, showing the multitude of information which can be derived for this research with this tool from claw marks to digit traces and displacement parameters (From Bates et al., 2008). 23
Figure 17. Example of swath implemented by LVIS (FromNational Aeronautics and Space Administration [NASA], 2011b).....24
Figure 18. Crane Glacier, Antarctica LVIS map in left image, LVIS scan and beam pattern shown on the right highlighting the complete coverage picture (After NASA, 2011).....25
Figure 19. Bathymetric LiDAR Coverage, Hilo Bay, HI (From Macon et al., 2008). 26
Figure 20. Example comparing river crossing profile of ground survey (dashed line) with LiDAR data results (solid line) (From Coutermarsh, 2003).....27
Figure 21. Example of how Laser landing sensors could be utilized in spacecraft landing scenarios (From Amzajerdian et al., 2011).....28
Figure 22. Current Concept for ICESat–2's 9 beam configuration (not to scale) (From Harding et al., 2010) 30
Figure 23. Comparison between conventional single pulse full waveform systems and micropulse photon counting systems measurement approaches of forest canopy structure (From Harding et al., 2011).....31
Figure 24. Examples of optical illusions. Left image: Lengths of the two horizontal lines appear different, but are the same. Center image: "White" square B in shadow and "black" square A both have the same absolute intensity value. Right image: As you move your eyes over figure, gray spots appear in the intersections (After Szeliski, 2010).....32
Figure 25. Vision–based system overview for automatic detection and extraction of road networks (From Poullis, 2008). 33
Figure 26. Point cloud cross section from study area where small empty space above trail surface is visible (between 40 m and 50 m on X–axis) (After Heezin Lee et al., 2005). 34
Figure 27. Left figure shows GPS points of actual trail, middle figure has visibility vectors computed of potential trails, and right figure is the winning candidate trail (From Heezin Lee et al., 2005). 35
Figure 28. Indian Creek Watershed Collection (From: Google Earth) 40
Figure 29. Lake Tahoe Basin collection, Cold Creek (From Google Earth).....41
Figure 30. Kahuku training area site 6 (From Google Earth) 43
Figure 31. ASCII dataset import menu on the left and LAS dataset import menu on the right. For ASCII, data is arranged as text in file by column as East, North, Z, and Intensity. For LAS, data can be imported with intensity or according to classification.....48
Figure 32. Indian Creek point cloud, all returns. Colors show relative elevation values in meters.....49
Figure 33. Indian Creek point cloud model information, all returns.....49

Figure 34. Lake Tahoe, Cold Creek point cloud, all returns. Colors show relative elevation values in meters. 50
Figure 35. Lake Tahoe, Cold Creek model information, all returns. 50
Figure 36. Kahuku point cloud, all returns. Colors show relative elevation values in meters. 51
Figure 37. Kahuku model information, all returns. 51
Figure 38. Bare earth extraction import menu. 53
Figure 39. Google Earth Image of Indian Creek Watershed survey area, each square forms a separate ASCII file covering about 1 km^2 53
Figure 40. Digital Elevation Model from Indian Creek watershed survey area revealing surface features beneath vegetation. 54
Figure 41. Google Earth image of Cold Creek survey area in Lake Tahoe Basin dataset. Survey area covers slightly more than 1 km^2 55
Figure 42. Digital Elevation Model from Cold Creek survey area in Lake Tahoe Basin revealing surface features beneath vegetation 55
Figure 43. Google Earth Image of Site 6 in Kahuku survey area, Oahu, HI. Area covers about 400m x400m. 56
Figure 44. Digital Elevation Model from Kahuku site 6 survey area revealing surface features beneath vegetation. 56
Figure 45. AGL Analyst menu, ground estimate calculated from surface model, break points added at 0.1m and 1.8m, points exported into LAS files 57
Figure 46. Birds–eye view of 3D point cloud in Lake Tahoe, Cold Creek from 0.1m to 1.8m. Linear gap in point cloud absent of points is clearly visible winding across the landscape, corresponding to identifiable trail on the DEM in Figure 47 58
Figure 47. Birds1eye view of DEM in Lake Tahoe, Cold Creek with trail clearly visible winding across the landscape corresponding to linear gap in point cloud absent of points from Figure 46. 59
Figure 48. Export Model menu for each surface model to be converted to image file for ENVI analysis 60
Figure 49. Grid Statistics Menu, Cold Creek: Number of Points for 0.1m to 1.8m AGL slice file was calculated at 1 meter spacing, and values saved in GEOTIFF format for subsequent ENVI image analysis 61
Figure 50. Lake Tahoe, Cold Creek survey area Number of Points for all points. Flight line overlap effects are clearly evident as strips of higher density points transiting the image. 61
Figure 51. Lake Tahoe, Cold Creek survey area Number of Points for 0.1 m to 1.8 m AGL point cloud slice. Flight line overlap effects are clearly evident 62
Figure 52. Topographic model parameters, selection of measures to compute, kernel Size and output to file. 63
Figure 53. Indian Creek topographic slope band. 64
Figure 54. Indian Creek topographic profile convexity band. 64
Figure 55. Indian Creek topographic plan convexity band. 64
Figure 56. Indian Creek topographic longitudinal convexity band. 65
Figure 57. Indian Creek topographic cross-sectional convexity band. 65

Figure 58. Layer Stacking Parameters input menu. Files are selected for stacking in order of precedence and output in re–sampled, 1 m^2 pixels. 66
Figure 59. Forward MNF Transform Parameters menu. Transform performed on Layer Stacked data files and output into MNF bands file for subsequent spectral analysis. 67
Figure 60. ROI Tool for selecting regions of suspected road/trail regions (Red points) and suspected non–road/trail regions (Green points).....68
Figure 61. Indian Creek survey area, Regions of Interest over MNF band 4, identifying roads/trails (red selections) and non–roads/trails (green selections). 69
Figure 62. N–D visualizer scatter plot utilizing MNF bands 2 through 7 for Indian Creek survey area.....69
Figure 63. Maximum Likelihood Parameters input menu. ROI regions are selected with a probability threshold of 0.5 and output to both class and rule files 70
Figure 64. Maximum Likelihood Classification result, probability threshold of 10%, applied to Indian Creek survey area. The red areas are classified as most likely to be trail. Vast areas of the survey area are unclassified at this threshold.....71
Figure 65. Maximum Likelihood Classification result, no probability threshold, applied to Indian Creek survey area. The red areas are classified as most likely to be road/trail. The green areas are classified as most likely to be other than road/trail.....71
Figure 66. MNF band 1 (left) and MNF band 2(right) images, overview. In band 1, lighter areas more likely to be trail. In band 2, darker areas more likely to be trail. 72
Figure 67. Regions (top) drawn over MNF band 1 image, red points identified as most likely trail, blue points as possibly trail, and green as not trail. N–D visualizer scatter plot (lower left) utilizing MNF bands 1 through 4, and scatter plot (lower right) utilizing MNF band 1 and band 2. 73
Figure 68. Maximum Likelihood Classification result applied to Lake Tahoe, Cold Creek survey area. The whiter the area, the more likely that it is a trail. Vast areas of the survey area are classified as trail using this method. 74
Figure 69. Subset of Lake Tahoe, Cold Creek survey area surrounding region of interest selected areas (upper left of figure that includes the green shaded region of nontrail points). Classified such that the whiter the area, the more likely it is a trail. 74
Figure 70. Kahuku survey area, Regions of Interest over MNF band 1, identifying roads/trails (red selections) and nonroads/trails (green selections). Differing shades of red and green are the result of further n–D visualizer analysis.....75
Figure 71. N–D Visualizer scatter plot of points selected in Regions of Interest and further selected and colored according to obvious point groupings. Red colored points which correspond to selected roads and trails clearly form a grouping orthogonal to the nonroad/trail points. 76

Figure 72. Kahuku survey area Maximum Likelihood Classification map identifying red colored areas as roads/trails, green colored areas as non–road/trails, black areas as not classified. 77
Figure 73. Kahuku Maximum Likelihood Probability "Rule" image distinguishing between the first three identified road/trail classes such that the whiter the area, the more probable that it is a road/trail. "Rule" image is the probability that a pixel vector matches the mean of the region of interest for the training set. 78
Figure 74. Birds–eye view of 3D point cloud in Lake Tahoe, Cold Creek from 0.1m to 1.8m. Linear gap in point cloud absent of points is clearly visible winding across the landscape, corresponding to identifiable trail on the DEM....80

THIS PAGE INTENTIONALLY LEFT BLANK

LIST OF TABLES

Table 1. Indian Creek Watershed Collection, Optech 25kHz specifications (Airborne 1) 40
Table 2. Lake Tahoe Collection, Leica ALS50 specifications (OpenTopography).....42
Table 3. Kahuku collection, Optech 3100 specifications (From Espinoza & Owens, 2007) 44

THIS PAGE INTENTIONALLY LEFT BLANK

LIST OF ACRONYMS AND ABBREVIATIONS

AGL	Above Ground Level
ALS	Airborne Laser Scanning
ALTM	Airborne Laser Terrain Mapper
AMUA	Ahtanum Multiple Use Area
ASCII	American Standard Code for Information Interchange
CALIPSO	Cloud-Aerosol LiDAR and Infrared Pathfinder Satellite Observation
CHARTS	Compact Hydrographic Airborne Rapid Total Survey
CNF	Colville National Forest
CW	Continuous Wave
DEM	Digital Elevation Model
DESDynI	Deformation, Ecosystem Structure and Dynamics of Ice
DSM	Digital Surface Model
DTM	Digital Terrain Model
EAR/IF	Earth Sciences Instrumentation and Facilities Program
EM	ElectroMagnetic
ENVI	Environment for Visualizing Images
FWD	Full Wave Digitizer
GaAs	Gallium Arsenide
GEOTIFF	Geostationary Earth Orbit Tagged Image File Format
GIS	Geographic Information System
GLAS	Geoscience Laser Altimeter System
GPS	Global Positioning System
ICESat	Ice, Cloud, and Land Elevation Satellite
IDL	Interactive Data Language
IMU	Inertial Measurement Unit
InSAR	Interferometric Synthetic Aperture Radar
ISS	International Space Station
JALBTCX	Joint Airborne LiDAR Bathymetry Technical Center of Expertise

LADAR	LAser Detection and Ranging
LiDAR	Light Detection And Ranging
LITE	LiDAR In Space Technology Experiment
LVIS	Laser Vegetation Imaging Sensor
MNF	Minimum Noise Fraction
NASA	National Aeronautics and Space Administration
Nd YAG	Neodymium-Doped Yttrium Aluminum Garnet
NGA	National Geospatial Intelligence Agency
PRF	Pulse Repetition Frequency
QTM	Quick Terrain Modeler
RADAR	Radio Detection and Ranging
RMSE	Root Mean Square Error
ROI	Region Of Interest
SIMPL	Slope Imaging Multi-Polarization Photon Counting LiDAR
SLA	Shuttle Laser Altimeter
SLICER	Scanning LiDAR Imager of Canopies by Echo Recovery
SNR	Signal to Noise Ratio
TP	Training Plots
USDA	U.S. Department of Agriculture
WSI	Watershed Sciences Incorporated

ACKNOWLEDGMENTS

Special Thanks to:

Dr. R. C. Olsen, Naval Postgraduate School

Angela Puetz, Naval Postgraduate School

Dr. Cajun James, Sierra Pacific Industries

Glen Rouse, Sierra Pacific Industries

Michael Umansky, Applied Imagery

Jerome Gregory, Airborne 1

Dr. Charalambos "Charis" Poullis, Cyprus University of Technology

Krista Lee, Naval Postgraduate School

Chelsea Esterline, Naval Postgraduate School

Sarah Carlisle, Naval Postgraduate School

Maj Frank Harmon, U.S. Army

The Staff at the El Prado Room

My Roommates: Ken, Mike, Clint and Scooter

Nate and Rikki for Pizza Night

Andrew for Thursday Cigar Night

7–11 Coffee

Rock Band 2

And most of all,

Thanks to my wife and children for their continued love and support:

Marianne, Nathaniel, Matthew, Jonathan and Theodore Muha!

THIS PAGE INTENTIONALLY LEFT BLANK

I. INTRODUCTION

A. PURPOSE OF RESEARCH

A critical component in land–management mission planning is accurate and up-to-date knowledge of the terrain. Airborne Laser Scanning (ALS) methods have been developed which can be exploited to produce high resolution 3–D topographic models. The ability to extract high precision Digital Elevation Models (DEMs) from collected point data allows for the added benefit of being able to "see" what is underneath vegetation at the time of collection. This capability is relevant in a variety of disciplines, including cartography, rural and urban development, geology, archaeology, forestry and watershed management, and military mission planning. Recognition of human activity beneath dense forest canopy, previously undetectable utilizing other methods, is of particular value for intelligence agencies in reconnaissance of criminal organizations or enemy combatants. The ability to automate the analysis of Light Detection and Ranging (LiDAR) data to detect landscape changes between subsequent collections would be a significant improvement over current methods. The purpose of this research is to evaluate the efficacy of LiDAR for automated road and trail detection beneath forest canopy in order to recognize these changes in landscape topography over time consistent with human activity.

B. OBJECTIVE

The primary objective of this thesis is to determine a method for analyzing LiDAR data in order to effectively recognize potential roads and trails under forest canopy with the intent to automate such a process. LiDAR data utilized in this research was collected in two different regions of California mixed conifer forest environments with different sensors and levels of point density (Indian Creek Watershed (2002) near Shasta–Trinity National Forest, and Cold Creek Watershed (2010) in the Lake Tahoe Basin). Commercial software used in this analysis includes Applied Imagery LLC's Quick Terrain Modeler (QTM) Version 7, ILAP Bare Earth Extraction Plug–In

developed by The John Hopkins University/Applied Physics Laboratory, and Environment for Visualizing Images (ENVI) 4.8.

Chapter II will provide a brief description of LiDAR, its historical development, and a review of current technologies. Remote sensing application and use by various disciplines for terrain analysis will be discussed in detail, including forestry and watershed, archaeology, government research, military, and space systems applications. This section will also include a brief description of current and emerging attempts at automation.

Chapter III will provide the structure of this problem and project along with a detailed description of each research area and accompanying data selected for analysis. Tools, inputs and evaluation techniques, as well as, a short explanation of some post–processing software used in this research, are described in this chapter.

Chapter IV will include the observations compiled from LiDAR point cloud data manipulation, including DEMs and grid statistic output following selected evaluation techniques. This chapter will also provide analysis of the observations extracted from results utilizing available software tools, and provide interpretation of these results compared to the expected outcome.

Chapters V and VI provide an overall summary of the analysis and conclusions derived from this research project.

II. BACKGROUND

A. LIDAR FUNDAMENTALS

LiDAR is laser (*l*ight *a*mplification by *s*timulated *e*mission of *r*adiation) scanning in which electromagnetic (EM) wave energy is transmitted in optical pulses, or by continuous wave signals, which reflects off of an object and returns to a receiving detector. The time traveled between pulses can be easily converted into a distance where R is the range to target and c is the speed of the EM radiation. In a continuous wave (CW) system, range is dependent on frequency *f* and phase difference ϕ of the ranging signal. If a multifrequency system is used, the frequency with the longest wavelength (λ_{long}) determines R_{max} and the frequency with the shortest wavelength (λ_{short}) determines range resolution and accuracy (Wehr & Lohr, 1999).

Pulse:

Range: $R = \frac{1}{2} c \cdot t_L$

Range Resolution: $\Delta R = \frac{1}{2} c \cdot \Delta t_L$

Max. Range: $R_{max} = \frac{1}{2} c \cdot t_{L\,max}$

Range Accuracy: $\sigma_R \sim \frac{c}{2} t_{rise} \cdot \frac{1}{\sqrt{S/N}}$

Sinusoidal CW-Modulation:

Travelling Time by Phase Difference: $\left.\begin{matrix} T \triangleq 2\pi \\ t_L \triangleq \Phi \end{matrix}\right\} \Rightarrow t_L = \frac{\Phi}{2\pi} \cdot T$

Range: $R = \frac{1}{2} c \cdot \frac{\Phi}{2\pi} \cdot T = \frac{\lambda}{4\pi} \cdot \Phi$

Max. Unamb. Range: $R_{max} = \frac{\lambda_{long}}{2}$

Range Resolution: $\Delta R = \frac{\lambda_{short}}{4\pi} \cdot \Delta\Phi$

Range Accuracy: $\sigma_R \sim \frac{\lambda_{short}}{4\pi} \cdot \frac{1}{\sqrt{S/N}}$

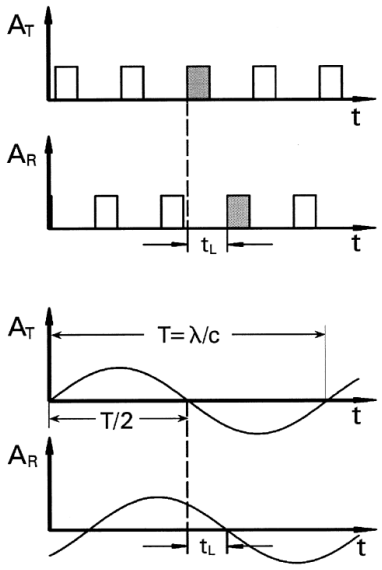

Figure 1. Measuring principle of pulse and CW lasers showing amplitudes of transmitted (A_t) and received (A_r) signals. (From Wehr & Lohr, 1999)

LiDAR can be delivered via terrestrial or airborne platforms, and can provide extremely high quality collections of three dimensional data. When delivered from an airborne platform, in combination with current global positioning system (GPS) technology, distance to target information and aircraft position can be used to accurately determine geo–referenced elevation information. Pulses are delivered across a landscape via cross–track scanning mirror, and occur at very high rates. Current LiDAR systems are capable of delivering a pulse repetition frequency (PRF) of hundreds of thousands of pulses every second, and multiple returns can be measured for each pulse. Discrete return, small footprint, airborne LIDAR systems were developed for the express purpose of mapping terrain (Wehr & Lohr, 1999).

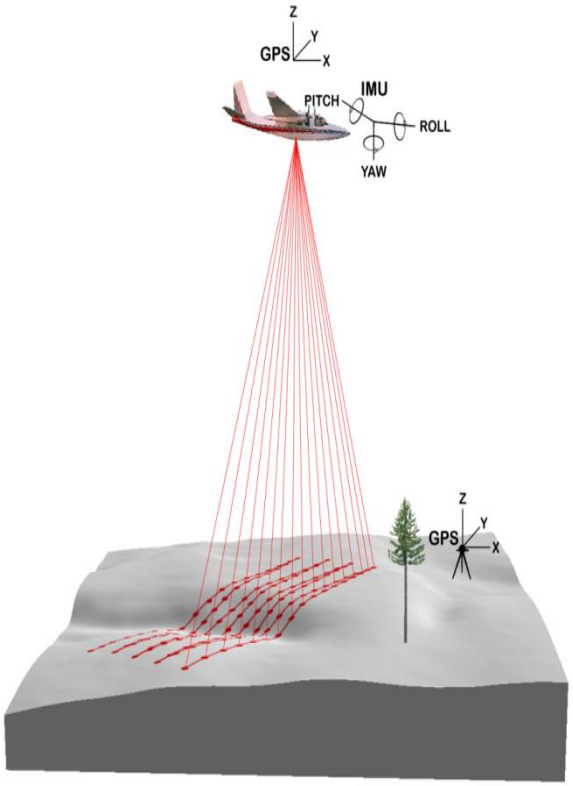

Figure 2. Rangefinding scanning and aircraft orientation (From McGaughey, Andersen, & Reutebuch, 2006)

Lasers that are primarily used in LiDAR applications include neodymium–doped yttrium aluminum garnet (Nd:YAG) at 1064 nm wavelengths and Gallium Arsenide (GaAs) at 840 nm. Scanning methods vary between single or oscillating plane mirrors, a spinning optical polygonal mirror, elliptically scanning nutating mirror, or a pair of tilted mirrors in linear fiber-optic arrays. A much more detailed description of these methods, components, and other basic LiDAR fundamentals can be found in this excellent reference (Shan & Toth, 2009).

B. HISTORY AND TECHNOLOGY

Ranging systems that utilize electromagnetic waves to locate a target by means of transmission and reception of reflection waves, have been in development for military application since the late 1930s, beginning with RADAR (Radio Detection and Ranging). Technological development has allowed ever–increasing frequencies, with corresponding shorter wavelengths, from radio frequencies, microwaves, infrared, light and beyond. LiDAR applications, also referred to as LADAR (LAser Detection and Ranging), were possible in the mid-1960s as Laser based sensors were first being successfully developed (Richmond & Cain, 2010). Key enabling technologies that precipitated airborne LiDAR development include GPS and suitable scanning mechanisms, such as rotating mirrors (Toth, 2009). Once GPS became widely deployed, airborne surveying was enabled because of very precise positioning capabilities. From the air, object elevations above ground level can be obtained very accurately and ground terrain features can be extracted from last pulse returns. GPS enables a common interface for combining other imagery products with LiDAR data to complement and enhance its utility.

Although remote sensing of the Earth, and its applications, is of most interest to this research, LiDAR frequencies are suited very well for accurately measuring aerosols and cloud particles above the earth, and this dominated the early use of LiDAR for atmospheric research and meteorology. This has continued through to the present, evidenced by the launch of the Cloud-Aerosol LiDAR and Infrared Pathfinder Satellite Observation (CALIPSO) in April 2006, which allows for 3D perspectives of clouds and aerosols in the atmosphere.

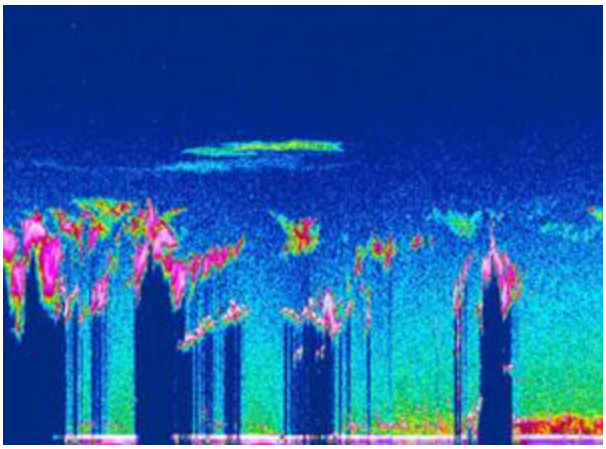

Figure 3. CALIPSO LiDAR collection, June 2006 from sea level to 30km (From National Aeronautics and Space Administration [NASA], 2011)

1. Airborne and Spaceborne LiDAR

Airborne LiDAR system components required for collection include a helicopter or light aircraft with a belly-loaded scanning laser emitter–receiver unit, a differentially-corrected GPS, stabilizing Inertial Measurement Unit (IMU) and robust computer for processing and data storage. Millions of points can be collected in a single survey numbering in the terabytes of data storage required. The purpose of the IMU is to determine the aircraft's attitude during data collection of roll, pitch, and yaw, as well as, altitude variations during flight. This is critical to ensuring high accuracy calculation of the laser relative to the earth's surface. Data is represented according to Cartesian XYZ point cloud coordinates from reflected signals. Signals can include multiple returns from a single pulse, dependent on how much light is partially blocked en-route to the ground, usually by passing through multi–storied vegetation (McGaughey et al., 2006). Typical vertical accuracy of current systems can be achieved down to less than 5 cm and with pulse rates up to 500 kHz (Leica Geosystems GIS & Mapping, LLC Product Information, 2011). Profile measurements are constructed from area scanning in cross-track and along track directions of the flight to produce the positions and elevations of collected points. Airborne LiDAR bathymetry systems which work a little differently, measure differential timing of reflected laser pulses from the water surface and underwater surface to determine very accurate water depth measurements (Heritage & Large, 2009).

Spaceborne LiDAR systems work in much the same way as airborne, but the characteristics of the components are much different, recognizing the constraints of orbital regime, as well as, increased distances from the target and speed over the ground (Shan & Toth, 2009).

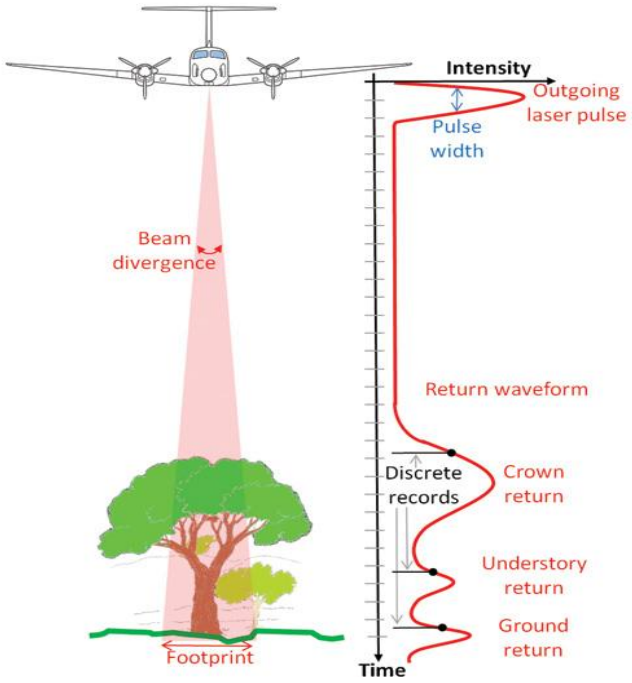

Figure 4. Illustration of LiDAR waveform and discrete recording characteristics (From Diaz, 2011)

Examples of topographic products derived from airborne collected raw point data include Digital Elevation Models (DEMs), Digital Terrain Models (DTMs), Digital Surface Models, (DSMs), Slope, Aspect, and Intensity images. These raster products are very useful, but a great deal of information can be derived from raw point data which allows us to identify and measure objects beneath other objects, conduct vertical obstruction analysis, and classify terrain based on statistical analysis of the data. Many man-made features are often smoothed out or omitted when creating a DEM (Applied Imagery).

a. Scanning assembly

Comprising the laser, scanning mechanics and optics, the scanner assembly is the heart of the LiDAR system. Laser systems typically operate between wavelengths of 800nm and 1550nm with spectral width typically between 0.1 and 0.5nm (Vosselman & Maas, 2010). Key considerations for laser scanning wavelengths include reflectivity properties of target objects, absorption of water in the visible part of the spectrum, and eye safety. Swath width is determined by scan angle, typically between 5˚ and 75°, and the height above ground. Similarly, footprint diameter of the laser is determined by the beam divergence, typically between 0.1mrad and 1mrad, and height above ground (Vosselman & Maas, 2010). The ranging resolution of LiDAR systems continues to improve dramatically, typically available at 1–2 cm. Point density on the ground has also improved over time as the PRF continues to increase. Multiple pulse technology has allowed laser pulses to be transmitted and received in overlapping rapid succession with data capture rates in the hundreds of kHz (Toth, 2009). Point density is governed by high PRF, small scanning angle, low aircraft cruising speeds and low survey heights AGL. Pulse systems produce stop signals, with separate returns of up to four echoes per pulse. Full waveform systems return an echo's complete shape at very high resolution. Full waveform systems are not currently widely used due to very high hardware and processing requirements, but show great promise as capabilities continue to improve (Vosselman & Maas, 2010).

Figure 5. Leica ALS70 LiDAR airborne system components including laser, scanner, range counting electronics, position/attitude measurement subsystem, flight planning and execution software (From Leica ALS70 brochure)

Scanning mechanisms typically use a single or pair of oscillating mirrors in a technique that results in a sawtoothed or sinusoidal pattern measured on the ground along the aircraft flight path. Along track and cross track point distances are variable with larger point distances found in middle of a swath, and smaller point distances at the end of the swath. Because scan angle and scan rate are variable, this mechanism can be configured to produce predefined point distances on the ground. Other systems include rotating polygonal mirrors, nutating mirrors producing an elliptical scan pattern, and linear glass fibre–optic arrays which results in scan lines that run parallel to the flight line (Shan & Toth, 2009). Flash LiDAR generates a complete 3D image in one shot instead of by scan utilizing coherent field superposition on the photodetector between returned signal and reference signal. This method has spatial resolution and range limitations inherent in the design (Vosselman & Maas, 2010).

b. GPS/IMU assemblies

GPS measures the positional information and the IMU measures orientation data, both essential for geo-locating each laser pulse. Position information is necessary at 2 Hz or higher and IMU frequencies of 100 Hz or higher for orientation needed in airborne assemblies (Heritage & Large, 2009). Platform coordinates can be determined to an accuracy of approximately 10 cm.

c. Control and data recording unit

Aircraft position data, sensor attitude data, laser pulse data and aircraft behavior and recording errors are all stored and controlled by this unit, synchronized by GPS time stamp. Extended processing allows creation of time–stamped point clouds to provide the end product. Modern scanners produce in excess of 20 Gbytes of scanning data per hour with only 0.1 Gbyte per hour of GPS/IMU data (Vosselman & Maas, 2010).

2. Terrestrial LiDAR

Ground-based LiDAR can achieve horizontal 3D images unattainable from overhead systems, excellent for many applications, especially urban planning, mapping, chronology and engineering surveying (Shan & Toth, 2009). With a tripod mounted, freely rotating LiDAR sensor on the ground, 360-degree "street scenes" can be created from pulses transmitted and reflected off of all objects within range of the system. This 3D point cloud allows for very accurate lateral details of buildings, vegetation, and other objects that cannot be retrieved from airborne systems. Vehicle mounted systems can also be employed utilizing GPS much like airborne platforms. A combination of airborne with terrestrial scanning collections can provide fused images of exceptional quality to get the whole picture (IKG Research).

C. LIDAR APPLICATIONS

1. Selected Forestry and Natural Resource Management Applications

LiDAR is very well suited to forestry and natural resource management applications because of the high quality three dimensional data collection it provides. In addition to terrain visualization, LiDAR produces multiple returns which allow for detailed analysis of vegetation, watershed topography, and slope stability.

a. Forest Inventory, Mapping and Watershed Management

Critical to inventory is accurate mapping of forested terrain, and the influence that different forest parameters have on the accuracy of LiDAR-derived terrain models. One study by the Pacific Northwest Research Station U.S. Department of Agriculture Forest Service (USDA) in heavily forested lands in western Washington determined that these models can be extremely accurate over mature forested areas, even at as little as 1 return/m^2. The study was conducted utilizing Saab TopEye LiDAR system mounted on a helicopter in the Spring of 1999, covering 5 km^2 and collecting over 37 million points with up to four returns per pulse.

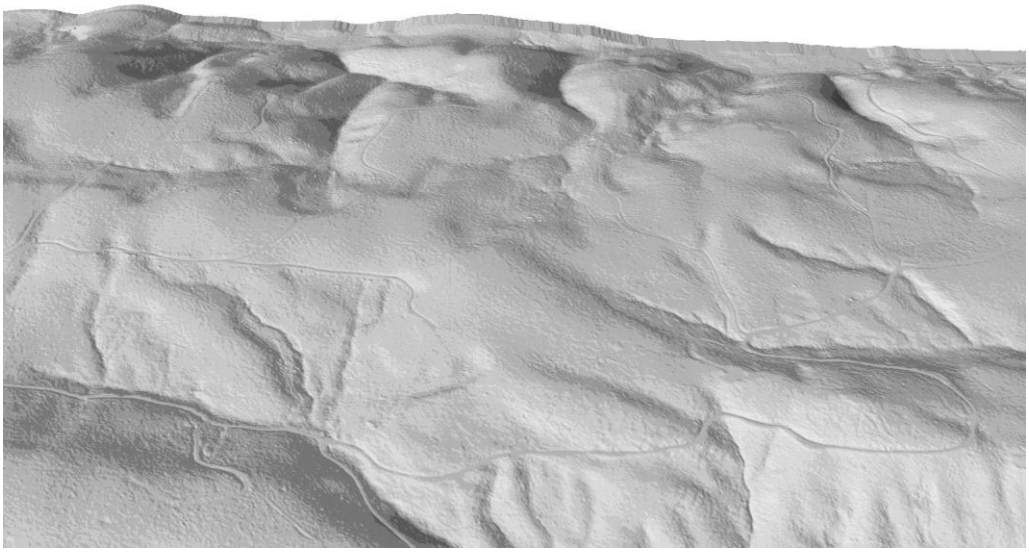

Figure 6. DEM formed from LiDAR survey under multistoried forest canopy (From Reutebuch, Andersen, & Carson, 2003)

Canopy classes studied included uncut, heavy and lightly thinned, as well as cleacut areas, with nearly 350 ground checkpoints to compare results against. It was found even at that time with relatively low resolution that the precise terrain modeling LiDAR provides of microtopography in a typical conifer forest, has excellent potential for many applications in the field of forestry (Reutebuch et al., 2003).

The ability to select out individual tree crowns from LiDAR intensity data, combined with the knowledge of forest type and stand characteristics, has allowed for some level of success in classification of tree species. A study funded by the Precision Forestry Cooperative at the University of Washington College of Forest Resources was conducted analyzing intensity values of two LiDAR data sets during leaf–on and leaf–off periods collected over Washington Park Arboretum in Seattle, Washington. Data collects were flown at 900m and 1200m AGL, with two different Optech LiDAR systems, achieving point densities at $5/m^2$ and $20/m^2$, respectively. Seven coniferous and eight broadleaved species were selected for analysis distinguishing broadleaved species from conifers, and making distinction between species within these broad groups, based on different reflective properties of the vegetation. The study noted that choosing data sets collected from the same LiDAR systems to compare against would probably yield more consistent results (Kim, McGaughey, Andersen, & Schreuder, 2009).

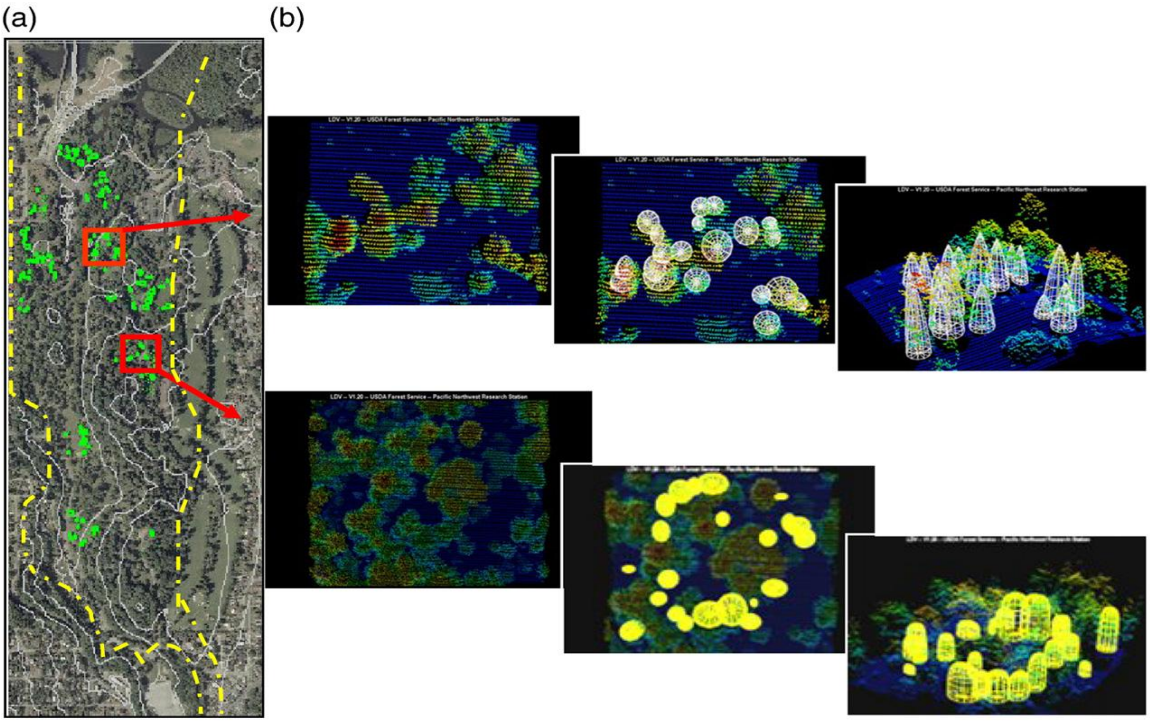

Figure 7. Display shows (a) Location of individual trees plotted over aerial photography and (b) LiDAR point clouds of individual trees selected out for study based on intensity values. Conifers are on top displayed in white, broadleaved species below displayed in yellow (From Kim et al., 2009)

Forest inventory of stand tree heights can be collected and extrapolated to larger areas based on landscape relationships utilizing LiDAR and imagery (Wulder & Seemann, 2003). Leaf area index can also be derived from LiDAR to provide estimates that are useful in explaining mass and energy exchanges in forest ecosystems (Jensen, Humes, Vierling, & Hudak, 2008). Another study compared the use of LiDAR data to intensive ground-based methods for characterization of streamside forest structure in order to assess the rate of delivery of large woody debris to streams. A strong correlation in accuracy between the two methods was observed, confirming the potential for LiDAR to provide capability as a tool for watershed assessment. Other potential applications were noted including stream shading studies and litterfall modeling, both important in the study of stream ecosystems (Fleece, 2002).

Terrestrial scanners have the potential to eventually replace current forest inventory methods in some situations, with supporting software that models production from standing forest volume to the mill's final output. Scanners can be deployed on slope independent terrain, effective up to 30 m per plot with less than 20 minutes for setup and collection time and 8 hours of operation under its own power (TreeMetrics Ltd., 2011). Scanners would not work well in stands with dense, brushy understory, both because of the difficulty in traversing this type of vegetation with the equipment, and because of the need for a clear field of view between the scanner and the timber.

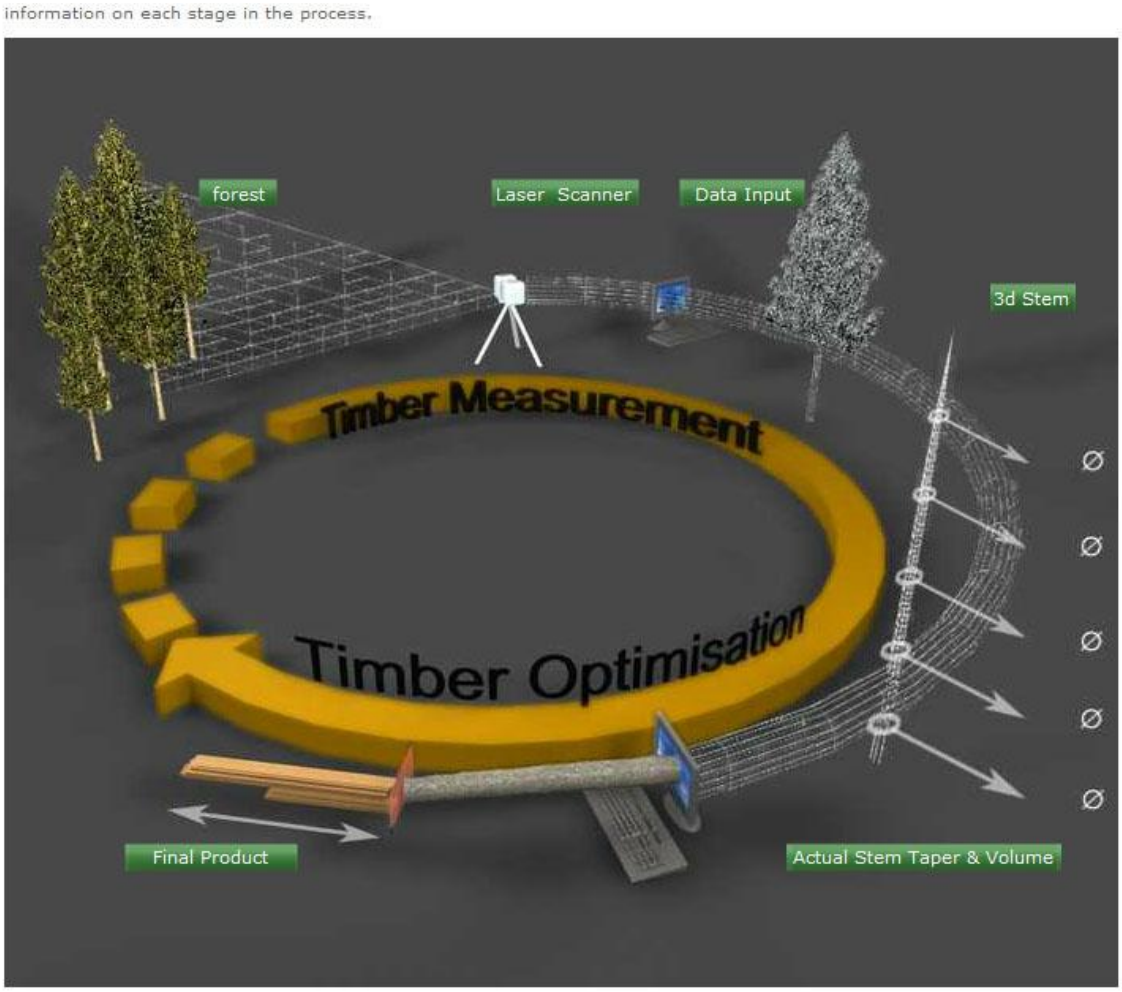

Figure 8. Description of specific method advocated by TreeMetrics software company for utilizing terrestrial LiDAR in timber measurement and optimization (From TreeMetrics, Ltd., 2011).

There is some question as to the economic viability of using airborne LiDAR in timber inventory. One 2004 study exploring cost considerations was conducted out of the Mississippi State University College of Forest Resources and Remote Sensing Technology Center on a 1200-acre study area located on the Lee Memorial Forest of Louisiana State University. This study found that timber inventory using LiDAR is not cost effective for determining timber volumes when compared to traditional methods due to the high cost of obtaining LiDAR data and the requirement for its use in a double-sampling approach. Although very effective for obtaining tree heights and trees per acre, airborne LiDAR does not give the highly accurate diameter, taper and understory stand characteristics that would be achieved from ground plot inventories. In this study, they found that as LiDAR plot costs fall below 35% of ground plot costs, double sampling with LiDAR becomes cost effective for coefficient of determination of 0.7 or greater (Tilley et al., 2004).

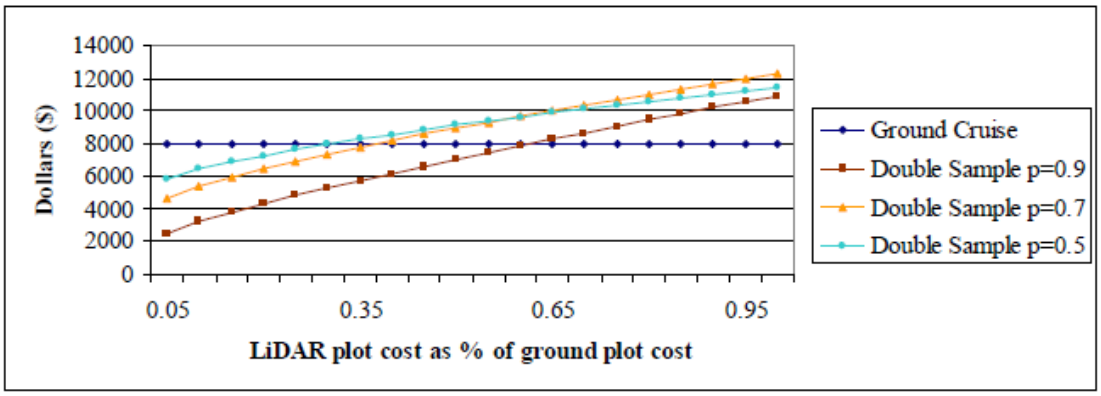

Figure 9. Total cost of a double sampling LiDAR cruise and a fixed plot ground cruise for three coefficients of determination and a range of relative plot costs for a 100,000 acre tract (From Tilley et al., 2004)

b. Stand Characterization

Forest stand structural characteristics can be accurately assessed from the capability of LiDAR to reflect from multiple levels of vegetation canopy. Typically one to four returns can be collected per pulse, effectively outlining individual trees, as well as, subcanopy characteristics. Useful products derived from these returns can include

forest biomass, canopy closure, carbon content, height distribution, and wildlife habitat based on stand characteristics (Reutebuch, Andersen, & McGaughey, 2005).

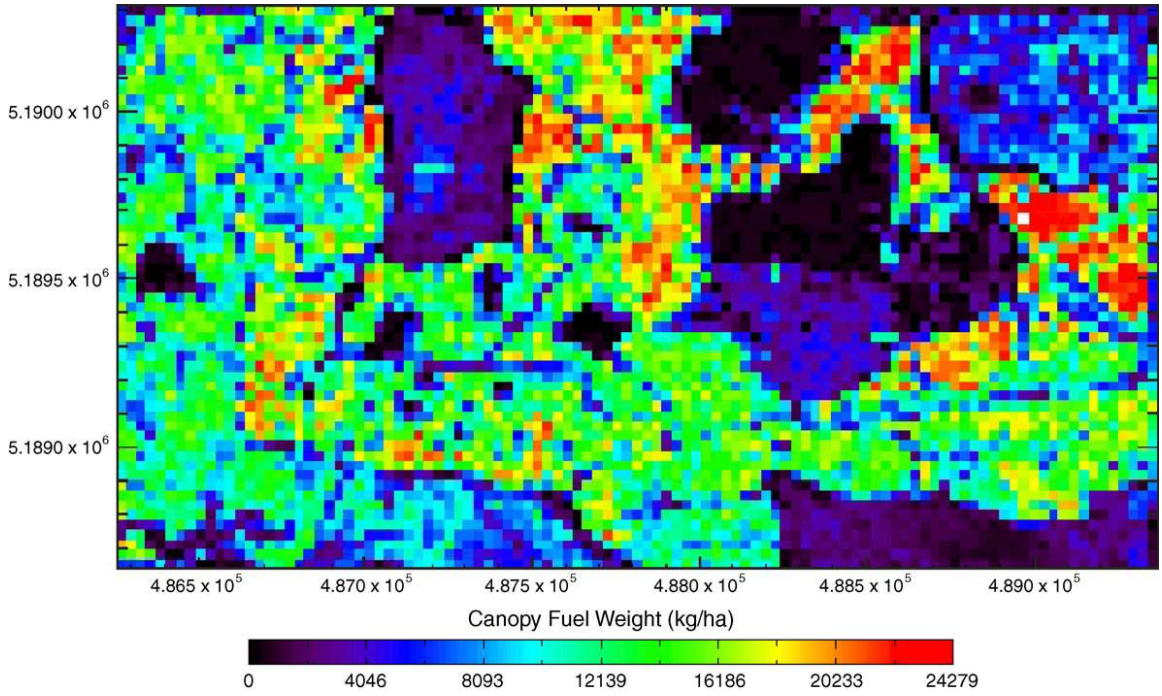

Figure 10. LiDAR derived forest canopy fuel weight map (30 m resolution) (From Andersen, McGaughey, & Reutebuch, 2005)

Fire behavior models which are driven by tree position, height, and crown diameter can be fed from LiDAR collections at greatly reduced cost compared to traditional forest inventory methods (Andersen et al., 2005).

Analyzing forest structure for predicting stand volume and growth is important for both commercial and ecological purposes. A study using LiDAR to estimate diameter and basal area distributions for prediction of stand volume and growth was conducted in Southeast Norway, covering 54 ground field plots distributed in differing combinations of age, site quality and species of trees. Plot volumes were calculated in these areas using traditional methods, then compared against LiDAR data results compiled from measurements of canopy height distributions further derived into diameter and basal area distributions. Optech's ALTM 1210 was used on a small aircraft flown at 650 m AGL at 75 m/s over 129 flight lines with 50% overlap between strips. It

was found that stem–frequency distributions can be adequately derived from LiDAR data and that a higher precision of volume predictions are possible when based on derived basal area distributions rather than diameter distributions (Gobakken, T., and Naesset, E., 2004).

A more recent study specifically looked at the strengths and limitations of LiDAR in assessing forest density and spatial configuration. This study looked at three separate forest areas within the rain-shadow of the Cascade Mountain Range in Washington State. Stands were specifically chosen to demonstrate heterogeneity in stand types, yet wide variation in vertical, horizontal, and density structures. LiDAR datasets were collected in June 2007 and 2008 with different sensors (Optech 3100 EA and Leica ALS50 Phase II) at different point densities (greater than 4 points/m^2 and greater than 8 points/m^2). The study concluded that aerial LiDAR is effective at producing precise estimates of tree densities for trees greater than 20 m, but severely underestimates tree densities of under and midstory canopies at these point densities (Richardson & Moskal, 2011).

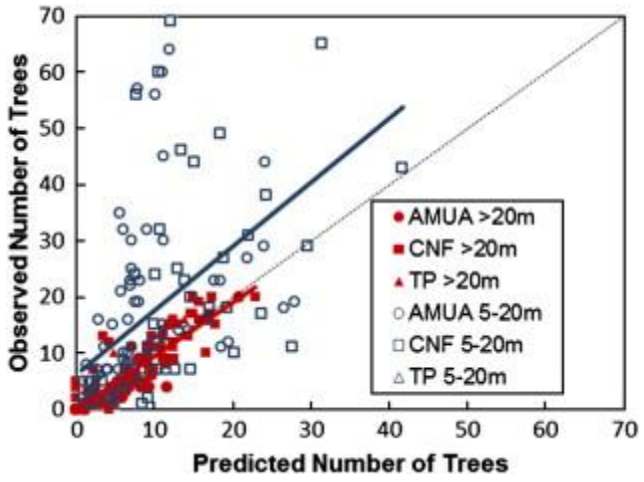

Figure 11. Comparison of predicted tree density to field measured tree density for all polts measured in the study for two height classes. The red icons are for trees greater than 20 m tall and the blue icons are for trees between 5m and 20 m tall. Locations are the Ahtanum Multiple Use Area (AMUA), Colville National Forest (CNF), and Training Plots (TP) (From Richardson & Moskal, 2011).

c. Forest Operations

LiDAR is potentially helpful for forestry production management operations in revealing existing road and skid trail networks located in a harvest area under dense forest canopy. A study that tested the accuracy of this claim was conducted in the Little Creek watershed on Swanton Pacific Ranch near Santa Cruz, CA, comparing the utilization of LiDAR data for road identification and mapping to traditional centerline survey on a typical forest haul road. Airborne LiDAR Data were collected using an Optech ALTM 3100 system. This survey provided high point densities greater than 12 pts/m^2, reducing to approximately 1 pt/m^2 in ground returns. Over 30 km of forest roads and trails in the study area were mapped resulting in 95% of manually digitized road lengths located within 1.5 m normal to the conventionally field surveyed centerline. Results showed exceptional accuracy from measurements of road position, length and gradient (White, Dietterick, Mastin, & Strohman, 2010). It can also be used to model new areas for roads, skid trail networks and log landings from extracted topographical data, as a supplement to field investigation. LiDAR was utilized in one study for mapping of the Tahoma State Forest south of Mt. Rainer as part of a forest operations harvest and transportation plan. Subsequently field verified, this study revealed the many benefits of reducing field time by utilizing LiDAR derived topography for identifying possible road and landing areas, planning for harvest system designs, and improving cost estimates over harvest activities.

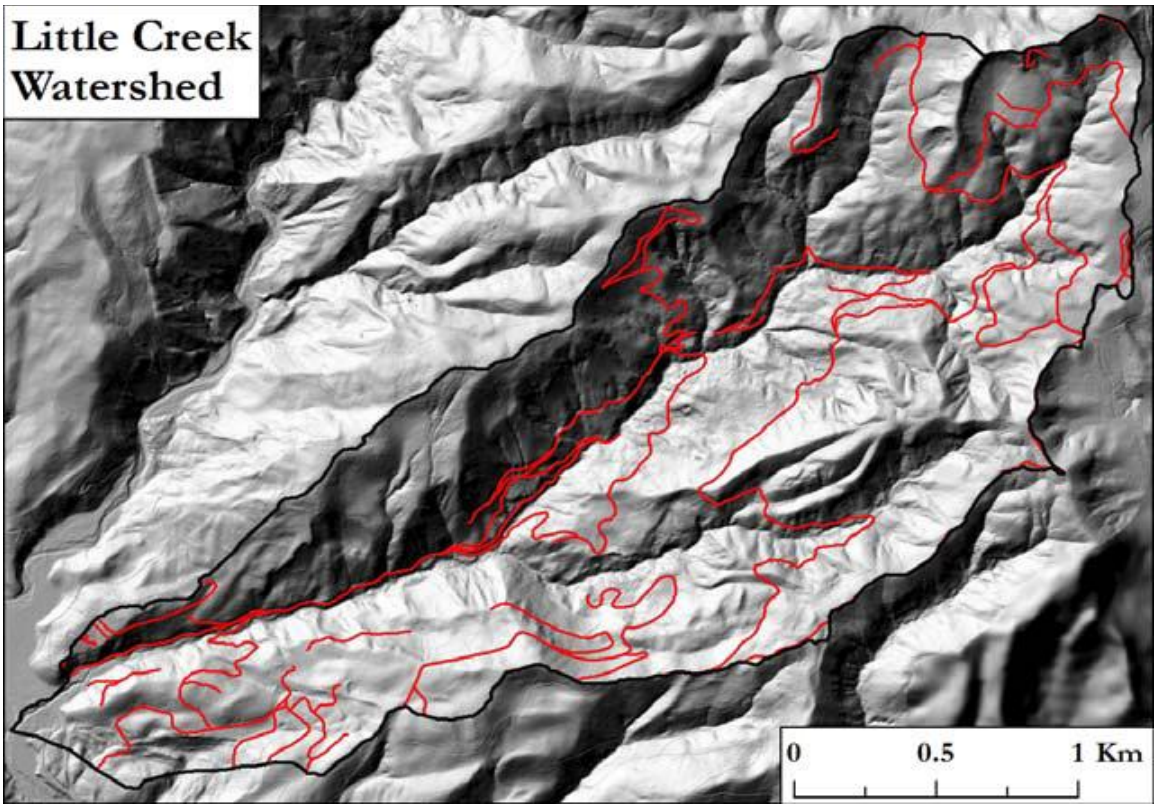

Figure 12. LiDAR–derived roads in the Little Creek watershed (From White et al., 2010)

Although LiDAR–derived models can greatly benefit pre–planning harvest and road design activities, ground inspection is still necessary in all forest management operations (Krogstad & Schiess, 2004). A model for estimating skidding costs of individual cut trees based on data retrieved from LiDAR to obtain terrain and tree information has been recently developed which can be used to generate optimal skid trail networks with adequate results (Contreras & Chung, 2011).

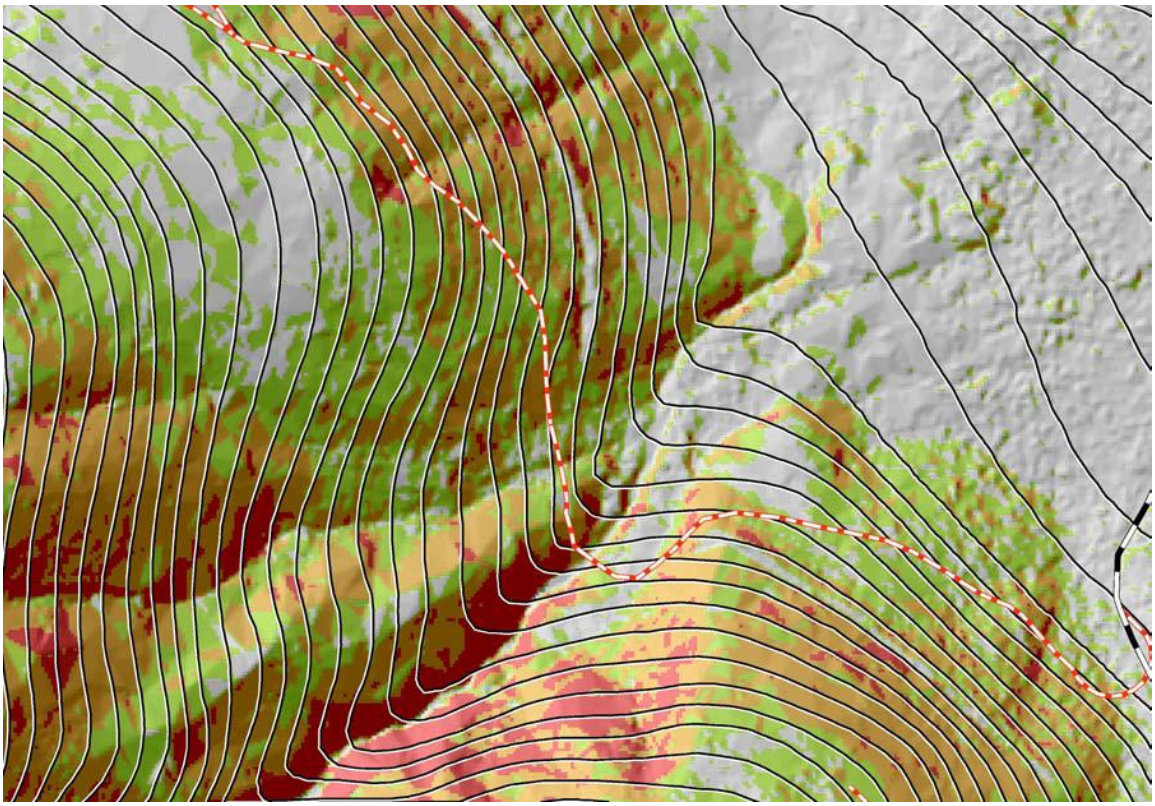

Figure 13. Contour lines overlayed on LiDAR-derived DEM with slope class coloring revealing the greater detail available than from working with Topographic map alone (After Krogstad & Schiess, 2004)

2. Selected Archaeology Applications

Mapping features underneath forest canopy makes LiDAR another effective tool in archaeology operations. LiDAR is sensitive to even small variations in height and, with vegetation removal tools, can reveal ancient earthworks in superior detail (Devereux, Amable, Crow, & Cliff, 2005).

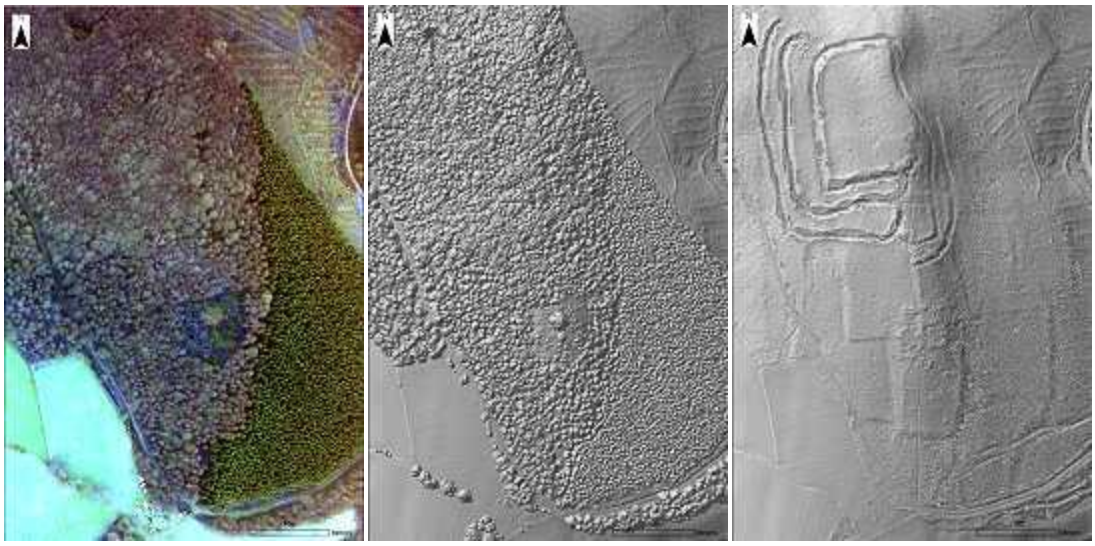

Figure 14. Prehistoric, fortified enclosure known as Welshbury Hill in the Forest of Dean, Gloucestershire, UK. Left image from digital imagery, center image is a LiDAR DTM, and right image is an extracted DEM (After Devereux et al., 2005)

Airborne LiDAR has been used to effectively penetrate jungle canopy in mapping of Mayan ruins in Central America, revealing higher spatial data results than previous ground surveys. Success was achieved by flying tight flight lines, including perpendicular passes, to ensure the probability of penetrating the thick canopy would be maximized. In addition, flights were conducted at low altitudes of 800 m AGL and low speeds around 150 knots utilizing Optech Inc.'s Gemini Airborne Laser Terrain Mapper (ALTM) to collect approximately 4.3 billion points resulting in 20 returns/m^2. The survey resulted in many new features of previously undiscovered Mayan sites, which would probably have remained hidden without the benefits of LiDAR (Diaz, 2011).

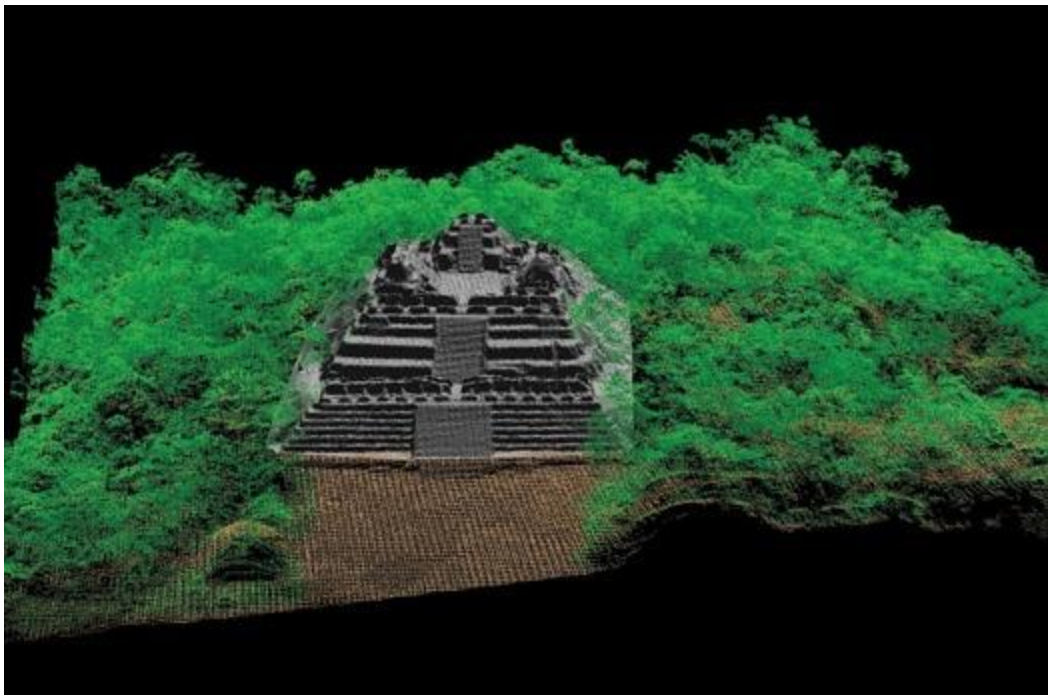

Figure 15. Rendering from airbone LiDAR point cloud surrounding Mayan pyramid (From Diaz, 2011)

Efforts have even been taken by Palaeontologists to model Dinosaur trackways utilizing the powerful detail of LiDAR–derived products to reveal intricacies of disturbed earth not otherwise obvious. One study reveals fossil tracks in high accuracy utilizing LiDAR at a location in the south-east Pyrenees Mountains on the Iberian peninsula. This capability can help Palaeontologists understand Dinosaur movement and kinematics. Using a RIEGL LMS-Z420i 3D terrestrial LiDAR scanner, providing up to 12000 points per second at a range of 800 m, very high resolution scans were obtained of individual fossil tracks, allowing the data to be visually analyzed in the digital environment, utilizing multivariate statistical methods. By comparing and integrating LiDAR collections with previous methods, it is expected that clearer interpretations of track morphology and formation can be derived than ever before (Bates, Manning, Vila, & Hodgetts, 2008).

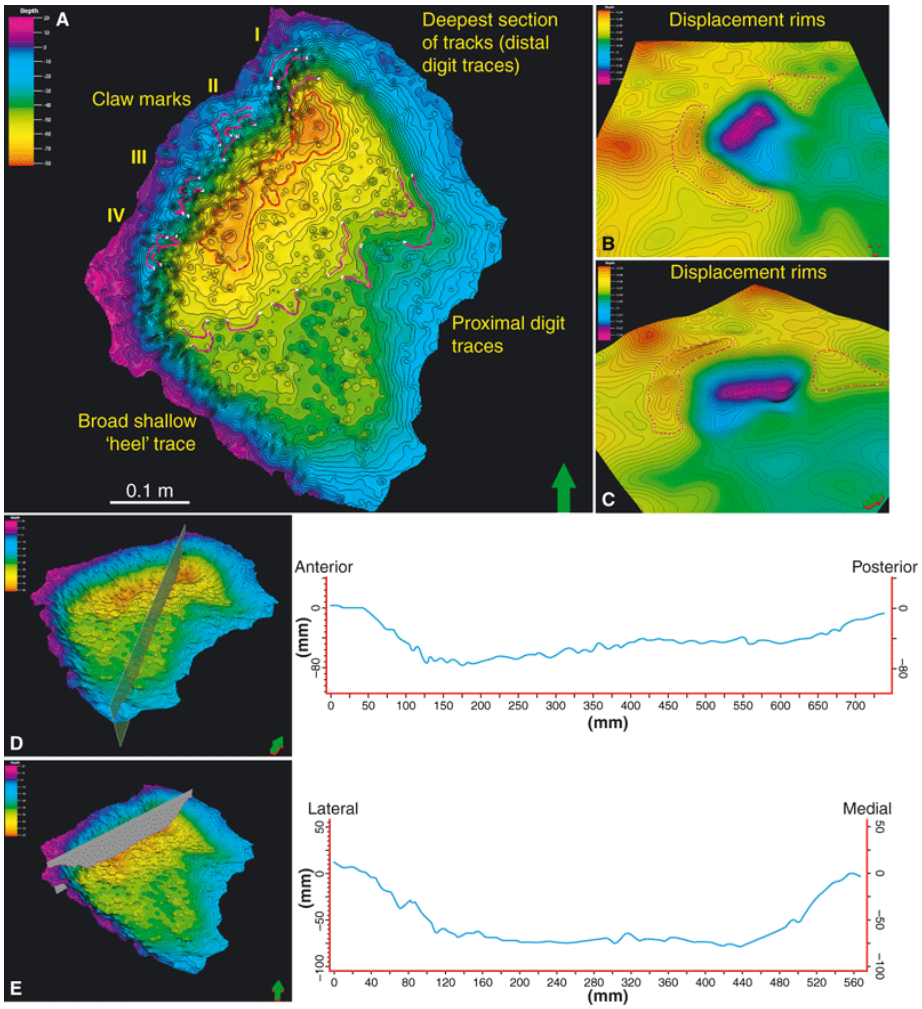

Figure 16. 3D LiDAR model of a Dinosaur track, showing the multitude of information which can be derived for this research with this tool from claw marks to digit traces and displacement parameters (From Bates et al., 2008).

3. Selected Government Research and Military Applications

The utility of LiDAR for government research or in military application is broad in scope, but most relevant, is the capability it provides for geographic situational awareness and intelligence collection.

a. Terrain Mapping and Vegetation Survey

Collections can be achieved relatively quickly via multiple air and/or ground-based platforms, providing focused or wide area collects for terrain mapping at high resolution. The National Geospatial-Intelligence Agency (NGA) provides imagery,

geospatial and targeting analysis, along with image sciences and modeling for U.S. national defense, disaster relief and safety of navigation. (NGA) In Afghanistan, NGA has deployed Flash LiDAR in aircraft to map the entire country, providing unrivaled terrain mapping in that part of the world for use by the warfighter in battlefield visualization, line-of-sight analysis and urban warfare planning (Walsh, 2011).

The NASA–Goddard Space Flight Center's Laser Remote Sensing Laboratory has designed, developed and operates the Laser Vegetation Imaging Sensor (LVIS). This LiDAR sensor is a scanning laser altimeter instrument, originally designed as a spaceborne platform, can be flown at high altitudes for very large collections over extensive areas for topography and vegetation survey. This sensor can cover 2 km swaths of surface from an altitude of 10 km.

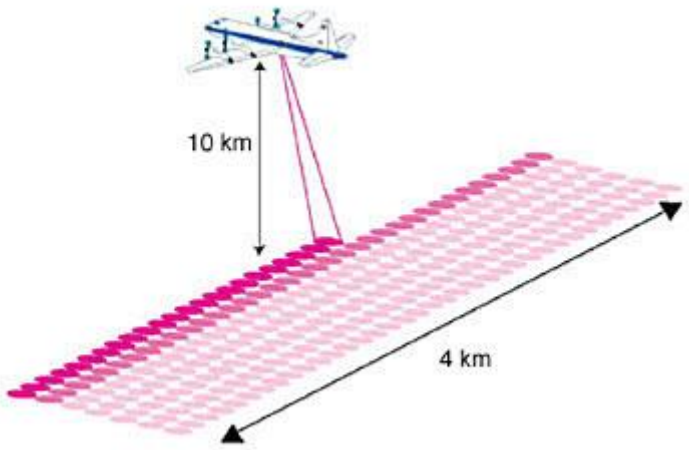

Figure 17. Example of swath implemented by LVIS (FromNational Aeronautics and Space Administration [NASA], 2011b)

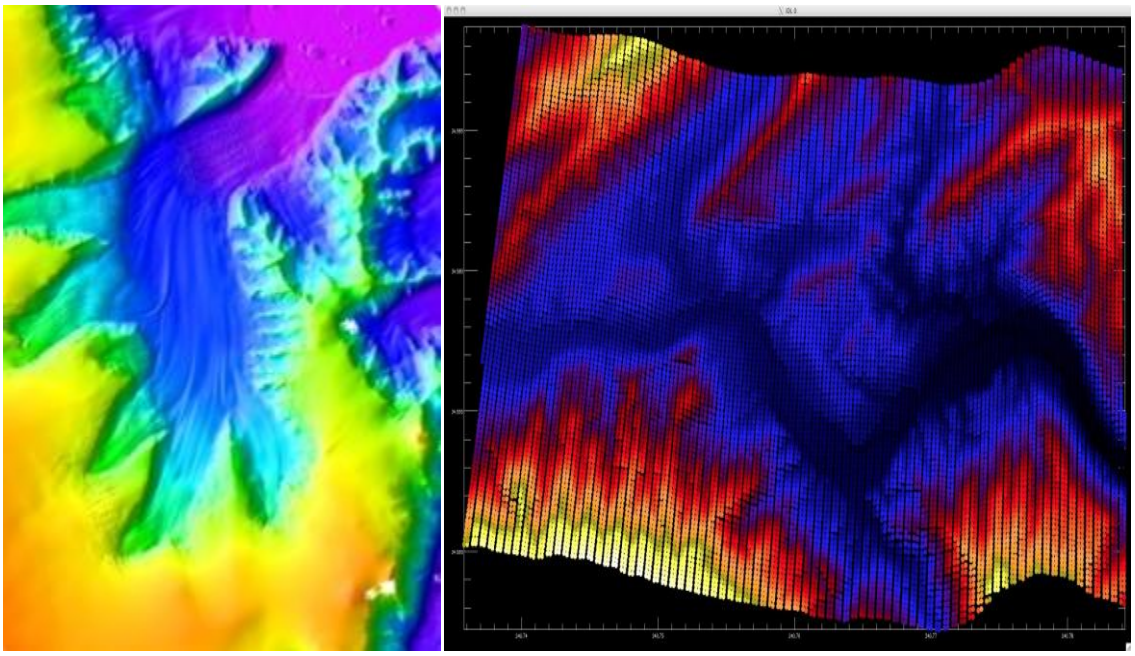

Figure 18. Crane Glacier, Antarctica LVIS map in left image, LVIS scan and beam pattern shown on the right highlighting the complete coverage picture (After NASA, 2011)

This research platform has been utilized to conduct major mapping projects of vegetation height and topography over the United States, Costa Rica, Canada, Antarctica and Greenland.

b. Bathymetry and Coastal Mapping

Although most relevant for oceanic coastline management, LiDAR survey of the land/sea interface in coastal mapping is of primary concern to the military in littoral transport, combat planning and mine detection by Navy and Marine forces. LiDAR reflections occur at the surface and sea floor, returning very accurate water depth results (Olsen, 2007). Coastline is a dynamic environment well suited to successive LiDAR collections of topographic and bathymetric data, concurrent with traditional hyperspectral imagery, which can be utilized to pinpoint changes over time. This has been well demonstrated with the Joint Airborne LiDAR Bathymetry Technical Center of Expertise (JALBTCX) mission, utilizing their in-house Compact Hydrographic Airborne Rapid Total Survey (CHARTS) system to monitor posthurricane storm impacts (Macon, Wozencraft, Joong Yong Park, & Tuell, 2008).

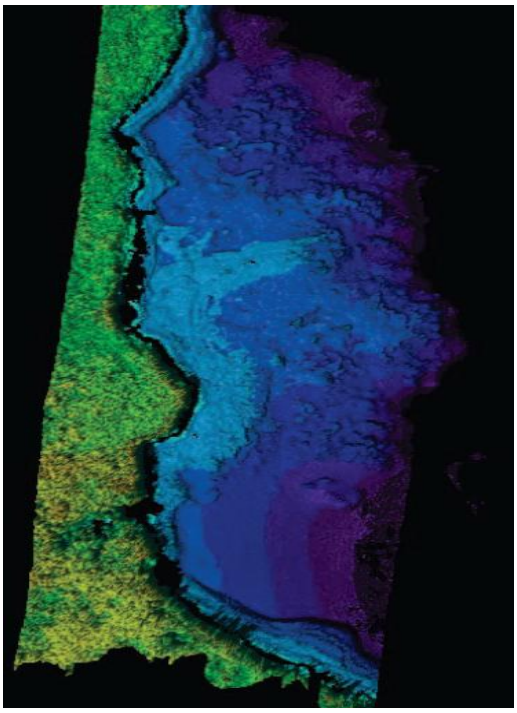

Figure 19. Bathymetric LiDAR Coverage, Hilo Bay, HI (From Macon et al., 2008).

c. Tactical River Crossings

The Army Corps of Engineers Cold Regions Research and Engineering Laboratory has compared conventional terrain analysis against LiDAR derived DEMs for determining suitable tactical river crossings. These DEMs were compared at crossing locations against measured data where conventional transit and tape surveys were performed. At each crossing site, riverbank profiles were constructed to visualize these comparisons between the DEM derived elevations and conventionally surveyed elevations. In most cases, they found that the LiDAR DEM matched the surveyed surface within 6 inches and 1 foot. Because of the increased resolution in bank slope profiles, along with accurate visual depictions of vegetation and road and trail recognition extracted from LiDAR data, this study noted an increase in over 70% in acceptable tactical river site selection rates over conventional methods (Coutermarsh, 2003).

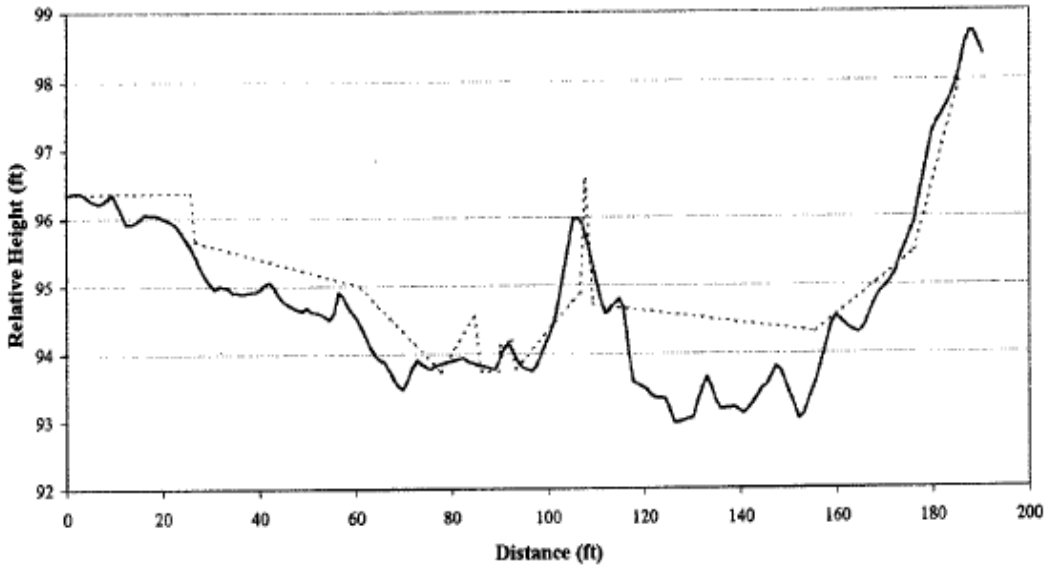

Figure 20. Example comparing river crossing profile of ground survey (dashed line) with LiDAR data results (solid line) (From Coutermarsh, 2003)

4. Selected Space–Based Applications

The history of LiDAR and other laser ranging altimetry in space missions can be traced back to the early days of NASA Goddard and their ionospheric research satellite BE–B (Explorer–22) launched in 1964 which carried a passive laser tracking reflector for orbit determination. Since that time, several LiDAR instruments have been successfully launched in lunar, planetary and asteroid mapping missions: Clementine (Moon), 1994; Mars Polar Lander, 1999; Hayabusa (Asteroid), 2003; and Phoenix (Mars) 2007 (National Aeronautics and Space Administration (NASA), 21 April 2011). Many more laser altimetry instruments have been utilized in space-based applications for accurate tracking and ranging, and most recently, precision activities from spacecraft docking with the International Space Station (ISS) to landing operations of crewed and robotic landing vehicles (Amzajerdian, Pierrottet, Petway, Hines, & Roback, 2011).

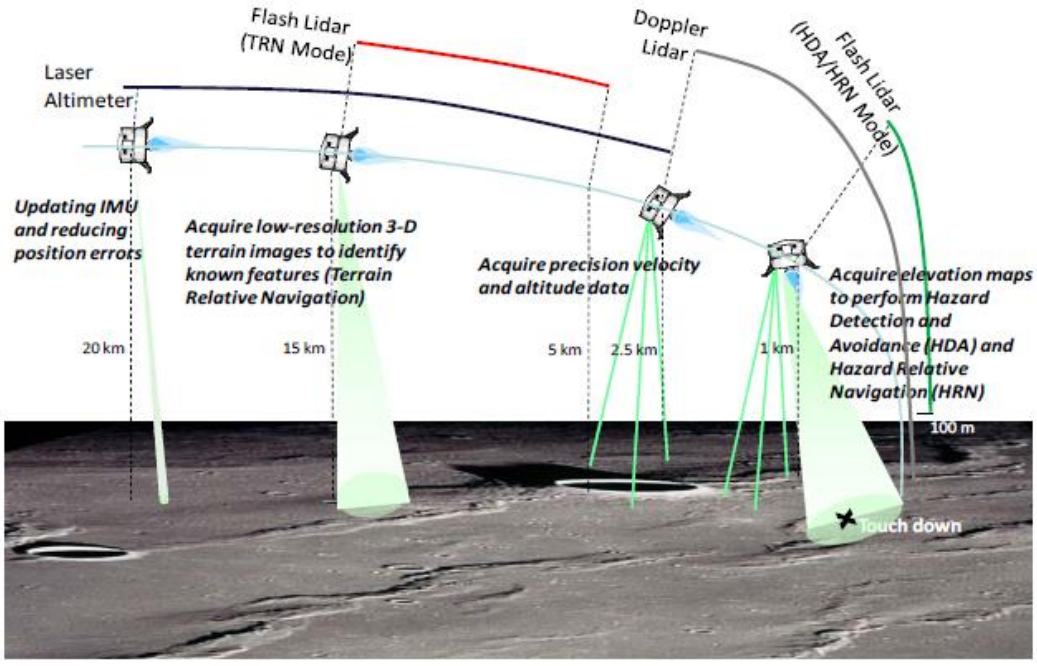

Figure 21. Example of how Laser landing sensors could be utilized in spacecraft landing scenarios (From Amzajerdian et al., 2011)

Listed below are selected missions utilizing LiDAR in space-to-earth based applications.

a. LiDAR In-Space Technology Experiment (LITE) and Shuttle Laser Altimeter (SLA)

This was NASA's first experimental mission with a space laser profiler aboard the Space Shuttle flight STS-64 in 1994. The primary purpose of this mission was looking at atmospheric, weather and climatic research rather than Earth's topography and utilized a very large power hungry Nd:YAG laser. The follow-up shuttle missions in 1996 and 1997 did look at surface relief and vegetation canopies using the lighter and smaller 1064 nm Q-switched diode-pumped Nd:YAG Shuttle Laser Altimeter providing important information on improving LiDAR systems capabilities from space platforms (Shan & Toth, 2009).

b. Geoscience Laser Altimeter System (GLAS)

Launched in 2003 and deorbited in 2010, the GLAS was developed as the primary instrument for NASA's Ice, Cloud, and Land Elevation Satellite (ICESat). This satellite's primary mission was to monitor the Earth's ice sheets for changes in elevations over time, determining their mass balance and to recognize their contribution to sea level changes. A secondary mission concentrated on finding detailed information on the global distribution of clouds and aerosols (Shan & Toth, 2009). The three passively switched Nd:YAG laser range finders made a total of 1.98 billion laser shot measurements of the Earth and its atmosphere over its seven year operating lifetime. Beyond its primary missions, the GLAS was used to measure vegetated surface areas as well (Shan & Toth, 2009).

c. ICESat–2 and Slope Imaging Multi-polarization Photon Counting LiDAR (SIMPL)

NASA's ICESat–2 mission, scheduled for launch in 2016, will employ a green 532 nm, micropulse, photon counting laser altimeter. SIMPL is an 11 KHz, 1064 nm near infrared, plane polarized micropulse laser, frequency doubled to 532 nm and split into four push-broom beams. This advanced technology uses single photon counting modules in order to achieve simultaneous surface sampling, capable of providing high vertical and spatial resolution measurements of forest canopy structure and excellent for determining above ground biomass estimates. This micropulse, photon counting laser will use a 9-beam configuration, much smaller pulse width (several nsec), high pulse repetition rate (10 to 15 kHz) and much lower pulse energy to conduct time-tagged single photon detection ranging at 532nm (D. Harding et al., 2010).

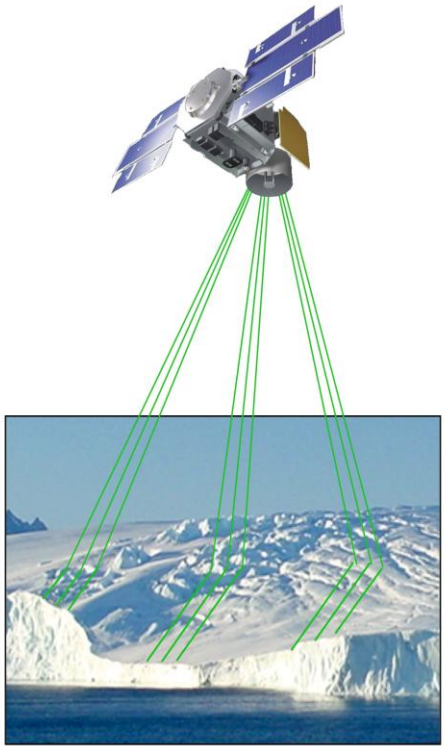

Figure 22. Current Concept for ICESat–2's 9 beam configuration (not to scale) (From Harding et al., 2010)

Because micropulse width is so much narrower and the timing precision is so much better, vertical resolution measurements will substantially improve over conventional waveform collections such as those carried on the original ICESat mission. ICESat 2 measures six profiles in pushbroom configurations with the output of a single laser split into six beams. The planned design has three tracks separated by 3 km for spatial coverage, each track separated by two profiles spaced cross-track. Each of these profiles will be sampled by 10-m diameter laser footprints and 0.7-m spacing between footprints, providing much better spatial resolution as well. Analysis of nine forest stands with different age, structure and tree composition were sampled using the SIMPL system confirmed that this new approach provides structure measurements with high vertical and spatial resolution (Harding, Dabney, & and Valett, 2011).

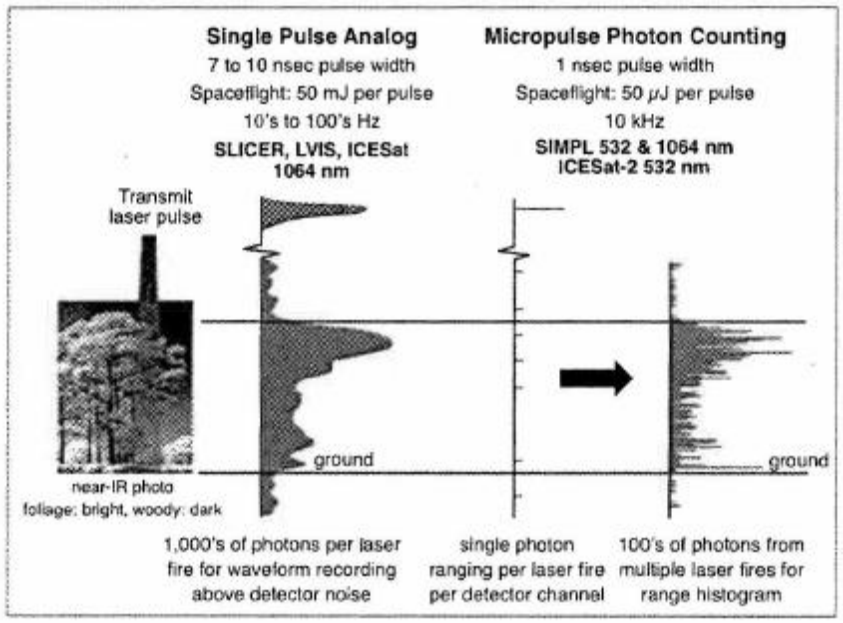

Figure 23. Comparison between conventional single pulse full waveform systems and micropulse photon counting systems measurement approaches of forest canopy structure (From Harding et al., 2011)

D. AUTOMATIC EXTRACTION OF FEATURES USING LIDAR

The desire to develop computer based techniques which can perceive a 3D interpretation of images that is comparable to the power of human vision is not new. Known as "computer vision," researchers have been working on this puzzle since the early 1970s. This effort is comparable to that of perceptual psychologists who continue to explore how our visual system truly works to interpret reality from an optical illusion (Szeliski, 2010).

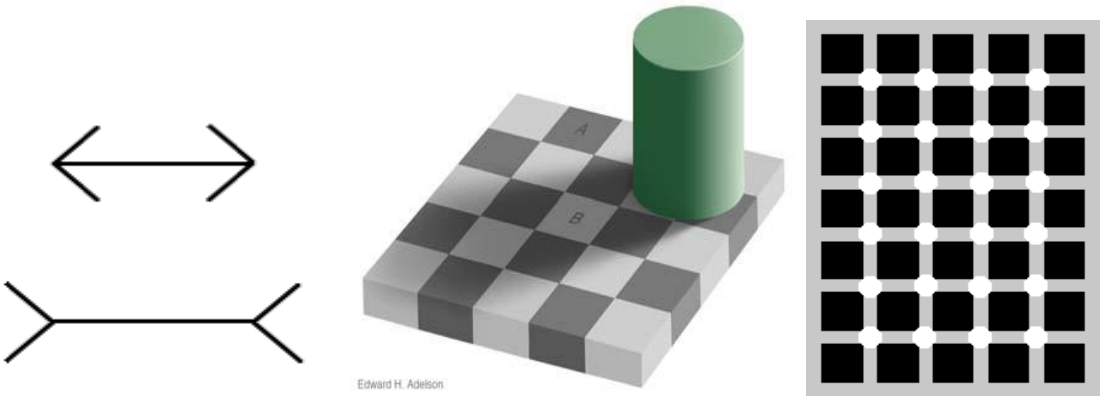

Figure 24. Examples of optical illusions. Left image: Lengths of the two horizontal lines appear different, but are the same. Center image: "White" square B in shadow and "black" square A both have the same absolute intensity value. Right image: As you move your eyes over figure, gray spots appear in the intersections (After Szeliski, 2010).

Computer vision algorithms attempt to model the world from a limited number of inputs and then extract this result to the whole in order to describe that world in a cognitive sense. This is an extremely challenging field that is continually advancing and which has many significant applications. Because LiDAR is also relatively new, attempts at automating data results for specific outputs has not been intensely studied as much as efforts aimed at describing imagery alone.

A very interesting effort applicable to this study is one of many being applied by members the University of Southern California Computer Graphics and Immersive Technologies Laboratory concerning computer based automation of LiDAR data. An integrated approach merges optimized segmentation techniques and perceptual grouping theory as part of a vision–based system for automatic detection of road networks from several sensor resources, including LiDAR (Poullis, 2008). In this study, it is recognized that pixel and region based efforts alone often fail when attempting to automatically extract road networks because of the wide variation of what defines a "road," including all of the occlusions that must be interpreted from imagery including cars, trees and shadows. The approach of these researchers addresses these problems and is summarized in Figure below. They first use Gabor Filtering followed by Tensor Voting to classify features. In correspondence with author Charalambos Poullis, PhD:

The reason for choosing tensor voting in the road extraction work was to overcome to problem of missing information caused by occlusion. Due to the global nature of tensor voting it can successfully recover missing information (up to a scale) based on neighborhood information, but at the expense of being a very slow process.

Road features are then segmented and labeled according to orientation, then extracted, modeled and linearized into a final road network. This study appears to have proven accurate and effective at identifying road networks in several urban environments, including LiDAR derived image in Baltimore, MD, demonstrated in the study.

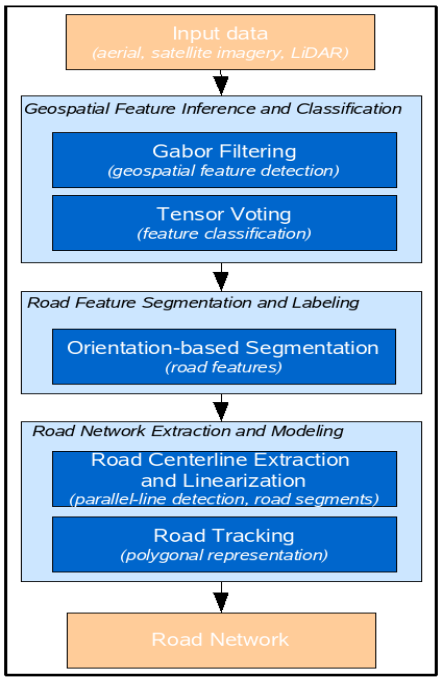

Figure 25. Vision–based system overview for automatic detection and extraction of road networks (From Poullis, 2008).

Another study conducted by the University of Florida Department of Electrical and Computer Engineering and Department of Civil and Coastal Engineering specifically targeted the problem of detecting forest trails under dense forest canopy from LiDAR utilizing an entirely separate methodology with unique results (Heezin Lee, Slatton, & Hojin Jhee, 2005). The study was conducted in dense mixed coniferous and deciduous forest in North Central Florida. In this study, foliage voids were identified in the point cloud data as potential trails based on the characteristics that the presence of a trail

implies an empty volume immediately above the trail surface. The study was imaged with an Optech 1233 system at 33 kHz from 600m AGL in two flight lines. Average point spacing was conducted at 2–2.5 returns/m^2. Penetrating shots through small gaps deep into the foliage resulted in an average of 0.25 returns/m^2. Expanding this idea into the implied linear nature of trail segments which require a vector of visibility between trail points, an identification algorithm was developed that connects candidate trail segments while discarding voids that are inherent where tree trunks reside.

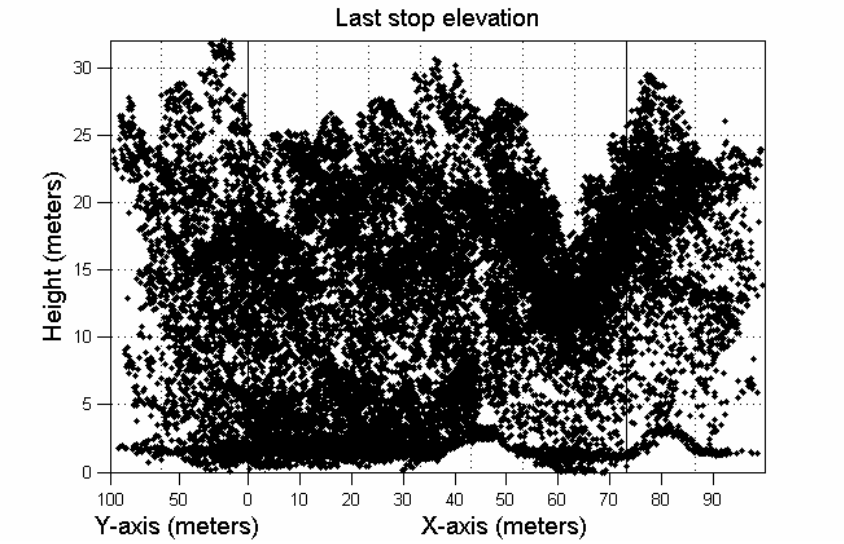

Figure 26. Point cloud cross section from study area where small empty space above trail surface is visible (between 40 m and 50 m on X–axis) (After Heezin Lee et al., 2005).

Applying geometric constraints of visibility vectors to remove vectors which are not trail, in tandem with visibility blockers and segmented ground points, walking trails under heavily vegetated areas were detected with winning trail candidates emerging. The longest trail segment remaining is selected as the final result. This approach shows great promise with future study to be conducted.

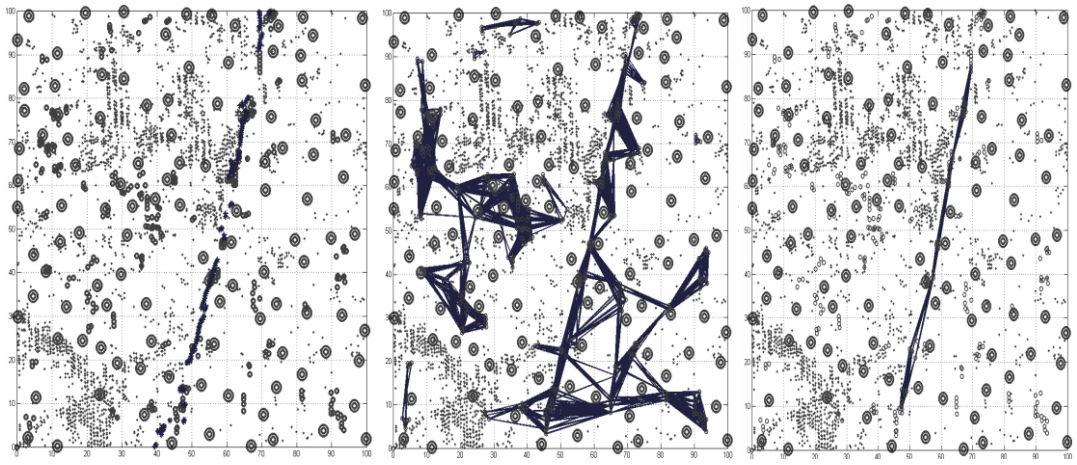

Figure 27. Left figure shows GPS points of actual trail, middle figure has visibility vectors computed of potential trails, and right figure is the winning candidate trail (From Heezin Lee et al., 2005).

THIS PAGE INTENTIONALLY LEFT BLANK

III. PROJECT DESCRIPTION

A. AUTOMATING TRAIL DETECTION BENEATH FOREST CANOPY

It has been demonstrated that visual inspection of DEMs extracted from LiDAR data can allow for reliable identification of roads and trails hidden under forest canopy in terrain analysis (Espinoza & Owens, 2007). This is important in several possible scenarios for military application, from locating logistics routes used by adversaries, to paths used by drug traffickers or terrorists attempting to conduct illicit operations. There is utility in this capability for the public sector as well, evidenced by the significant increase in large-scale narcotics operations being conducted by Mexican drug cartels in California National Forests. This has become dangerous to forestry and land management professionals working in woodland areas who face booby traps and armed gunmen protecting hidden drug farms. It is also detrimental to the environment due to the potential habitat destruction and contamination that results from fire and harmful cultivation practices (McGirk, 2009; BBC News, 2011).

Unfortunately, human analysis of large data sets can lack timeliness due to inefficiencies of the labor-intensive processes required in creating products extracted from this raw data. The ability to utilize an automated procedure that would reliably recognize roads and trails extracted from raw data, and output a product in a timely manner for further utilization, would be an important improvement over current methods. In this project, several sets of data covering multiple forest types were evaluated using grid statistics and AGL analysis of points to isolate unique trail characteristics on a DEM and point cloud outputs.

To approach the problem, the first question to ask is what makes a trail unique? A trail is produced by repeated compression or scarring of the earth by a small-footprint medium, be it a human foot, a bicycle tire, or animal tracks. The size of the trail will vary in width and depth and height (thinking in 3D), dependent on the nature of the objects "making" the trail. Trail surface deformation can include changes to convexity or concavity, deviation from surrounding terrain slope characteristics, and exposure of soil,

rock or different levels of forest floor detritus. What is unique when looking at a trail from a 3D perspective, is the recognition that a well-used trail will have voids in vegetation generally from the forest floor to the height of the object traversing the trail. This will be more obvious in multistoried stands with a heavy understory. Because a trail should be the lowest point in each localized area, we can expect that last return points that reflect from a trail surface will be recorded as ground points, and any points immediately surrounding these points at a higher AGL will most likely be vegetation. Another consideration of trails is the intensity at which light reflects off of different surfaces. Depending on the nature of exposed soils, reflectivity can be expected to differ between a well-traversed area and the surrounding vegetated landscape.

Roads are similar to trails; the primary difference is that they are generally designed for specific wheeled or tracked vehicles, require some level of earth cut and fill to provide smooth slope deviations amenable to the capabilities of the vehicles for which they are designed, and they are often surfaced by rock or pavement if intended for regular use. Forest roads are often designed to allow adequate water drainage to pass over, adjacent, or under surfaces, according to multiple road design techniques. These include water-barring, culvert emplacement, and slope manipulation. Depending on the road surface, evidence of vehicle travel may also reveal predictable tire depression within the road confines. Road networks can also be very predictable in forest environments, depending on steepness of terrain. Main roads often parallel main watercourses, work from the highest elevations to the lowest elevations, following the shortest feasible distance between two points along course slopes which are less than 10%. This means that roads traversing up steep, hilly terrain, can be expected to have multiple switchbacks, and perpendicular watercourse crossings. Clearly, reflectivity off of paved road surfaces should result in very different returns from local surrounding materials, whether vegetation or soil. “Skid” trails are called such because they are utilized in forestry operations for “skidding” logs by tracked or wheeled vehicles from point of where trees have been cut to landings on main roads where they are subsequently loaded on trucks for haul. These “trails” display most of the same characteristics of roads in width, earth cut, and network grid between nearest main roads, but often occur traversing much steeper

slopes. What is different is that once logging operations have concluded, these trails are quickly overgrown again with first brush and other native vegetation, followed by trees. Skid trails can be expected to show up very well on DEMs because of these obvious changes to slope and movement of earth in predictable patterns across a managed forest floor, but may not be obvious from above ground point cloud representations.

Knowing some of these considerations about road and trail characteristics, image processing techniques can be chosen which capitalize on exploiting them. Techniques were applied to point cloud data to visualize those points that occur in the trail "zone" up to 1.8 m and converted to images. Additional images were extracted using topographic tools covering slope, convexity and curvature parameters. On these images, regions of interest were identified which could be used to recognize linear features on a local level, as to whether they were road, trail or other. Using all available image bands, pixels were separated out into classes that represent each surface feature and the results were subsequently applied using a maximum likelihood probability technique across an entire sample area.

B. DATA AND SITE DESCRIPTION

1. Indian Creek Watershed

Data from the Indian Creek Watershed in Trinity County, California, were collected by Airborne 1 Corporation for Sierra Pacific Industries Indian Creek LiDAR mapping project on July 7, 2001. This data were at the lowest point density of the three collections at around 3 points/m^2. The collection area consists of low-elevation conifer forest, consisting primarily of Douglas fir, Digger Pine and Live Oak. The most significant conifer concentrations are on north-facing slopes. There are also large areas of brush on south facing slopes that are probably the result of a previous forest fire. Bisecting the collection area from East to West is Indian Creek itself, paralleled by Indian Creek Road. The collection area contains other named roads including Mule Gulch Road and Joseph Gulch Road, as well as several small structures and one small pond.

Sensor	Optech 25kHz
Collection Date	1. July 7, 2001
Collection Rate	2. 25,000 pulses/second
Altitude	3. 1600 m AGL
Overlap	4. 50%
Scan Angle	5. ± 12° from nadir
Point Spacing	6. 1.5 m posting
Platform	7. Fixed wing twin prop (Parte Navia)

Table 1. Indian Creek Watershed Collection, Optech 25kHz specifications (Airborne 1)

Figure 28. Indian Creek Watershed Collection (From: Google Earth)

2. Lake Tahoe Basin

Data from the Lake Tahoe Basin on the California/Nevada border were collected by Watershed Sciences, Inc (WSI) from August 11 to August 24, 2010. Data were provided by the Tahoe Regional Planning Agency and the U.S. Geological Survey and made publicly available on the OpenTopography website, http://www.opentopography.org/index.php. OpenTopography is based at San Diego Supercomputer Center, University of California at San Diego, and is operated in tandem with the School of Earth and Space Exploration and Arizona State University. It receives funding from the National Science Foundation and NASA and receives operational support from the National Space Foundation: Earth Sciences Instrumentation and Facilities Program (EAR/IF) and the Office of Cyberinfrastructure. OpenTopography is a valuable public resource for obtaining high resolution topographic data sets in a myriad of locations throughout the U.S and beyond (currently Greenland and Haiti).

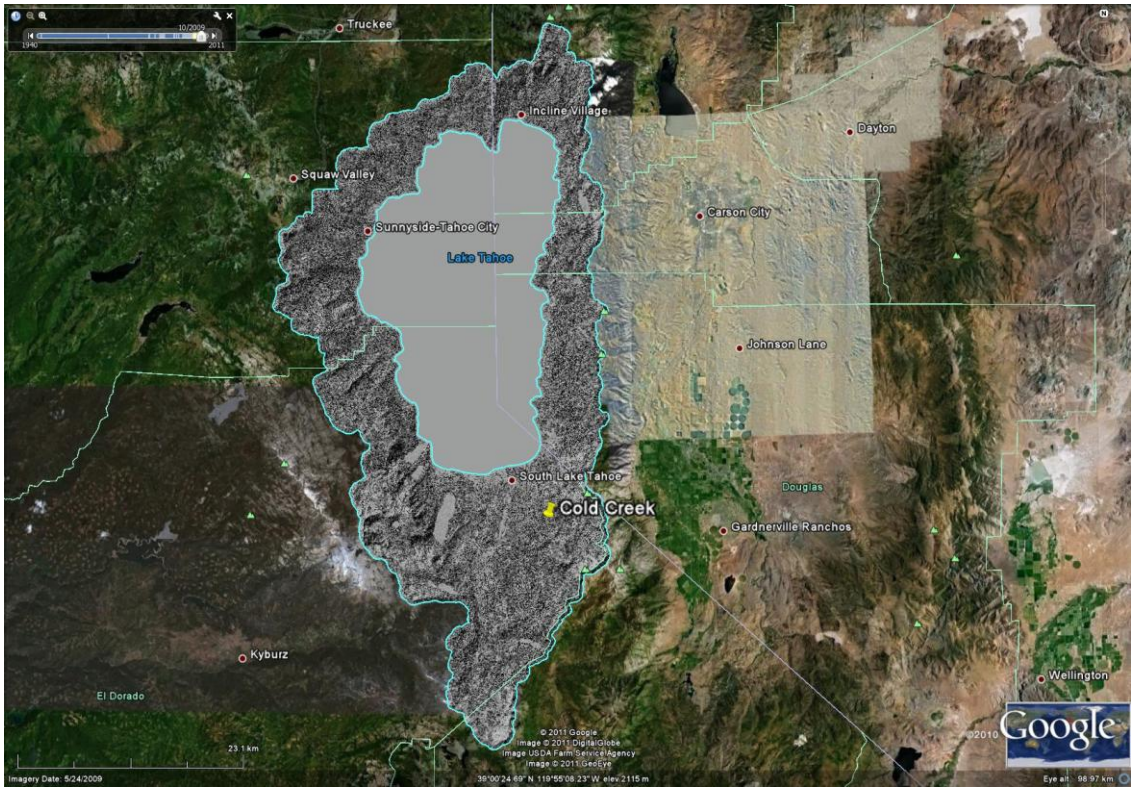

Figure 29. Lake Tahoe Basin collection, Cold Creek (From Google Earth)

The Lake Tahoe Basin dataset covers nearly 1000 sq. km. and more than 12 billion points. This LiDAR survey used two Leica ALS50 Phase II laser systems flown on a small Cessna Carvan 208B plane. Pulse rates were at 83 – 105.9 kHz and this aircraft was flown at between 900–1300 m AGL. Funded by the Bureau of Land Management, this dataset contains an average shot density of over 11 pts per m^2 and 2.26 pts per m^2 average ground point density (see Table 2 for breakdown).

This area is dominated by high elevation conifer forest, mostly more conical Ponderosa Pine, Sugar Pine, and perhaps White Fir, more widely spaced, with little understory vegetation except in exposed open brushy areas and along watercourses. There is significant downed woody debris and rocky ground. The survey area is relatively flat, except for along Cold Creek watercourse which traverses the Northern half. A large cleared power-line right of way passes through the Southern half of the survey area, and the Northeast corner contains a portion of a South Lake Tahoe neighborhood containing vacation home structures.

Sensor	(2) Leica ALS50 Phase II
Collection Date	8. Aug 11 – 24, 2010
Collection Rate	9. 83,000 – 105,900 pulses/second
Altitude	10. 900 – 1300 m AGL
Spot Distribution	11. > 8 pulses per m^2
Scan Angle	12. ± 14° from nadir
Vertical Accuracy	13. 3.5 cm RMSE
Platform	14. Cessna Caravan 208B

Table 2. Lake Tahoe Collection, Leica ALS50 specifications (OpenTopography)

3. Kahuku Training Area

Data from the Kahuku Training Area in northern Oahu, Hawaii, was collected in March 2005 and obtained from the NGA. This portion of the data set was chosen for analysis because of work done previously in this area to specifically identify roads and trails under canopy from LiDAR derived products, followed by extensive ground-truth work in the area in May 2007. Specifics of this study can be found in Espinoza and Owens (2007).

Figure 30. Kahuku training area site 6 (From Google Earth)

Data were collected from a custom Optech 3100 system mounted on a Bell 206 Jet Ranger helicopter. Site 6 was selected from this collection, which has an approximate total area of 400 x 400 m. Unique to this collection was the attempt made in the flight profile to simulate a step-stare mode during collection. Also of note was the use of a Full Wave Digitizer (FWD) to collect clearer definition of understory vegetation at high densities. See Table 3 for specific collection information.

The area was described in this previous work as being amid lowland mesic grasslands and forests with rugged mountainous terrain and varying degrees of vegetation. Site 6 contains a hilltop in the Southeast corner which has a significant sloping terrain toward the North/Northwest into a heavily vegetated canyon running the diagonal of the area, before gaining elevation again toward the Northwest corner. There is a primary road traversing around the hilltop, and a nonoccluded ridgetop dirt road that runs the length of the scene heavily travelled by "offroad" vehicles. Several trails have been mapped during ground truth work conducted by Espinoza and Owens (2007).

Sensor	Optech ALTM 3100
Collection Date	March 2005
Collection Rate	70,000 pulses/second
Wavelength	1064 nm (NIR)
Altitude	2,000 ft and 6,562 Ft
Spot Distribution	Sawtooth
Pulse Return Classification	Intelligent Waveform Digitizer
	8 bits @ 1nsec sample interval per pulse
	(max 50 kHz)
Ground Spatial Resolution	1ft (@ 2,000 ft. Altitude) 1 m (@ 6,562 ft. Altitude)
Platform	Bell 206 Jet Ranger Helicopter

Table 3. Kahuku collection, Optech 3100 specifications
(From Espinoza & Owens, 2007)

C. PROCESSING SOFTWARE

1. Quick Terrain Modeler, Version 7.1.4

Quick Terrain Modeler is designed by Applied Imagery for use as LiDAR visual exploitation software to provide 3D point cloud and terrain visualization utilities that are very powerful and user-friendly. This software was the primary analysis tool used in this study to build DEMs from point clouds, crop point clouds at user defined AGL selection,

run grid statistics on data, and export GEOTIFF images for further analysis. Also used was the ILAP Bare Earth Extraction Plug-In developed by The John Hopkins University/Applied Physics Laboratory to create DEMs, object files and cloud files which allowed for creating two point clouds at one user defined AGL cutoff between each files' set of points. It was also possible to export files for integration with Google Earth imagery.

2. Environment for Visualizing Images (ENVI) + Interactive Data Language (IDL), Version 4.8

ENVI is powerful image processing software that allows for comprehensive data visualization and analysis of images. Images exported from Quick Terrain Modeler were fed into ENVI for analysis with Topographic Tools and Spectral Tools imbedded in the program for real-time extraction from multiple bands, then classification was applied to extract global results. Use of these tools will be described in detail in the next few chapters.

THIS PAGE INTENTIONALLY LEFT BLANK

IV. OBSERVATIONS AND ANALYSIS

A. DATA PREPARATION

1. Quick Terrain Modeler

a. Data Import

Raw LiDAR data is available in many different formats. The two file types selected in this study are ASCII XYZ files with the Indian Creek and Kahuku datasets and LAS files with the Tahoe dataset. The ASCII XYZ file format consists simply of a series of data in X, Y and Z Cartesian coordinate style columns, each representing Easting, Northing and Altitude for each point. In addition, intensity values were included in the fourth column of each dataset. The generic formats are converted into software specific forms to be used with QTM. Model formats can be created as Gridded Surface (.qtt), Point Cloud (.qtc) or as Point Cloud with Attribute Table (.qta). The Gridded Surface model takes the points and creates a 2.5-D surface over the points, much like laying a tablecloth across a dataset. When applied to all points, this can be very useful for quickly identifying buildings and vegetated areas, but is not very useful for picking out "hidden" surface features. The Point Cloud is a 3D representation of the points in the dataset, and with the attribute table, allows per point attributes that can be further evaluated in statistical analysis.

(1) Indian Creek. In the case of Indian Creek, files were arranged according to first returns and last returns. All files were first imported in order to get an idea of the dimensions of the survey area and then selected files identified based on which would provide the best representation of trails and roads for this study. These files[1] were imported from both first and last returns in Point Cloud format, then merged together into one 3D Point Cloud file.[2] With all returns, point density is at 3 points per m^2 and each point 0.6 m apart on average. Data were not classified according to returns

[1] 000020.xyz, 000032.xyz

[2] Indian_Creek.qtc

into categories of ground or vegetation type, so it was not possible to import them with an attribute table (this is a characteristic of the xyz ASCII format).

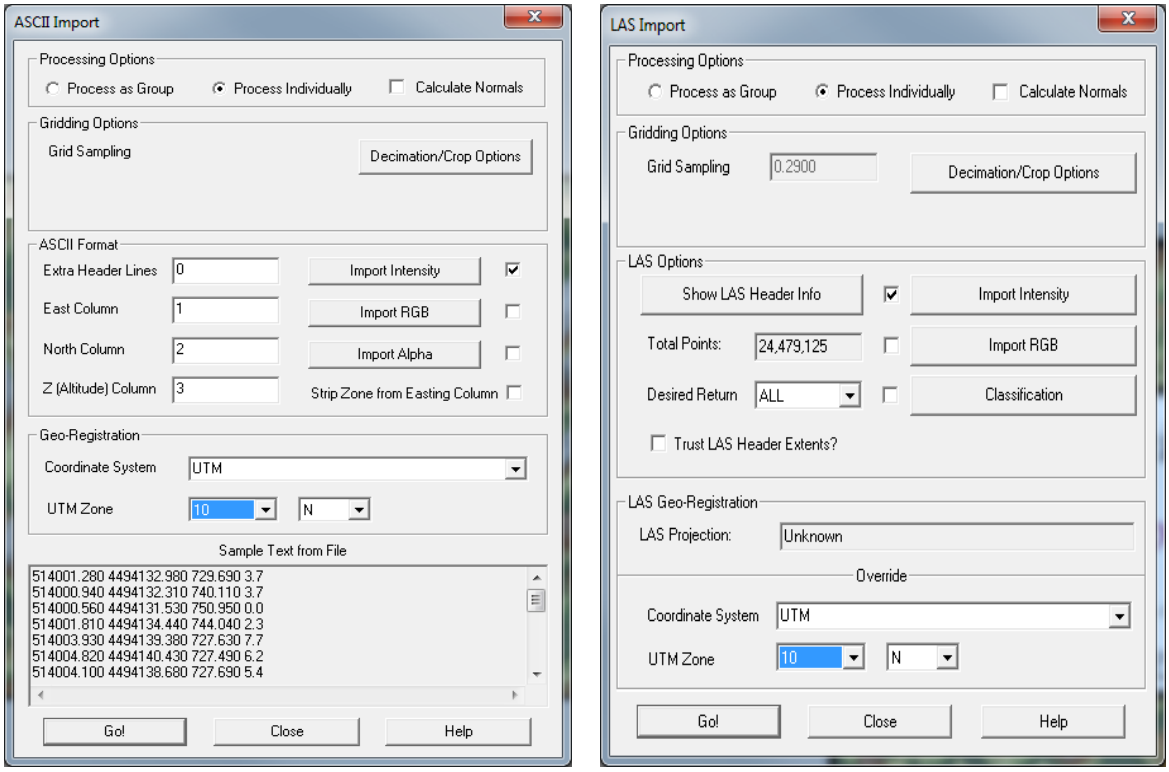

Figure 31. ASCII dataset import menu on the left and LAS dataset import menu on the right. For ASCII, data is arranged as text in file by column as East, North, Z, and Intensity. For LAS, data can be imported with intensity or according to classification.

(2) Lake Tahoe. Lake Tahoe data were downloaded in Laser Point File, LAS format.[3] This is a common file format extension for LiDAR data, and this data contains classification of points allowing for import into a 3D attribute table point cloud file[4] with all returns, as well as, importation directly into a surface model for only ground returns[5] at 0.29m default resolution. With all returns, point density is at over 16 points per m^2 and each point 0.25 m apart on average.

[3] 3179_080911.las

[4] Tahoe_ColdCreek.qtc

[5] Tahoe_ColdCreek.qtt

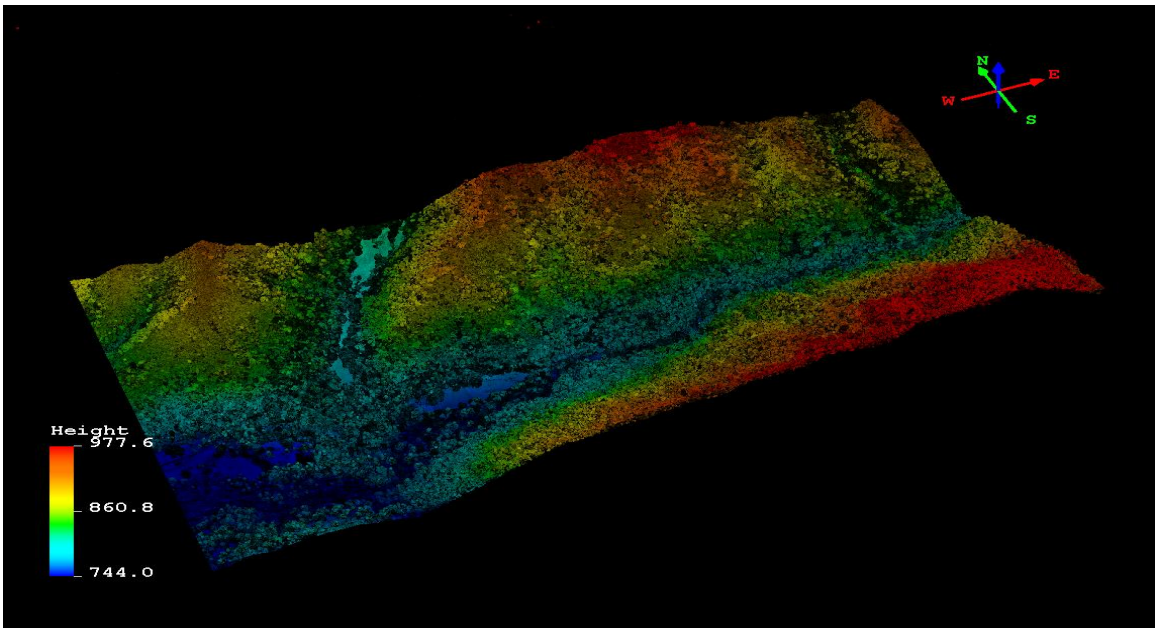

Figure 32. Indian Creek point cloud, all returns. Colors show relative elevation values in meters.

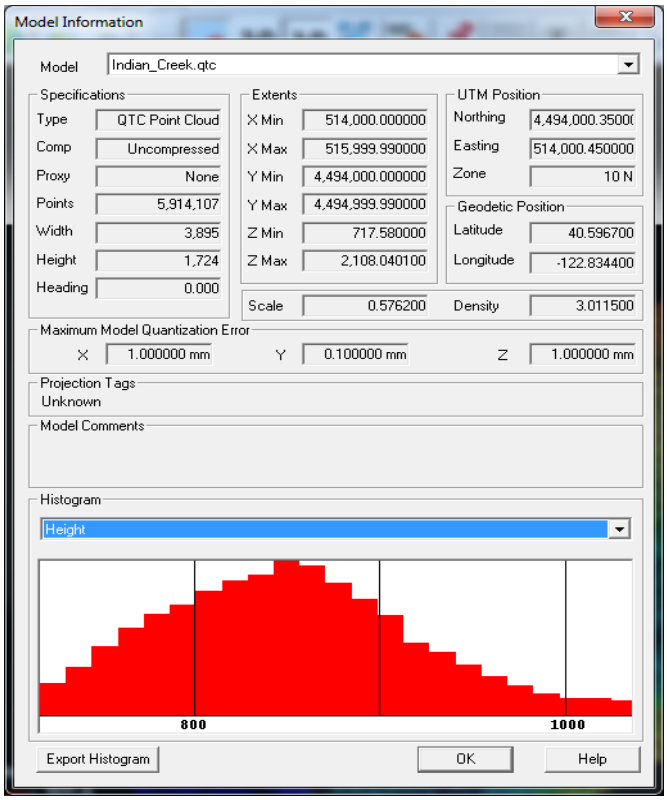

Figure 33. Indian Creek point cloud model information, all returns.

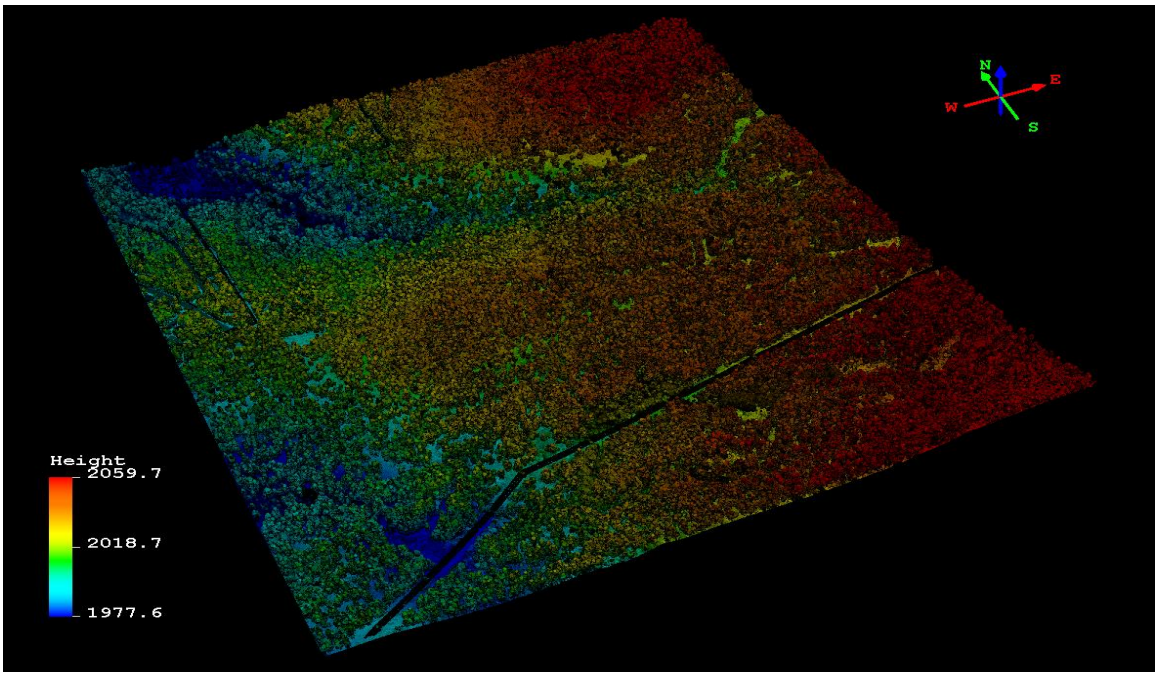

Figure 34. Lake Tahoe, Cold Creek point cloud, all returns. Colors show relative elevation values in meters.

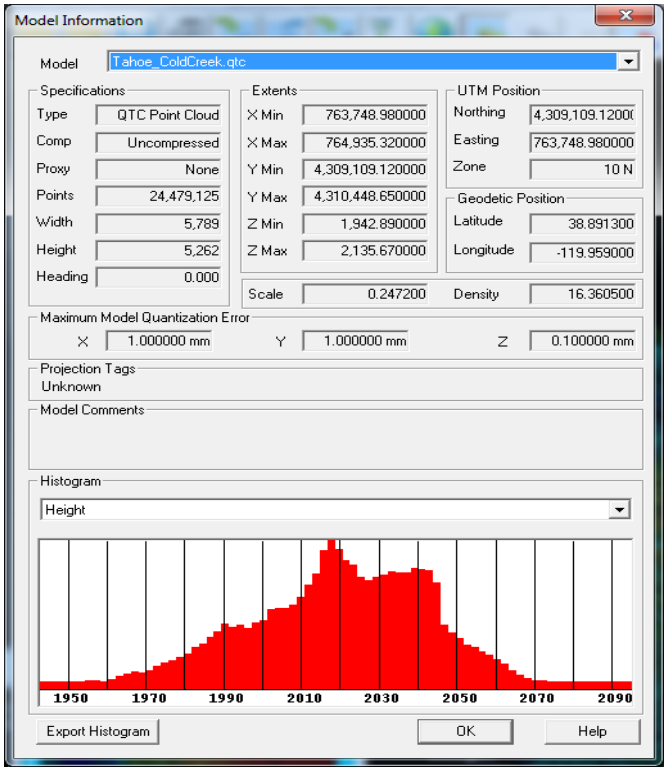

Figure 35. Lake Tahoe, Cold Creek model information, all returns.

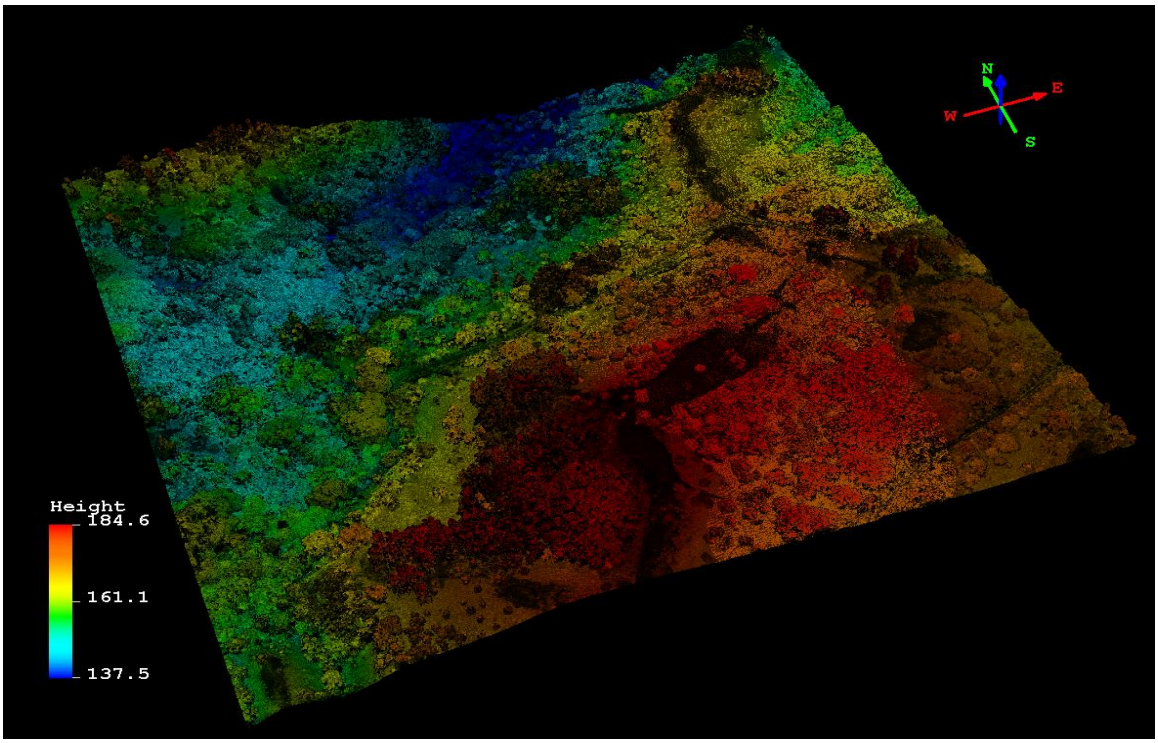

Figure 36. Kahuku point cloud, all returns. Colors show relative elevation values in meters.

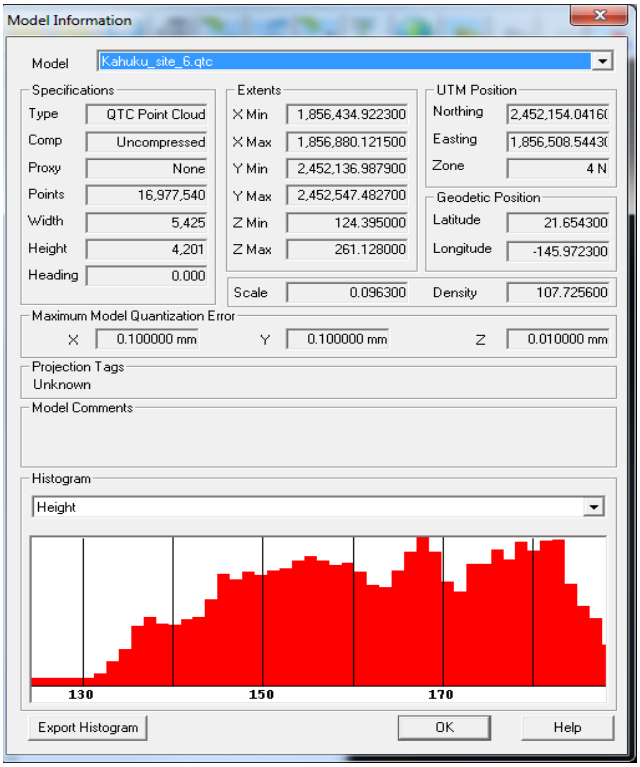

Figure 37. Kahuku model information, all returns.

(3) Kahuku. Kahuku data were already available in point cloud format in legacy files from earlier thesis work (Espinoza & Owens, 2007) and separated into point cloud, target files and surface files. Point cloud files were combined in their Site 6 area to create one file with all returns for further analysis.[6] With all returns, point density is at over 107 points per m^2 and each point 0.0963 m apart on average.

b. DEM Creation

Digital Elevation Models are created to represent the ground surface and exclude all above ground features such as vegetation or structures. From this product, it is easy to visually obtain surface features that are normally occluded by trees, such as roads, trails, watercourses and landslides.

(1) Indian Creek. In order to create a DEM from this dataset, the ILAP Bare Earth Extraction Plugin was utilized. With this application, many different parameters can be experimented with when attempting to create the best quality DEM for analysis.[7] Unique to this application, an object layer can be created consisting of points up to a user–defined AGL upper limit, and a Cloud layer consisting of all points above the user–defined limit. Although an object layer file was created up to approximately 1.8 meters AGL with the idea that this is the zone of points of interest for recognizing trails and roads,[8] this file was not looked at in the analysis. Instead, the AGL analyst option available in QTM (described below) was used in order to stay consistent in method across all three data sets. The resolution of the DEM could only be taken to about 2 meters before sacrificing quality to various artifacts known as "Crystal Forest." These are areas where thick foliage may become incorrectly marked as surface due to areas of few returns off of real ground. A surface mode sampling input equivalent to 1 meter resolution was used. Roads, skid trails, watercourses, and potential trails are clearly observable, even in this low point density dataset.

---

[6] Kahuku_site_6.qtc

[7] Indian_Creek_surface.qtt

[8] Indian_Creek_object.qtc

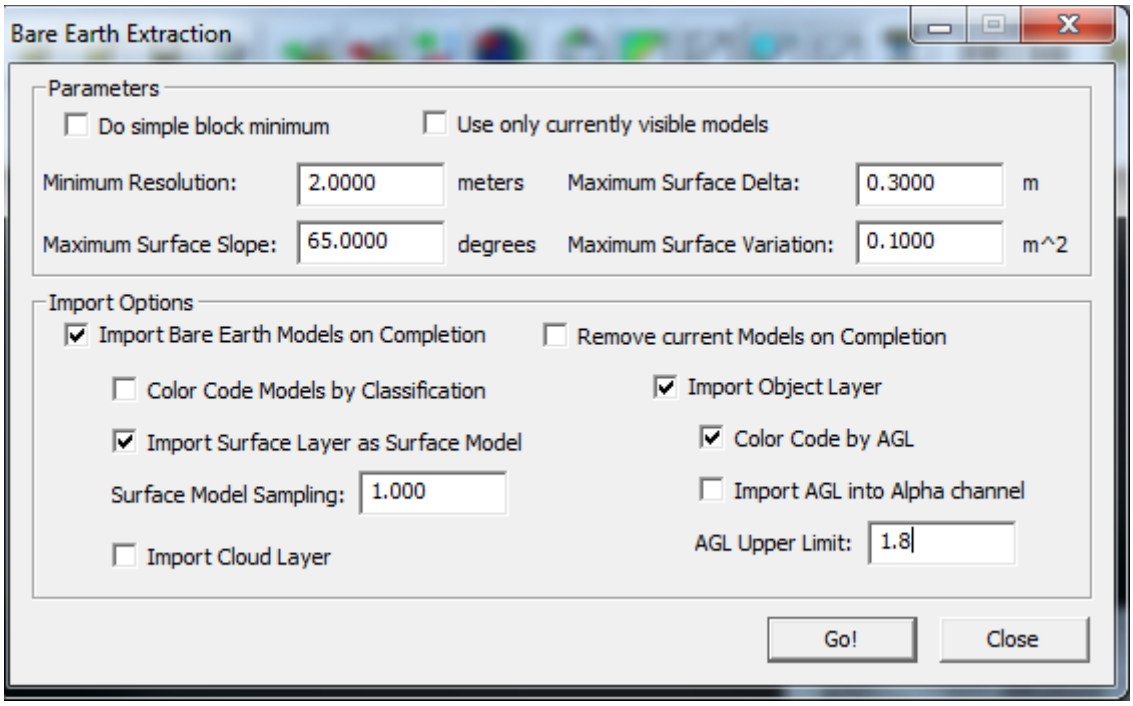

Figure 38. Bare earth extraction import menu.

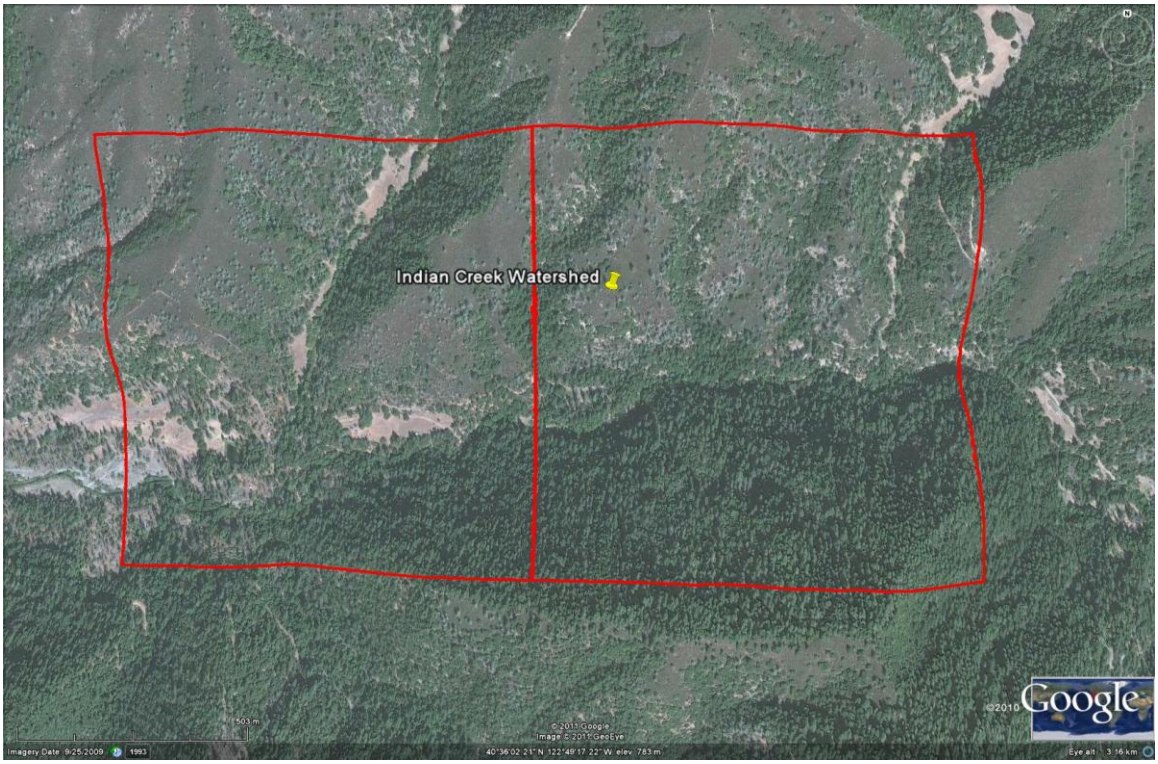

Figure 39. Google Earth Image of Indian Creek Watershed survey area, each square forms a separate ASCII file covering about 1 km^2

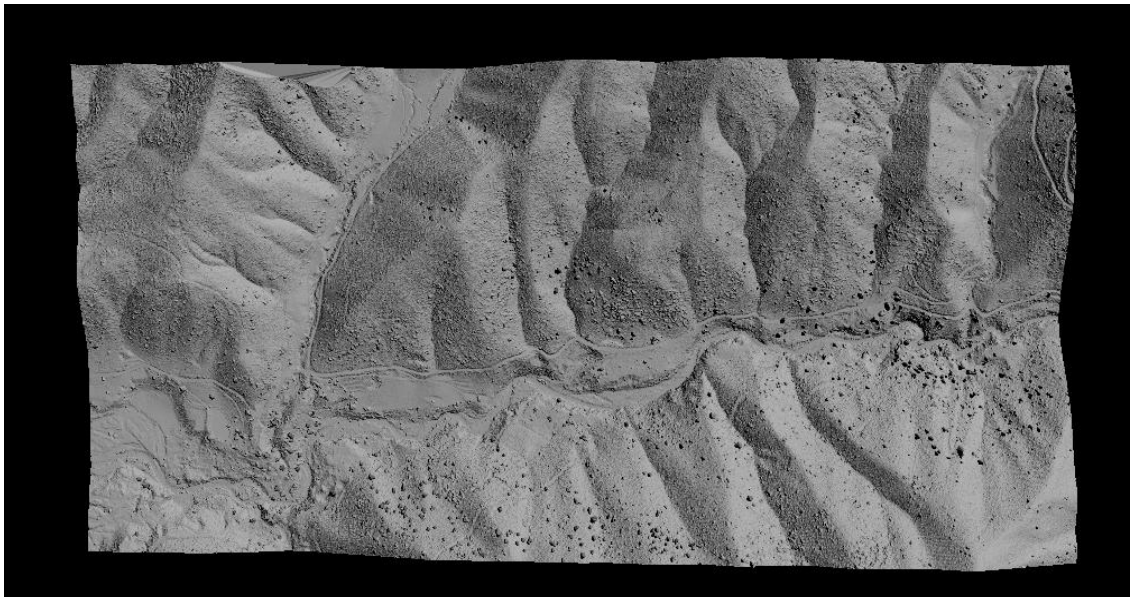

Figure 40. Digital Elevation Model from Indian Creek watershed survey area revealing surface features beneath vegetation.

(2) Lake Tahoe, Cold Creek. The LAS file was directly imported into a surface file by specifying that only ground classified points be considered.[9] With the higher point density, the resolution is very good at 0.29 m resolution with minimal artifacts. This dataset has much flatter terrain, yet roads, watercourses, and even trails can be easily observed.

(3) Kahuku. The high point density of this dataset allowed for the creation of a relatively high surface model sampling at 0.5 m between points using the Bare Earth Extraction Plug–in with resolution at 0.5 m, but the very dense vegetation also resulted in a large number of artifacts.[10] With this product, it is easy to see the roads, and surface drainage patterns in the open areas very clearly. Finding the trails that were heavily ground truthed in the area are not clearly observed on any DEM created in this analysis.

[9] Tahoe_ColdCreek.qtt

[10] Kahuku_site_6_surface.qtt

Figure 41. Google Earth image of Cold Creek survey area in Lake Tahoe Basin dataset. Survey area covers slightly more than 1 km^2

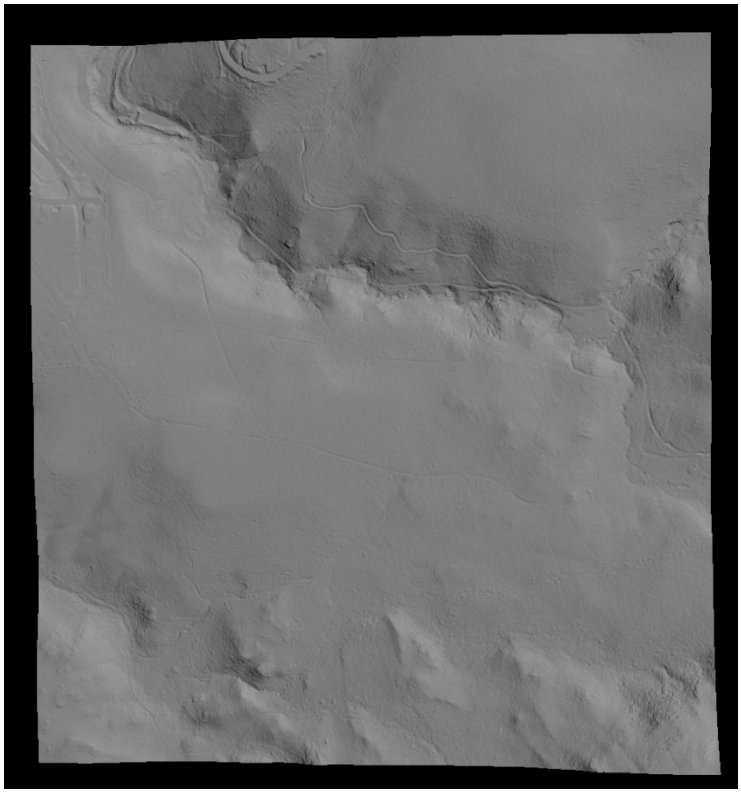

Figure 42. Digital Elevation Model from Cold Creek survey area in Lake Tahoe Basin revealing surface features beneath vegetation

Figure 43. Google Earth Image of Site 6 in Kahuku survey area, Oahu, HI. Area covers about 400m x400m.

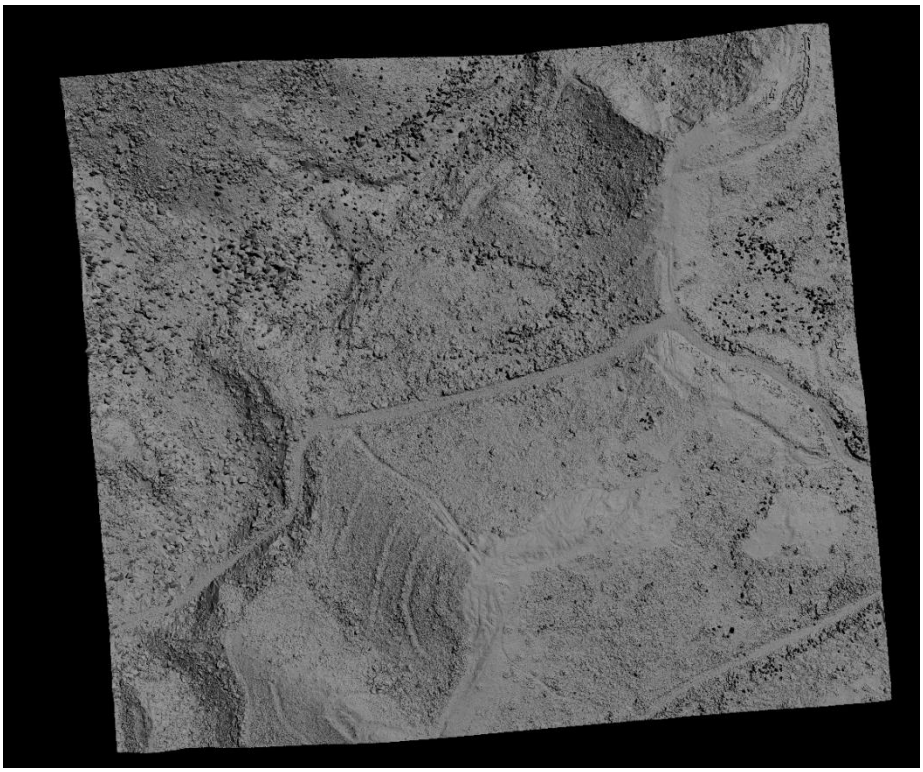

Figure 44. Digital Elevation Model from Kahuku site 6 survey area revealing surface features beneath vegetation.

c. AGL Analyst

Above Ground Level (AGL) analysis in QTM allows measurement of features relative to the ground, as opposed to measurement relative to absolute elevation. This is very useful for peeling back the canopy into user–defined slices to concentrate on just those points, or portions of the canopy of interest. For this study, concentration was placed on those points located just above the ground points to about 1.8 meters for analysis. This is the area where changes in the surrounding vegetative layer would be expected to have recognizable linear features, such as trails and roads.

The AGL Analyst tool in QTM utilizes information from the surface model compared to the point cloud model to build above ground analysis for every point. Break points can then be added to isolate points within elevation classes, and then these points can be displayed and/or exported into their own individual models. Break points for each data set were added at 0.1m and 1.8 m (room for 6 foot human on a trail). Then only these points within this range were exported into separate LAS files[11] for further analysis.

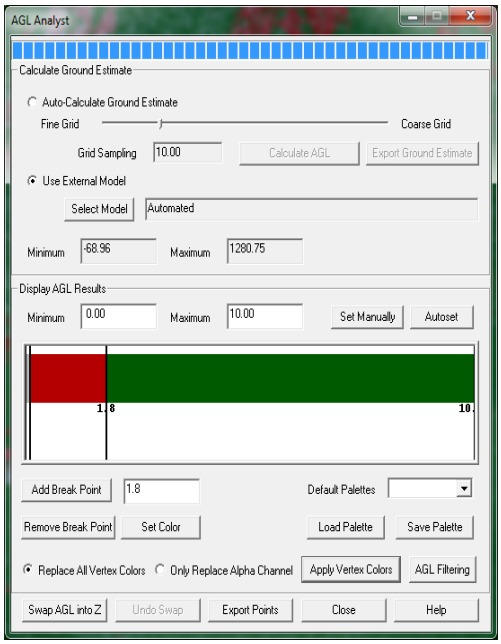

Figure 45. AGL Analyst menu, ground estimate calculated from surface model, break points added at 0.1m and 1.8m, points exported into LAS files

[11] Indian_Creek_Slice.las, Cold_Creek_Slice.las, Kahuku_Slice.las

With Indian Creek and Cold Creek data sets, linear gaps absent of points within this 3D point cloud slice corresponding to roads/trails are clearly visible across the landscape. In each case, it requires use of QTM's 3D zoom features, and manipulation of point size to visually enhance this result. Each have similar understory characteristics, with Indian Creek containing a greater vegetated understory and Cold Creek a relatively open understory. With the Kahuku data set, these gaps were not clearly evident beneath the thick vegetation, but still useful at identifying the main road through the survey area. This data set has the greatest point density, but also the most vegetated landscape. Trails known to be present under the canopy from ground truth are not evident on the DEM and not evident within this point cloud slice, probably due to the result that light penetration through the dense foliage, flown with this method, is still not sufficient to extract the desired information.

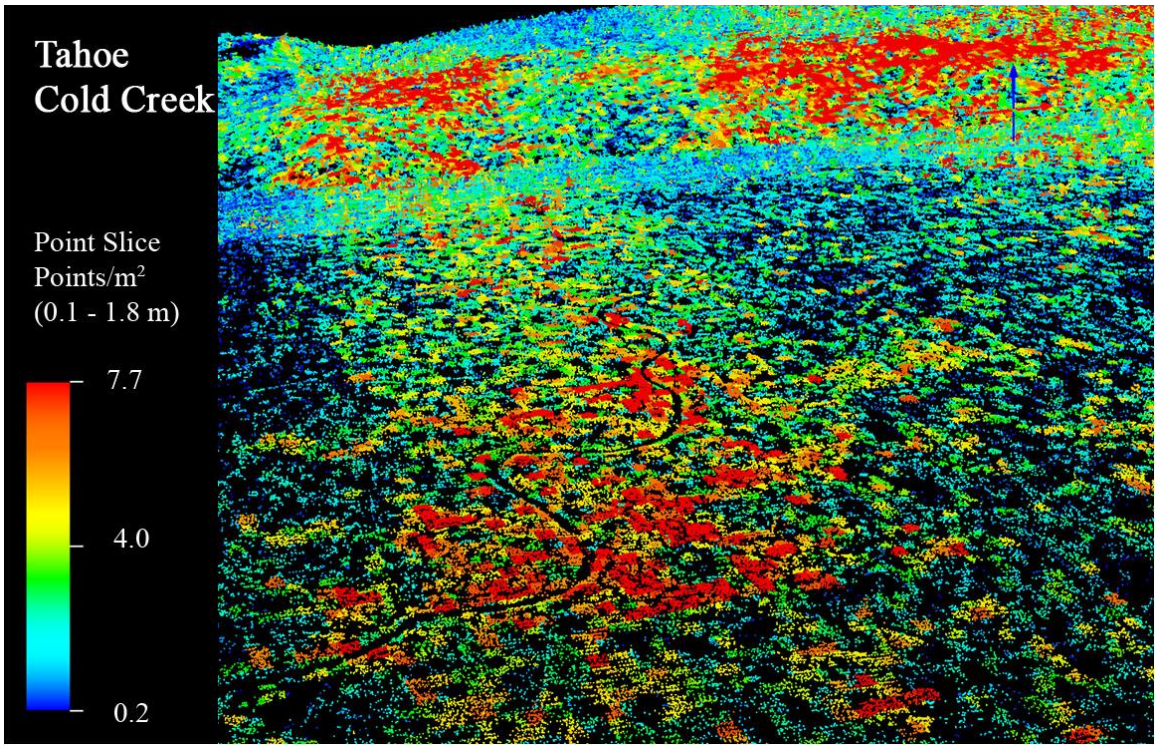

Figure 46. Birds–eye view of 3D point cloud in Lake Tahoe, Cold Creek from 0.1m to 1.8m. Linear gap in point cloud absent of points is clearly visible winding across the landscape, corresponding to identifiable trail on the DEM in Figure 47

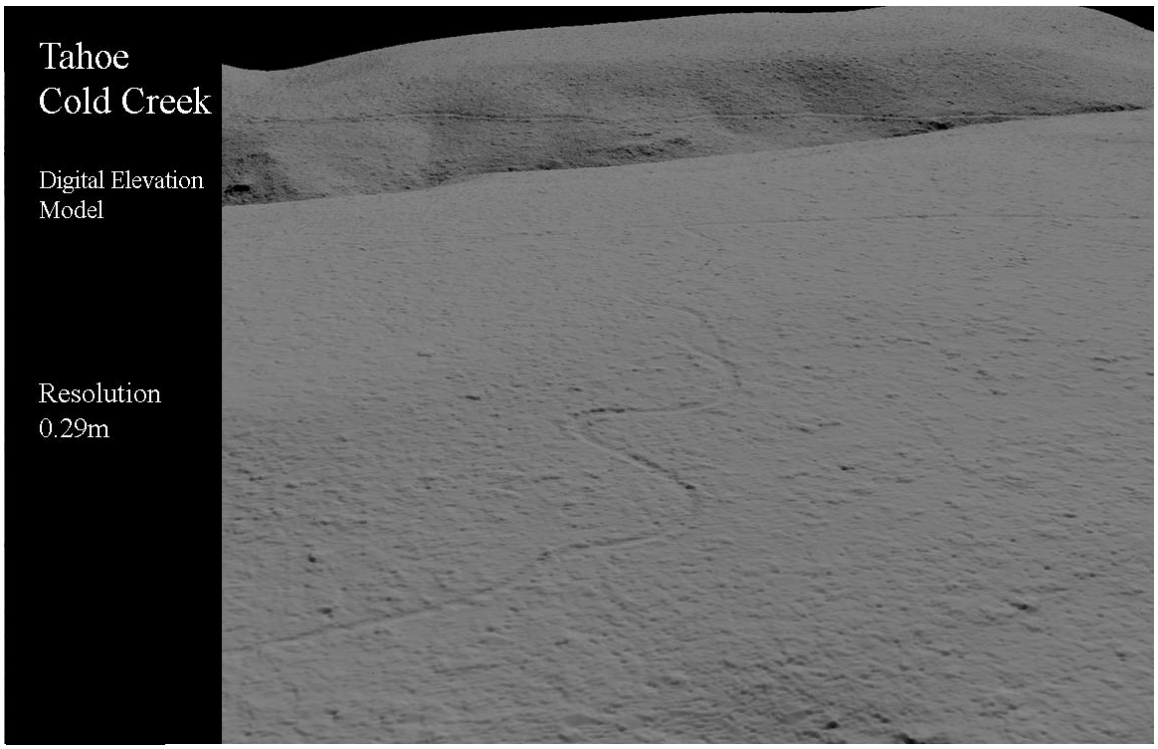

Figure 47. Birds1eye view of DEM in Lake Tahoe, Cold Creek with trail clearly visible winding across the landscape corresponding to linear gap in point cloud absent of points from Figure 46.

d. Image File Creation and Export

In order to utilize ENVI for image analysis, QTM files need to be converted and exported into appropriate image files. Each DEM model was exported in GEOTIFF (32–bit DEM) image format.[12]

[12] Indian_Creek_dem.tif, Cold_Creek_dem.tif, Kahuku_dem.tif

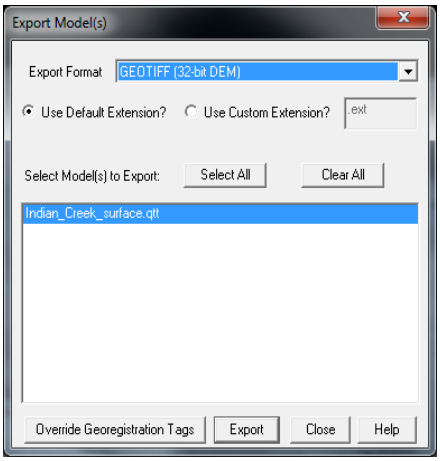

Figure 48. Export Model menu for each surface model to be converted to image file for ENVI analysis

After exporting these files, Grid Statistics were performed on each AGL point cloud LAS file slice and "Number of Points" was selected as a variable at a spacing of 0.5 meter for Kahuku, 1 meter for Cold Creek, and 2 meter spacing for Indian Creek data. These files were then exported, each retaining their number values, in GEOTIFF format.[13] In creating these point density images, collection methods are clearly evident where flight lines overlap with corresponding large variations in point density numbers. Figure 50 shows the number of points statistics on the Cold Creek full point cloud and Figure 51 shows the number of points statistics on the corresponding AGL point cloud slice. These variations should be taken into consideration during any subsequent analysis.

[13] Indian_Creek_Slice_Density.tif, Cold_Creek_Slice_Density.tif, Kahuku_Slice_Density.tif

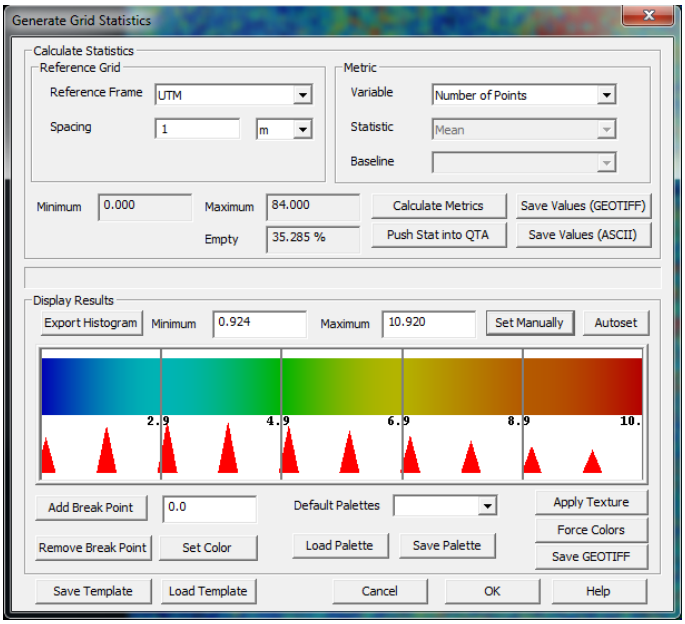

Figure 49. Grid Statistics Menu, Cold Creek: Number of Points for 0.1m to 1.8m AGL slice file was calculated at 1 meter spacing, and values saved in GEOTIFF format for subsequent ENVI image analysis

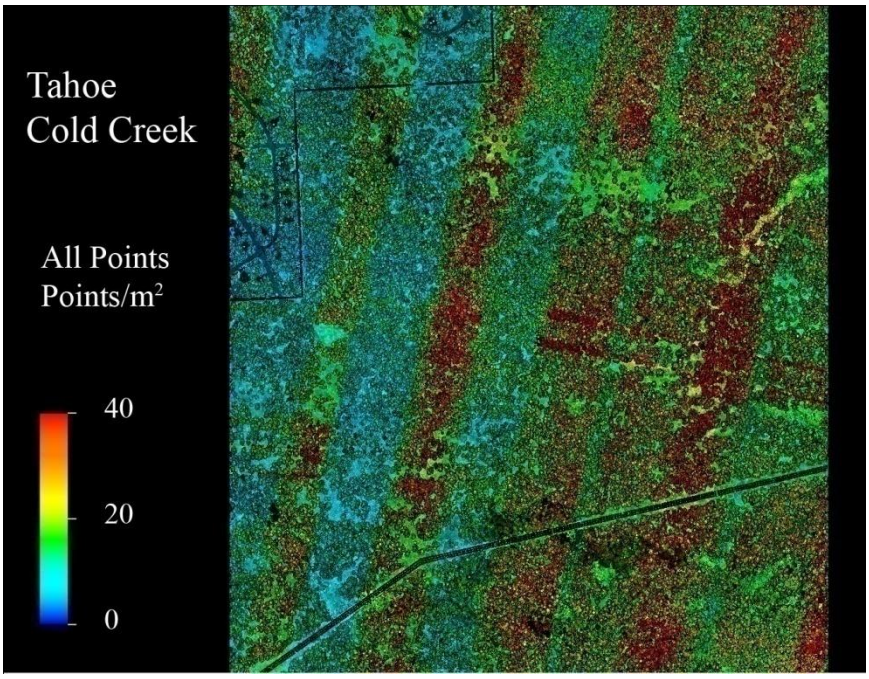

Figure 50. Lake Tahoe, Cold Creek survey area Number of Points for all points. Flight line overlap effects are clearly evident as strips of higher density points transiting the image.

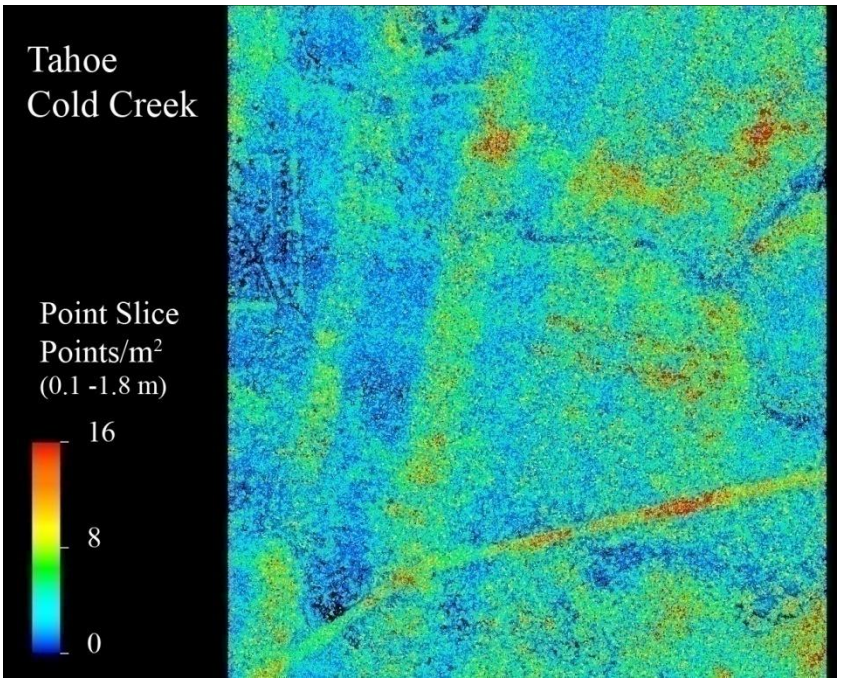

Figure 51. Lake Tahoe, Cold Creek survey area Number of Points for 0.1 m to 1.8 m AGL point cloud slice. Flight line overlap effects are clearly evident

2. ENVI

a. Topographic Modeling

Topographic tools in ENVI extract internal information from the image files created in QTM by fitting a quadratic surface to the digital information data and taking derivatives. Topographic outputs include slope, aspect, shaded relief, convexity, minimum and maximum curvature information, as well as, an RMSE image, all as separate bands. The creation of these bands is based on input of kernel size and file digital elevation data from original image. Slope and convexity bands were selected for analysis as most relevant for this study, utilizing the DEM image from each survey area. The default Topographic Kernel size at 3.[14]

[14] Indian_Creek_Topo.dat, Cold_Creek_Topo.dat, Kahuku_Topo.dat

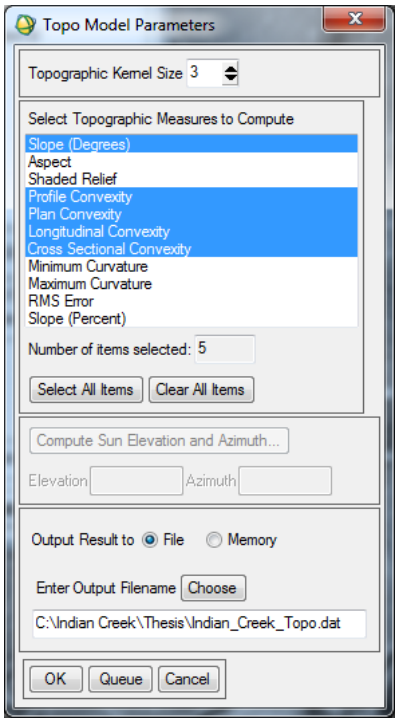

Figure 52. Topographic model parameters, selection of measures to compute, kernel Size and output to file.

Slope is measured in degrees, or percent from the horizontal, depending on band selected. Profile Convexity measures rate of change of the slope along the profile (intersecting with the plane of the z axis and aspect direction). Plan Convexity is in the plane of the z axis, intersecting with the XY plane, and measures the rate of change of the aspect along the plan. Longitudinal Convexity intersects with the plane of the slope normal and aspect direction, measuring the surface curvature orthogonal in the down slope direction. Cross Sectional Convexity intersects with the plane of the slope normal and perpendicular to the aspect direction, measuring the surface curvature orthogonal in the cross slope direction (ENVI, 2003). Evaluation of these bands, along with the additional Number of Points image band in the "trail zone," was the source for attempted isolation and identification of roads and trails for classification, and subsequent automation. Figure 53 through Figure 57 show representative output images from Indian Creek dataset.

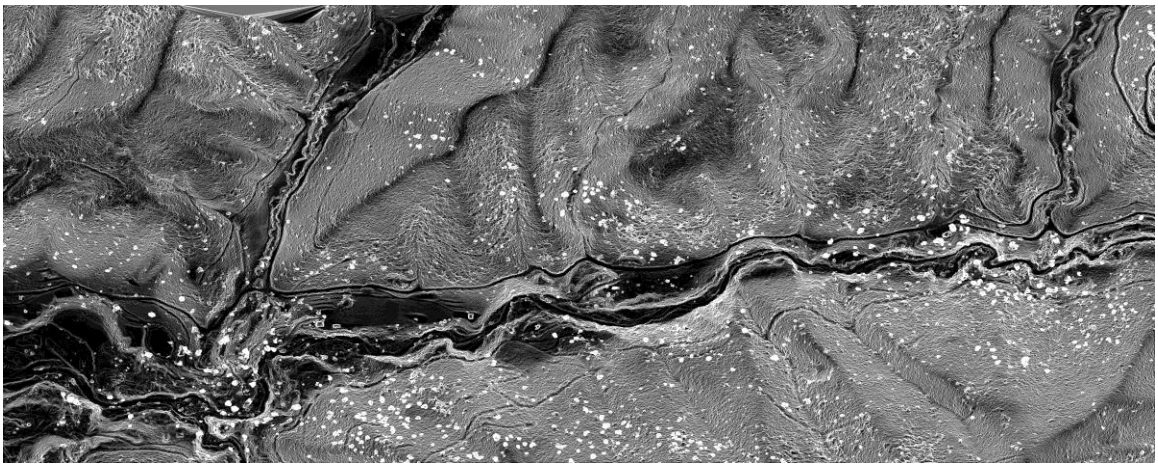

Figure 53. Indian Creek topographic slope band.

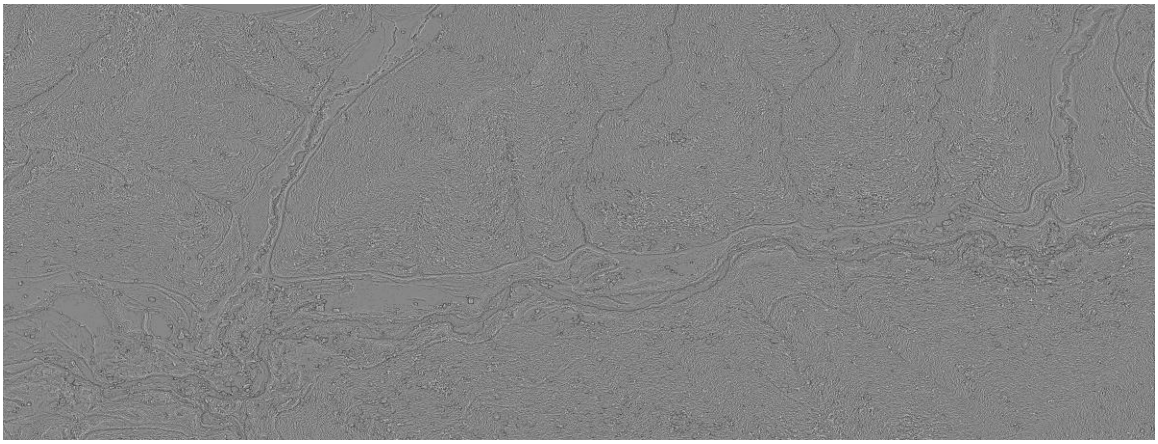

Figure 54. Indian Creek topographic profile convexity band.

Figure 55. Indian Creek topographic plan convexity band.

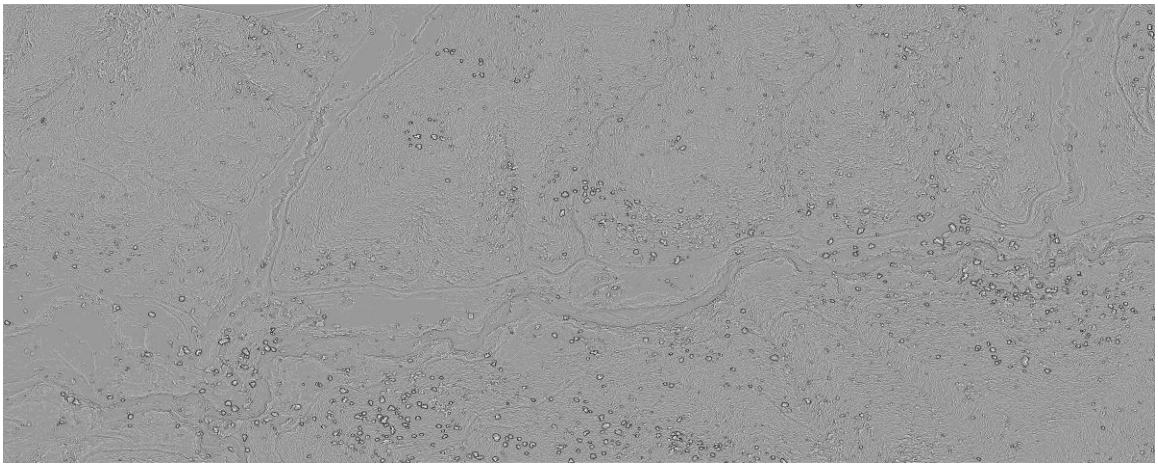

Figure 56. Indian Creek topographic longitudinal convexity band.

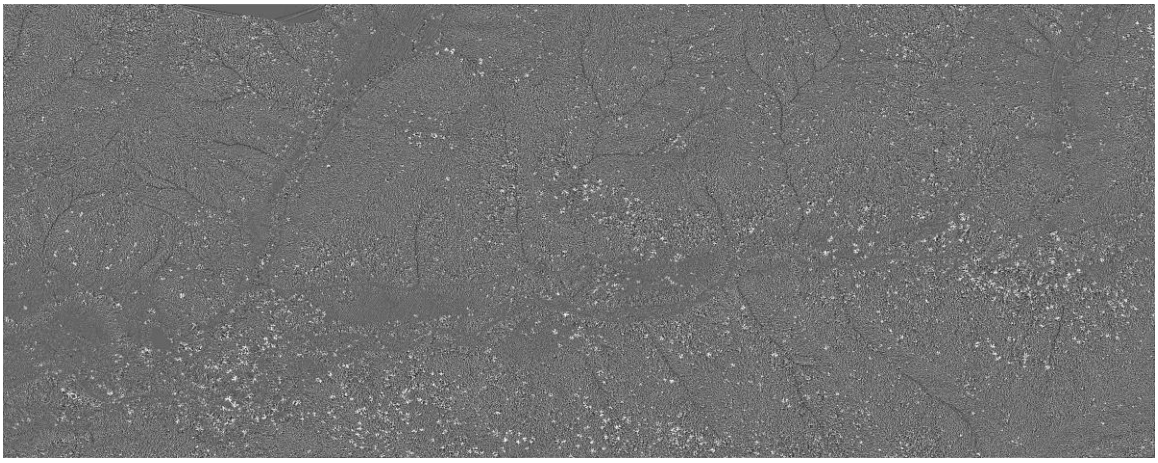

Figure 57. Indian Creek topographic cross-sectional convexity band.

b. Image Preparation and Layer Stacking

When images are exported from QTM, they are often in slightly different spatial sizes depending on defined DEM resolution and point slice image spacing selections. Also, the point slice image is exported with values of –9999.0 in pixels where there is an absence of points. These results must be corrected before proceeding with analysis. The point slice image problem was corrected within ENVI to facilitate routine analysis by setting all of these –9999.0 values to zero.

To enable simultaneous geographic analysis between the desired bands, spatial sizes must be equivalent. This was accomplished by Layer Stacking, in the Basic

Tools menu, to build a multiband file from all three geo–referenced images. Files were stacked from each survey area in order of precedence: Topo file, DEM file, updated point slice file. Exclusive range was selected to ensure that the output file would contain only data where files overlap. The output file projection was set corresponding to the input files, with pixel sizes at 1 m^2, and resampled according to Cubic Convolution.[15] Cubic Convolution uses 16 pixels to approximate the sinc function using cubic polynomials to resample the image. This method produces an image product that is smooth in appearance as a final analysis product (Richards & Jia, 2006).

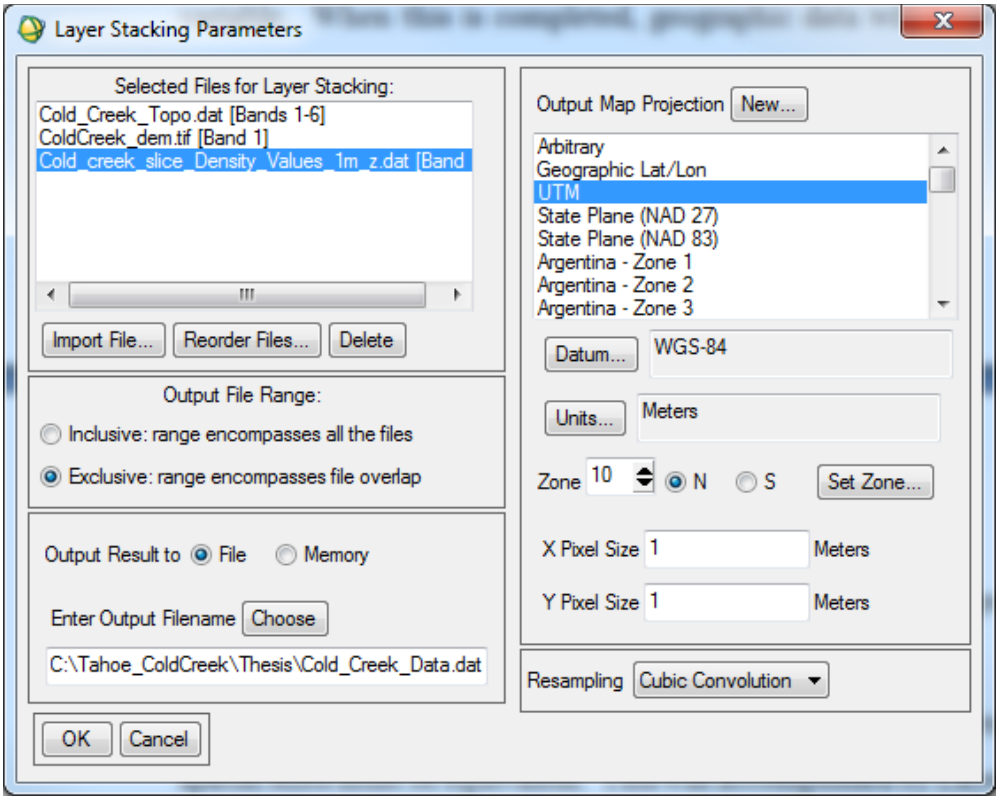

Figure 58. Layer Stacking Parameters input menu. Files are selected for stacking in order of precedence and output in re–sampled, 1 m^2 pixels.

c. Minimum Noise Fraction (MNF) Transform

Analysis of the multi-layer datasets was explored with principal components and the MNF transforms. This projection weighs the bands as a function of

[15] Indian_Creek_Data.dat, Kahuku_Data.dat, Cold_Creek_Data.dat

the Signal to Noise Ratio (SNR). A forward transform rotation was performed to estimate noise statistics from the data, and output MNF bands into a file for further spectral analysis.[16] The goal here was to project the data into a coordinate system that makes it most obvious which bands provide the best data for road and trail identification.

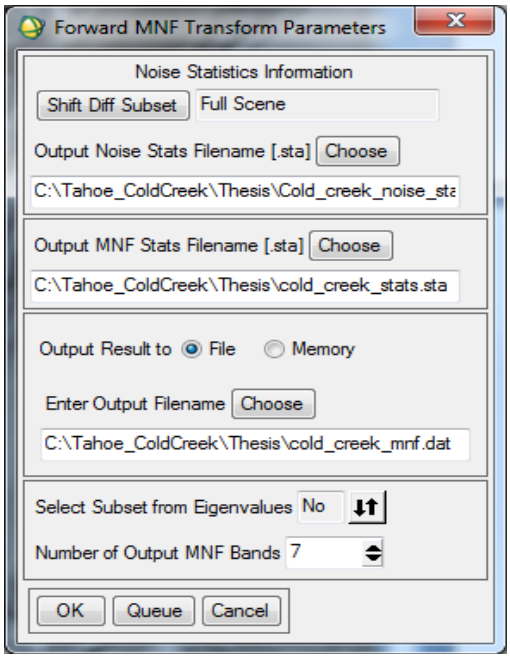

Figure 59. Forward MNF Transform Parameters menu. Transform performed on Layer Stacked data files and output into MNF bands file for subsequent spectral analysis.

B. DATA SPECTRAL ANALYSIS

1. Indian Creek

a. Region of Interest Selection

Examining the MNF, band 4 revealed that darker areas were more likely to be trail. Polygon regions were drawn within known roads and suspected skid trails and carefully traced within these smaller linear features suspected to be "trail–like." Polygon regions were also drawn over differing non–trail areas across the survey area. The tool that allows this is called the ROI Tool within ENVI which was used to visually draw

[16] Indian_Creek_mnf.dat, Kahuku_mnf.dat, Cold_Creek_mnf.dat

distinction between trail and non-trail areas within these identified regions. Different colors were used to distinguish between selected points in each region. These regions containing both trail and non–trail pixels were then exported into the n–D Visualizer to see the distribution of points within these regions between bands.

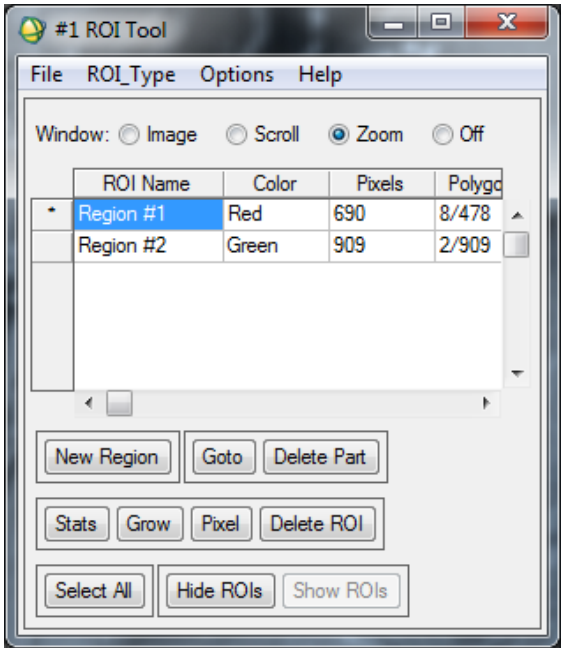

Figure 60. ROI Tool for selecting regions of suspected road/trail regions (Red points) and suspected non–road/trail regions (Green points)

b. n–Dimensional Visualizer Analysis

The n–Dimensional Visualizer provides a format for visualizing all selected bands in their several dimensions in order to check the separability of selected ROIs in a scatter plot. After export into n–D Visualizer, location, identification and clustering of trail points from non–trail points was very easily accomplished based on MNF band differences. Outlying points were then removed in the clusters to reveal a well behaved distribution of trail and non–trail points.

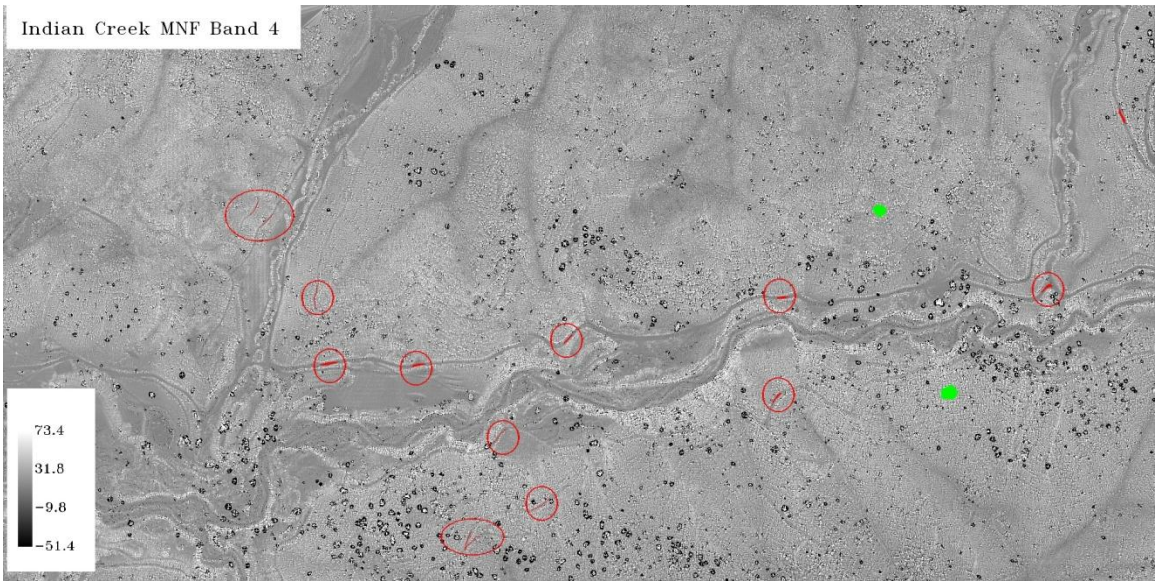

Figure 61. Indian Creek survey area, Regions of Interest over MNF band 4, identifying roads/trails (red selections) and non–roads/trails (green selections).

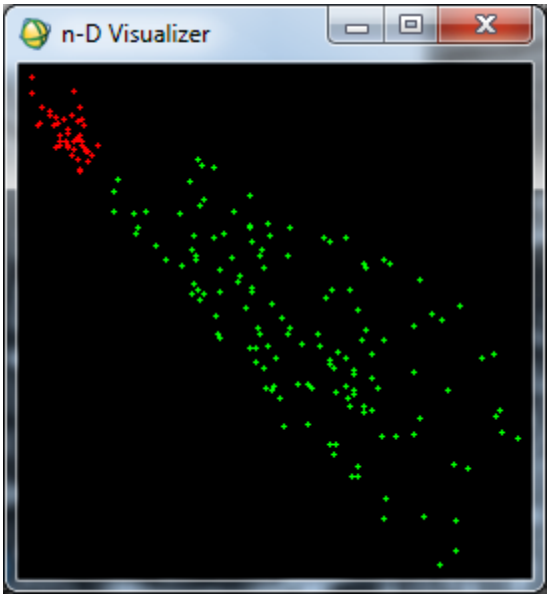

Figure 62. N–D visualizer scatter plot utilizing MNF bands 2 through 7 for Indian Creek survey area

c. Maximum Likelihood Classification

Maximum likelihood classification assumes a normal distribution of each class in each band identified as road/trail and not road/trail. This tool then calculates the

probability that a given pixel in the entire landscape belongs to that specific class (ENVI, 2004). Once classes were identified using the n–d visualizer, maximum likelihood classification was performed with these inputs on MNF spectral bands 2–7 at a probability threshold of 0.1 and output to a class file and a rule file.[17] The probability threshold was set at 10% such that pixels with probabilities less than this threshold would not be classified. At any threshold higher than 25%, points came back without any classification results. Only without a probability threshold were non–road/trail points classified at all with this method. Classification results correctly identify most all roads/skid trails visible on DEM, however, across the landscape, false positives are prevalent in flat ground along the creeks, and low slope areas along ridges.

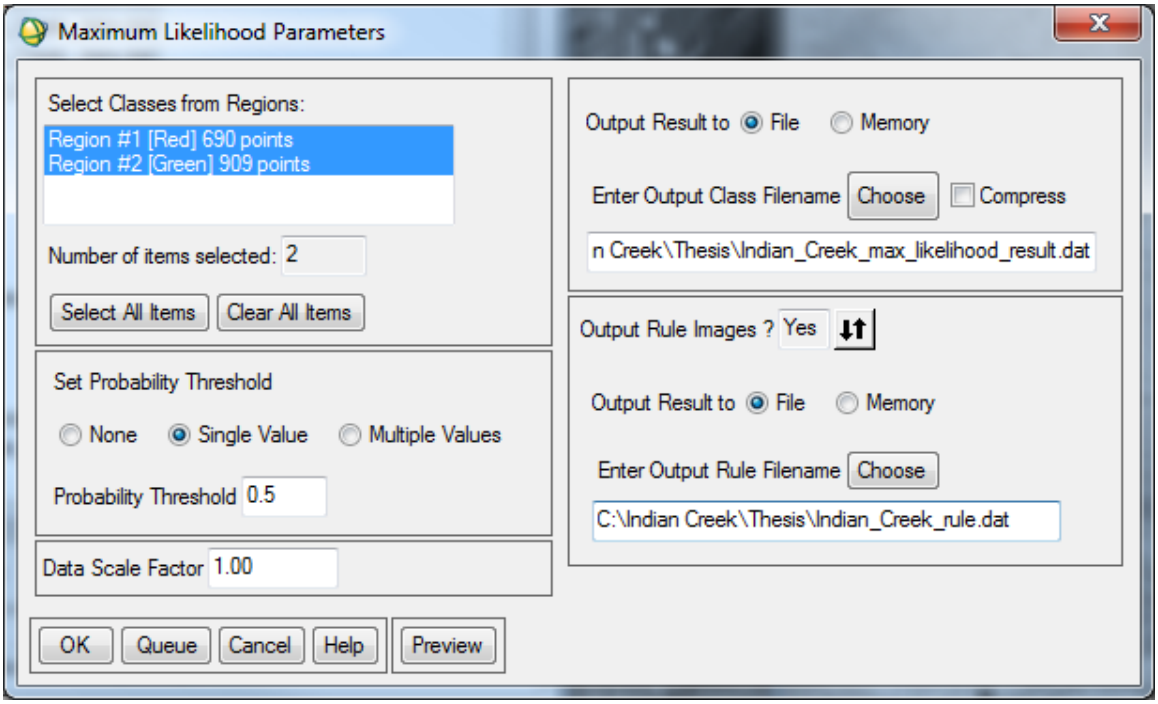

Figure 63. Maximum Likelihood Parameters input menu. ROI regions are selected with a probability threshold of 0.5 and output to both class and rule files

[17] Indian_Creek_max_likelihood_result.dat, Indian_Creek_rule.dat

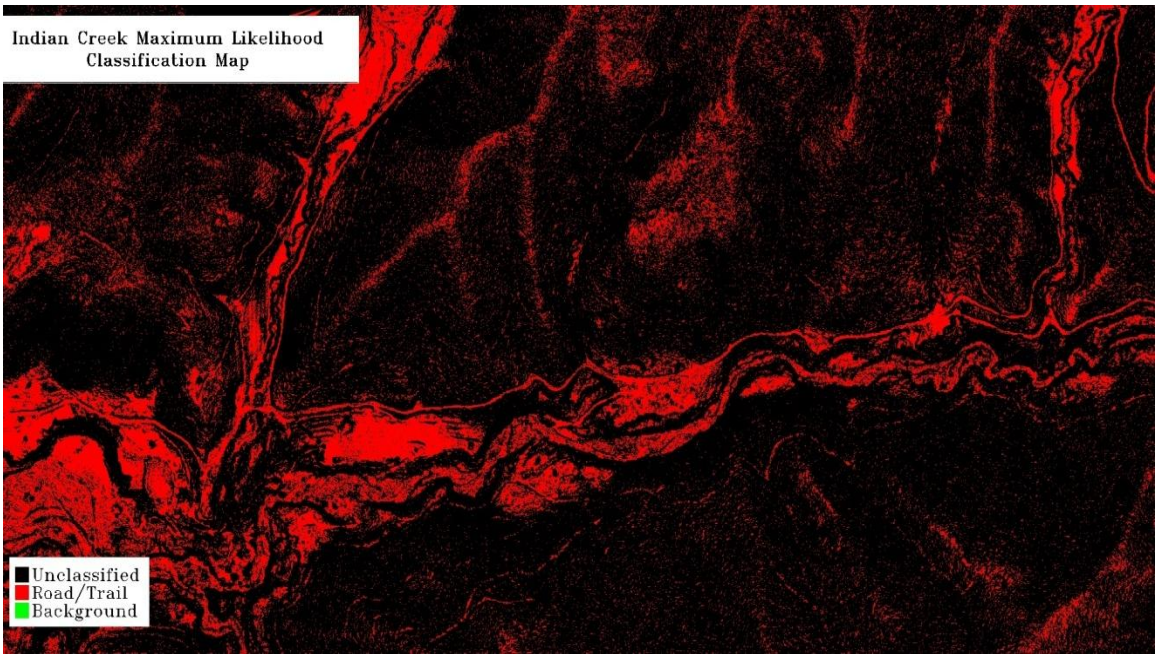

Figure 64. Maximum Likelihood Classification result, probability threshold of 10%, applied to Indian Creek survey area. The red areas are classified as most likely to be trail. Vast areas of the survey area are unclassified at this threshold.

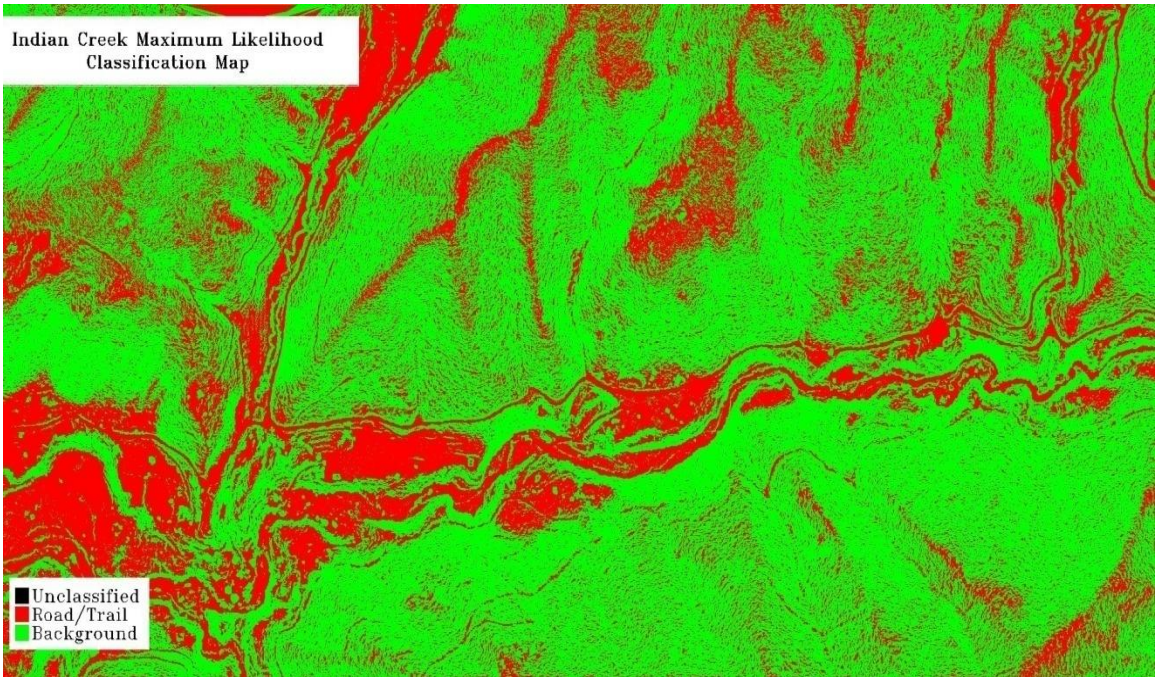

Figure 65. Maximum Likelihood Classification result, no probability threshold, applied to Indian Creek survey area. The red areas are classified as most likely to be road/trail. The green areas are classified as most likely to be other than road/trail.

2. Lake Tahoe, Cold Creek

a. Region of Interest Selection

Examining the MNF bands, band 1 revealed that lighter areas were more likely to be road/trail and band 2 revealed that darker areas were more likely to be road/trail. Band 1 was utilized for defining trail and non trail regions of interest for selection. A polygon region was drawn over an obvious trail, containing both trail and non–trail pixels for export into n–D Visualizer to see the distribution of points within this region between bands.

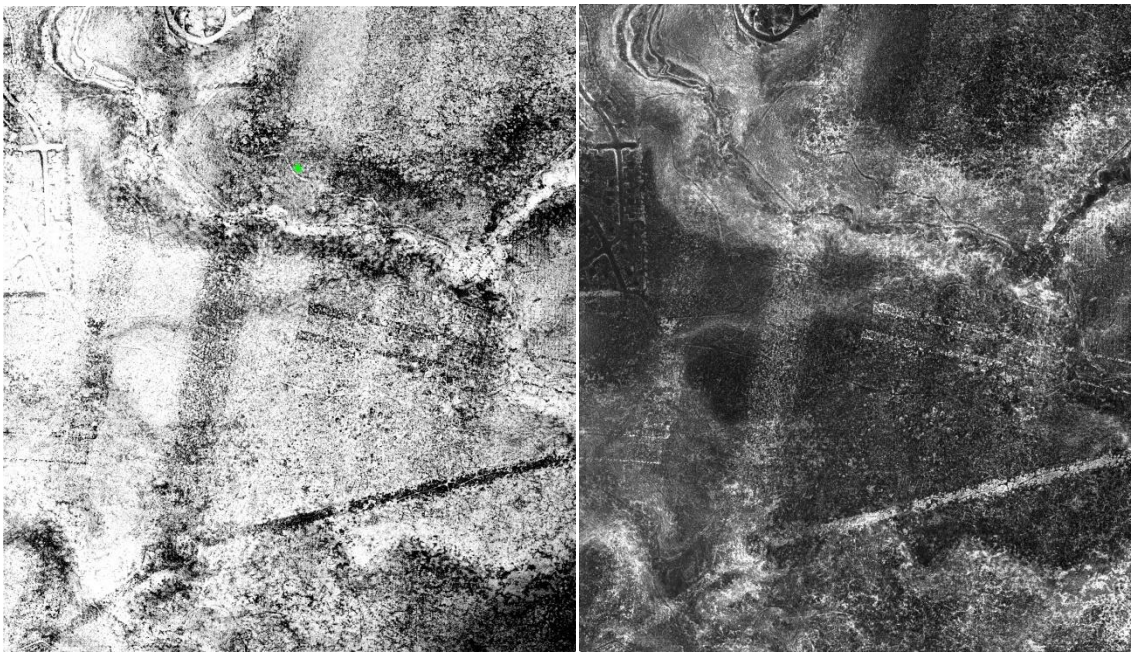

Figure 66. MNF band 1 (left) and MNF band 2(right) images, overview. In band 1, lighter areas more likely to be trail. In band 2, darker areas more likely to be trail.

b. n–Dimensional Visualizer Analysis

After export into the n–D Visualizer, location, identification and clustering of trail points from non–trail points was performed based on MNF band differences. Outlying points were then removed in the clusters and another region drawn of only non–trail points in order to further distinguish between trail and non–trail.

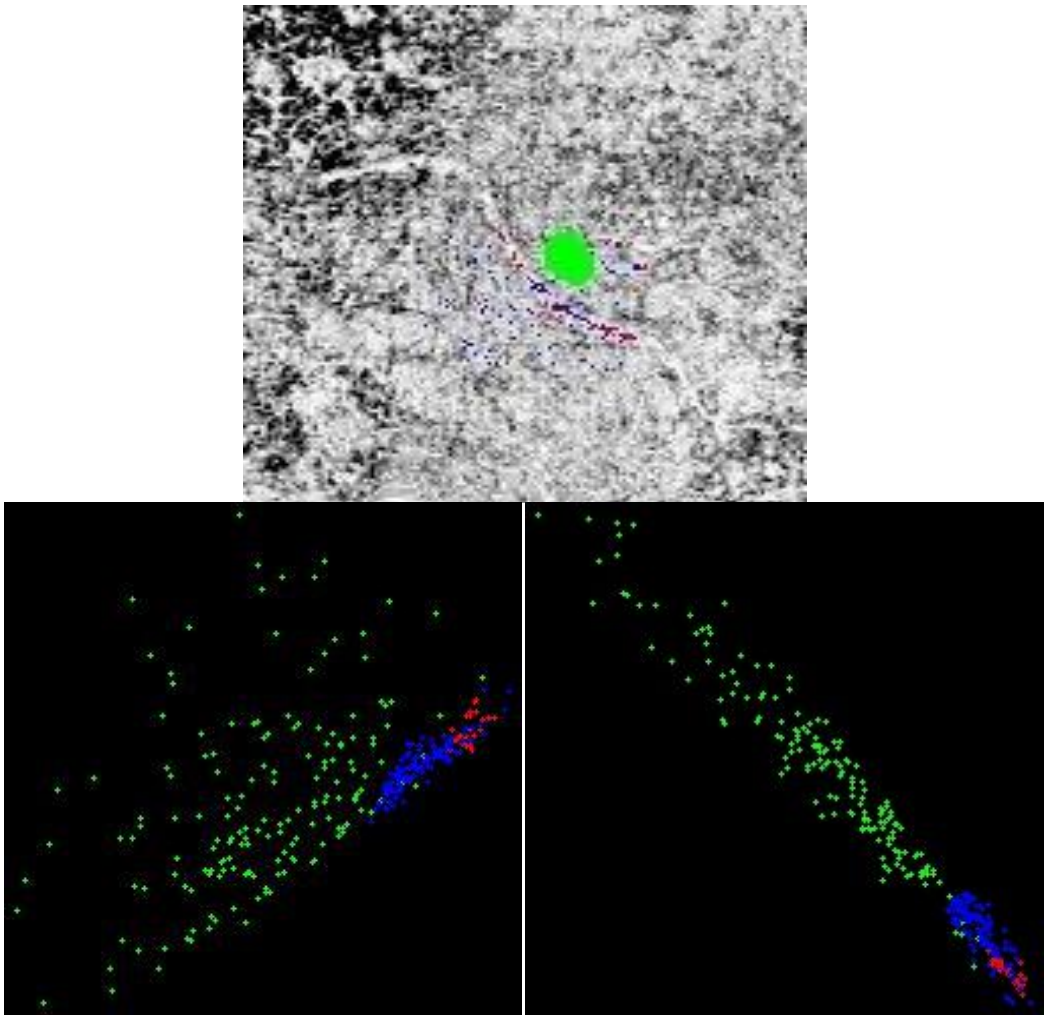

Figure 67. Regions (top) drawn over MNF band 1 image, red points identified as most likely trail, blue points as possibly trail, and green as not trail. N–D visualizer scatter plot (lower left) utilizing MNF bands 1 through 4, and scatter plot (lower right) utilizing MNF band 1 and band 2.

c. Maximum Likelihood Classification

Once identified, maximum likelihood classification was performed with these inputs on MNF spectral bands 1–4 at a probability threshold of 0.5 and output to a class file and a rule file.[18] Classification results correctly identify some trails, particularly within the area immediately adjacent to the region of interest selections; however, across the landscape, false positives far outnumber positive results, rendering

[18] Cold_Creek_max_likelihood_result.dat, Cold_Creek_rule.dat

this classification scheme as thoroughly ineffective. The "trail" identified areas correspond to the lowest slope terrain across the survey area.

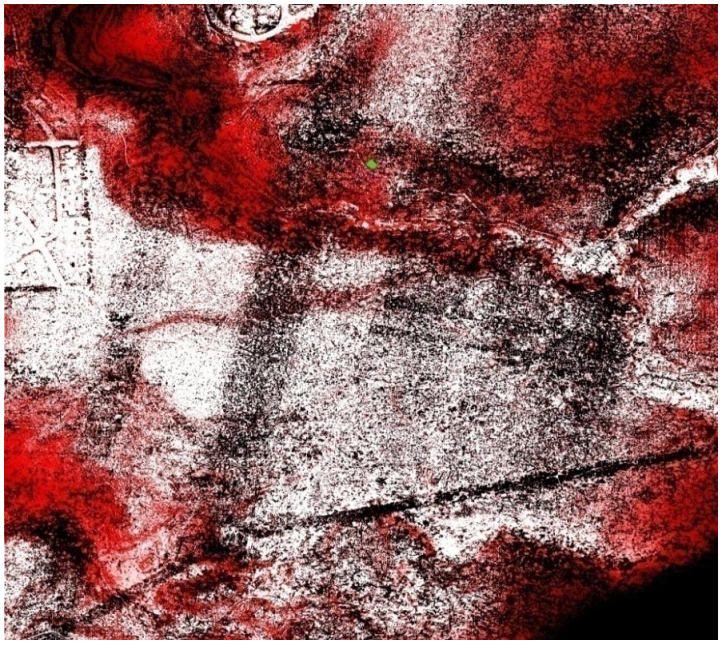

Figure 68. Maximum Likelihood Classification result applied to Lake Tahoe, Cold Creek survey area. The whiter the area, the more likely that it is a trail. Vast areas of the survey area are classified as trail using this method.

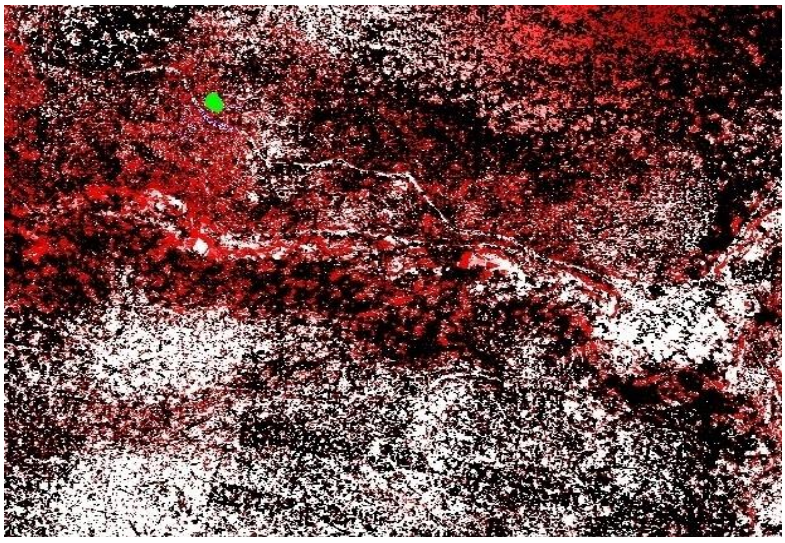

Figure 69. Subset of Lake Tahoe, Cold Creek survey area surrounding region of interest selected areas (upper left of figure that includes the green shaded region of nontrail points). Classified such that the whiter the area, the more likely it is a trail.

3. Kahuku

a. Region of Interest Selection

Examining the MNF bands, band 1 revealed that lighter areas were more likely to be road/trail and this band was utilized for defining trail and non trail regions of interest for selection. Polygon regions were drawn within known roads and other bare earth areas supporting vehicular travel. Polygon regions were also drawn over differing non–trail areas across the survey area. Lastly, positive areas of ground–truthed trails were carefully traced as identified in previous work (Espinoza & Owens, 2007). These regions containing both trail and non–trail pixels were then exported into the n–D Visualizer to see the distribution of points within these regions between bands.

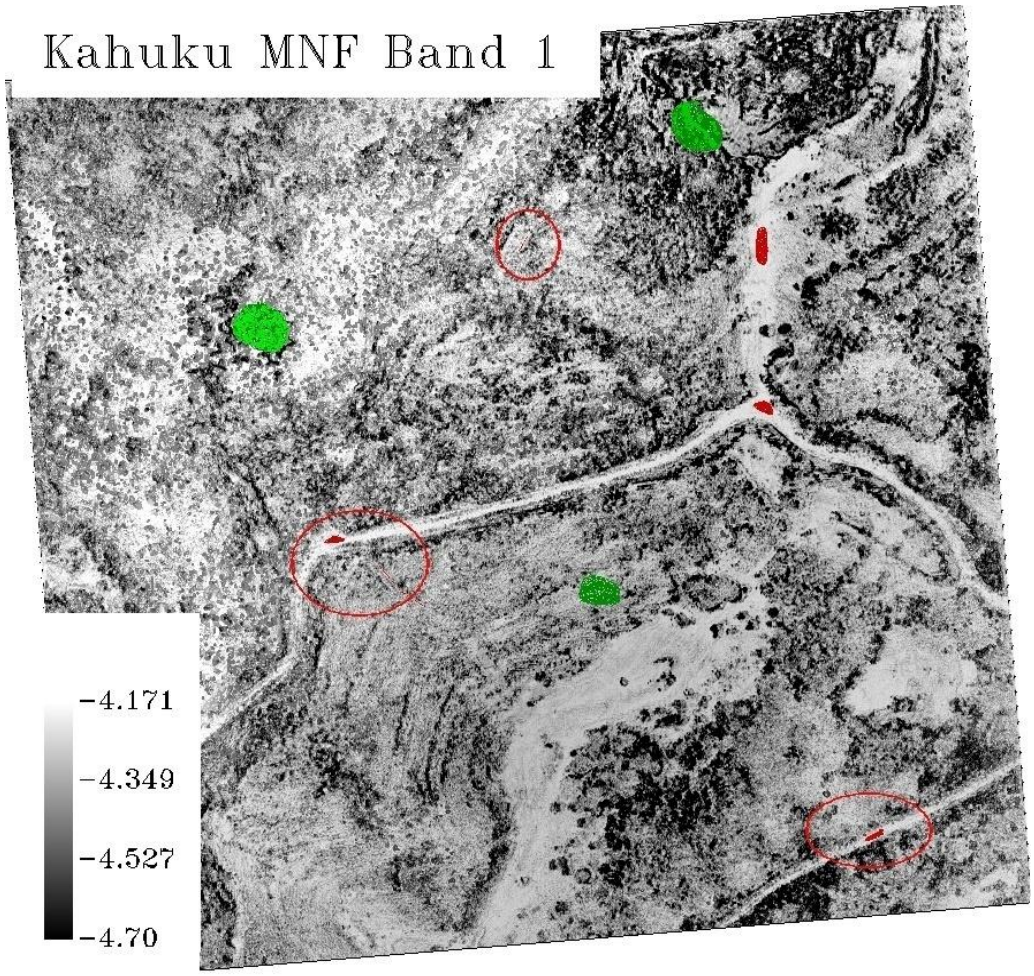

Figure 70. Kahuku survey area, Regions of Interest over MNF band 1, identifying roads/trails (red selections) and nonroads/trails (green selections). Differing shades of red and green are the result of further n–D visualizer analysis.

b. n–Dimensional Visualizer Analysis

After export into n–D Visualizer, the location, identification and clustering of trail points from non–trail points was performed based on MNF band differences. Outlying points were then removed in the clusters and further classified according to variations of red and green based on clusters within regions. Those regions identified as road/trail are clearly orthogonal to all other non–trail classified points in this analysis.

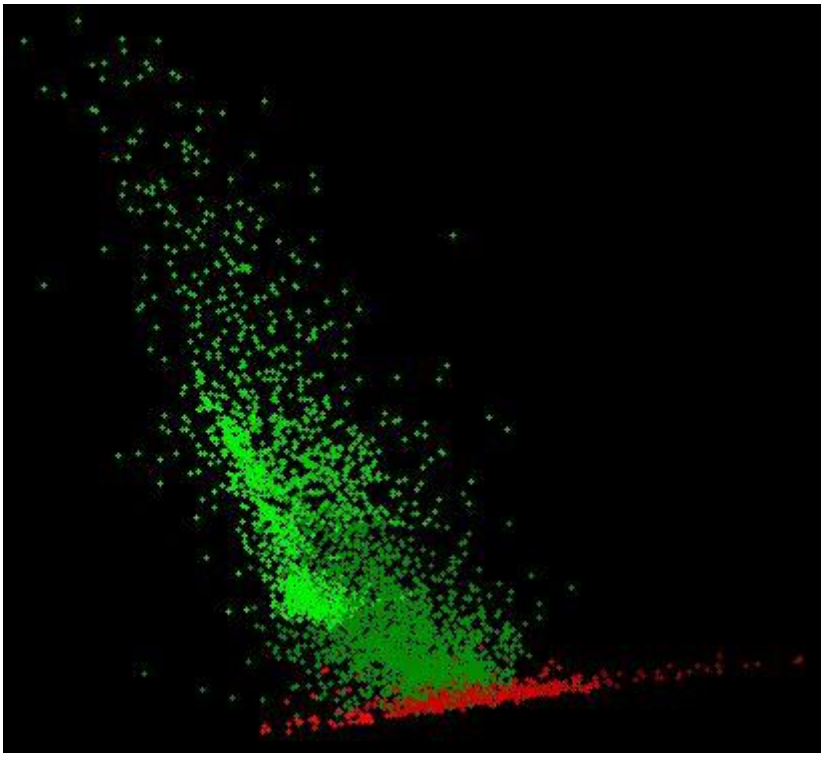

Figure 71. N–D Visualizer scatter plot of points selected in Regions of Interest and further selected and colored according to obvious point groupings. Red colored points which correspond to selected roads and trails clearly form a grouping orthogonal to the nonroad/trail points.

c. Maximum Likelihood Classification

Once points were separately identified, maximum likelihood classification was performed with these inputs on MNF spectral bands 1 through 4 at a probability threshold of 0.5 and output to a class file and a rule file.[19] Classification results correctly identify the majority of roads; however, large areas of exposed ground along a ridgetop

[19] Kahuku_max_likelihood_result.dat, Kahuku_rule.dat

that traverses the figure from the northeast corner, south toward the middle/center of the survey area, was also identified as road. This ridgetop area shows evidence of off–road vehicle activity, and clearly demonstrates characteristics synonymous with those of roads. This classification method fails to identify any of the known ground–truthed trails beneath vegetated areas in any useful classifiable way. If they do fall within the classification category, it is scattered and random, not clearly linear. In comparison with imagery over the same area, roads that are identified by this method are those which remain mostly exposed in any case and are not largely occluded by vegetation.

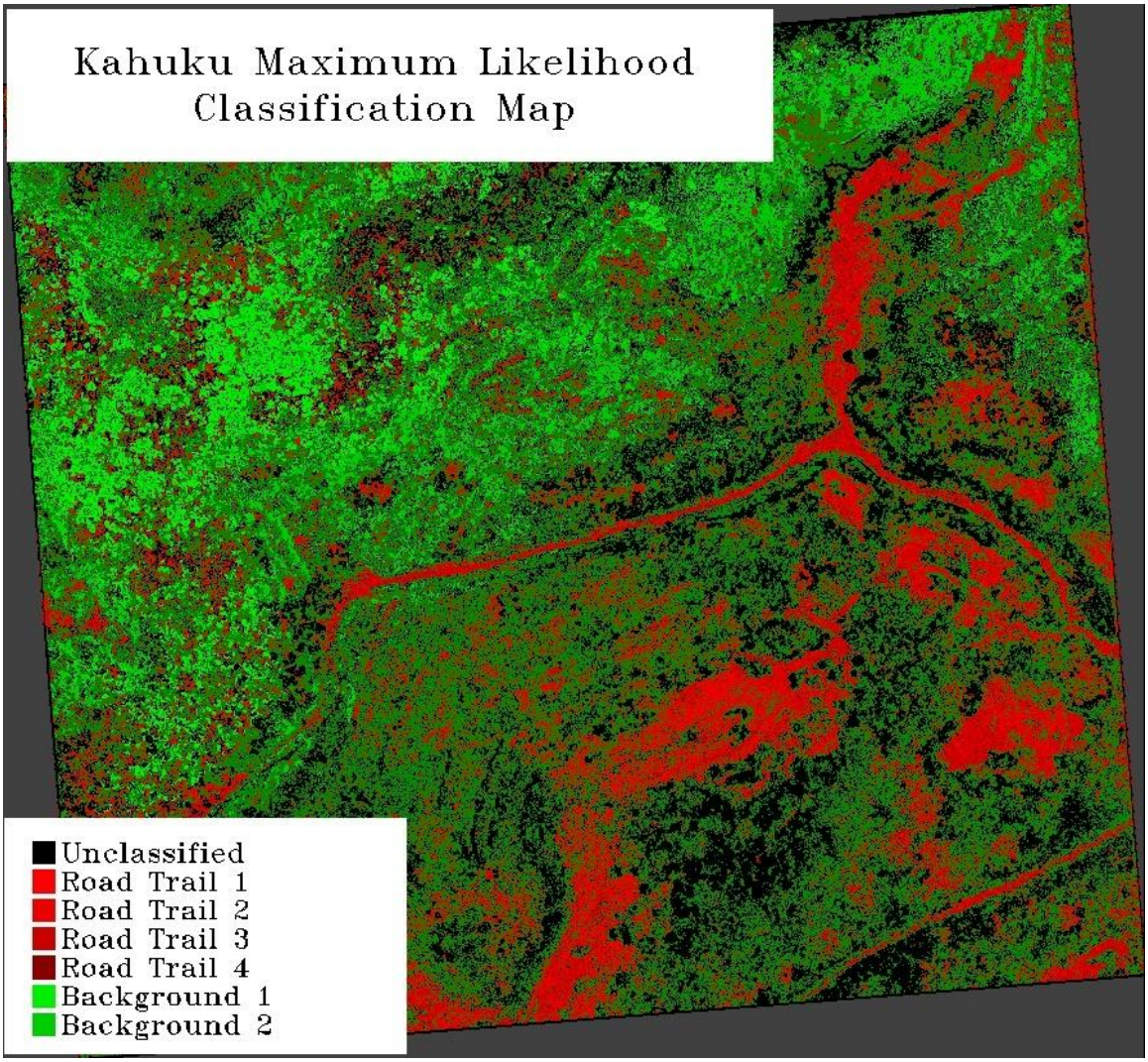

Figure 72. Kahuku survey area Maximum Likelihood Classification map identifying red colored areas as roads/trails, green colored areas as non–road/trails, black areas as not classified.

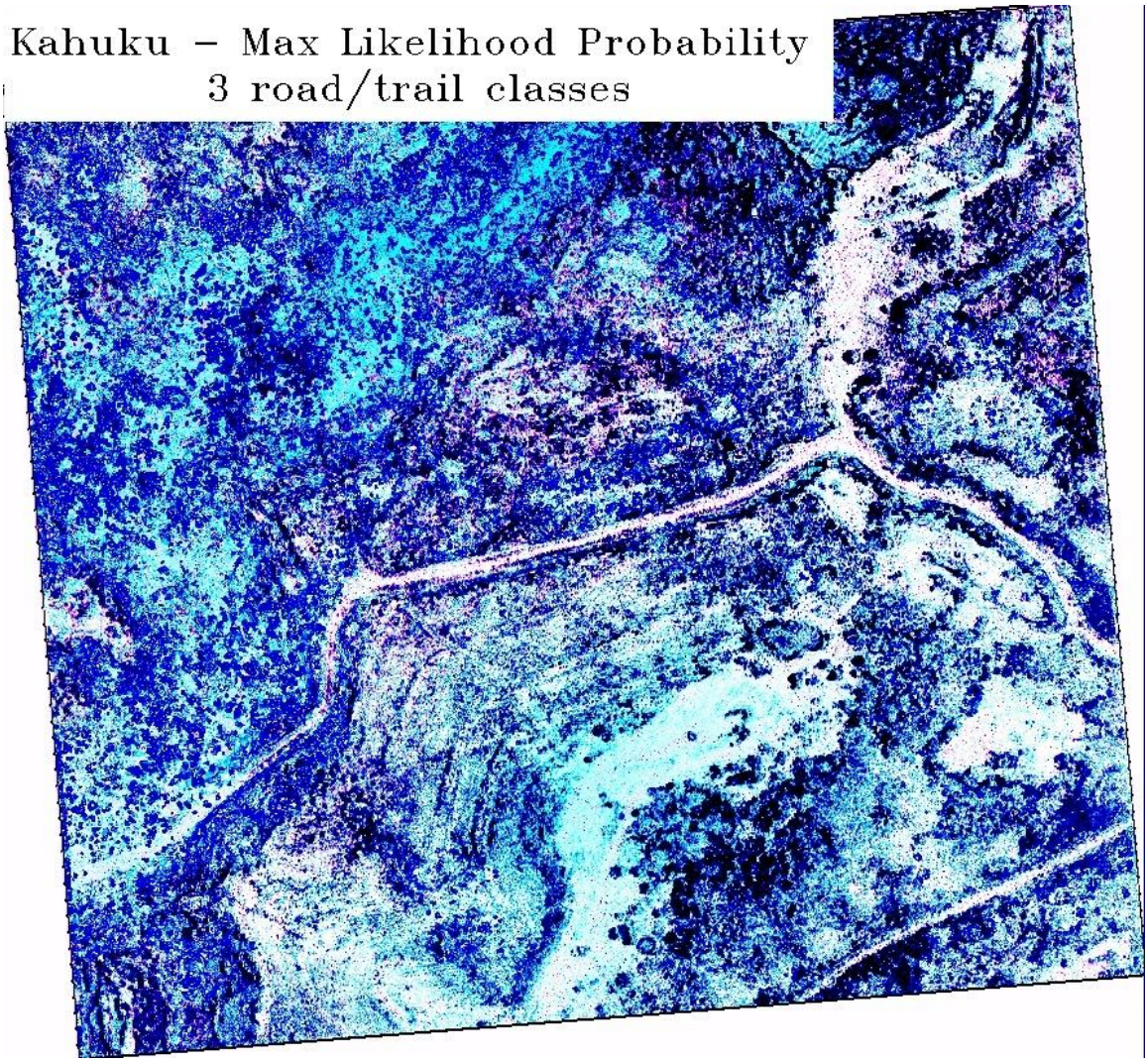

Figure 73. Kahuku Maximum Likelihood Probability "Rule" image distinguishing between the first three identified road/trail classes such that the whiter the area, the more probable that it is a road/trail. "Rule" image is the probability that a pixel vector matches the mean of the region of interest for the training set.

V. SUMMARY

The comprehensive summary of this research, represented by the observations and analysis in Chapter IV, yield interesting, if not impressive results using this method. By looking at three very different sets of data from three distinct forest environments, the attempt was made to model results of any successful automation regimen which could be applicable to a variety of situations. This experiment looked at three image products to assess the data for automated classification: QTM extracted DEM, ENVI Topographic Modeling results of area slope and convexity, and QTM Point Density Grid Statistics on number of points in "trail" zone between 0.1 m and 1.8m AGL.

For Indian Creek, it was observed that even with low point density data, a descriptive DEM was created which revealed roads, watercourses, and some skid trails under trees very visible. Topographic modeling of the data were useful at helping to further visually identify roads and skid trails, particularly the Slope and Profile Convexity bands. When taking a point "slice" between 0.1m and 1.8m AGL, linear gaps absent of points corresponding to road and skid trail locations were very easily recognizable with this data, even at point densities less than 1 per m^2. All bands were layer stacked and smoothed with an MNF transform. MNF band 4 of the data provided the best discriminating image on which to segregate road and skid trail points from background points. Maximum likelihood classification results using a 10% probability threshold identified roads and skid trails, but also misidentified flat areas, watercourses, and ridge–tops as also being probable roads/trails.

For Lake Tahoe, Cold Creek, it was observed that with the higher point density data, a much higher quality DEM could be created which effectively revealed roads, structures, downed woody debris and even trails under vegetation. This area had more level terrain with open canopy and a more open understory than the other two data sets. Topographic modeling of the data were useful to further visually identify roads and trails, particularly the Slope, Profile and Plan Convexity bands.

When taking the point "slice" between 0.1m and 1.8m AGL, the linear gaps absent of points corresponding to trail locations were also easily recognizable with the data, particularly in the higher point density flight line overlaps. Point density images contained significant variability due to these flight line overlap zones which was evident throughout all further analysis. All bands were layer stacked and smoothed with an MNF transform. MNF bands 1 and 2 were most useful in observing roads by dark or light coloring compared with the surrounding landscape. MNF band 1 was chosen on which to segregate trail from non–trail on the most obvious visually identifiable feature in the survey area. Maximum likelihood classification results using a 50% probability threshold, identified trails in the immediate vicinity of areas where trail/non–trail regions were selected for analysis, but also identified the majority of low slope areas across the landscape as most probable trail.

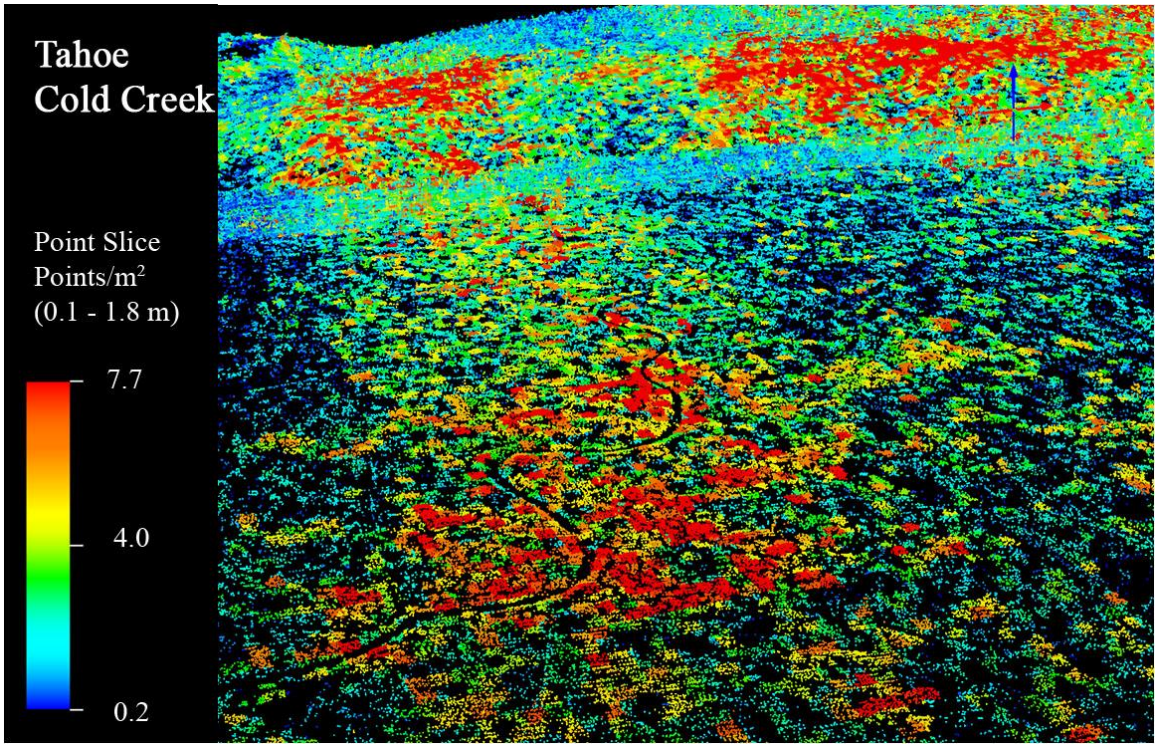

Figure 74. Birds–eye view of 3D point cloud in Lake Tahoe, Cold Creek from 0.1m to 1.8m. Linear gap in point cloud absent of points is clearly visible winding across the landscape, corresponding to identifiable trail on the DEM

For Kahuku, Oahu, HI data, it was observed that, even with the extremely high point density, DEM quality suffers where vegetation is thickest, rendering most trails hidden. This area has a mix of steep and flat terrain, but very thick "jungle" type vegetation was a barrier to field identified trails. Topographic modeling of the data were useful for further visually identifying the roads and a few trails, particularly the Slope and Profile Convexity bands. When taking the point "slice" between 0.1m and 1.8m AGL, linear gaps were only obvious around the major roadway in the survey area. Known trails in the survey area were not obviously identifiable from the point cloud slice. All bands were layer stacked and smoothed with an MNF transform. MNF bands 1 through 4 were most useful in observing the roads and few trails. MNF band 1 was chosen on which to segregate trail, road, and non–trail regions. Maximum likelihood classification results using a 50% probability threshold, identified roads very well, but also identified most all exposed ground across the ridge–tops as road, although at a lower probability. The results failed to reveal classification of any known trails beneath forest canopy.

For all three areas and data sets, automated classification utilizing this method was inconsistent and unsuccessful.

THIS PAGE INTENTIONALLY LEFT BLANK

VI. CONCLUSION

The primary objective of this thesis was to determine an acceptable method for evaluating LiDAR data in order to effectively recognize potential roads and trails under forest canopy with the intent to automate such a process. Although methods used in this study were effective in providing means by which manual visual recognition of roads and trails under forest canopy were enhanced, automated classification by these methods were ineffective and remain unacceptable without further research.

The utility and effectiveness of airborne LiDAR for producing data from which high quality 3D topographic models can be derived for use in military and forestry applications has been shown. Quality of DEMs produced from LiDAR data is dependent on point cloud densities and vegetation densities, and the ability to "see" beneath the vegetation clearly is also affected. Although it was attempted to model results for successful automation by looking at three very different sets of data from three distinct forest environments, more consistent results would be probably be obtained by comparing these sites with equivalent point density data sets. Unfortunately, having equivalent data set collections across multiple locations would be cost–prohibitive and difficult to arrange.

Subsequent efforts should be explored with efforts aimed at Gabor filtering, Tensor Voting, Visibility Vectoring and other computer vision techniques mentioned in Chapter II, D. These methods may be more successful, in combination or separately from methods applied in this study, at further delineating between the data. Also, it was decided to concentrate on point density as a contributing factor, whereas other grid statistics outputs from QTM (intensity, second–order slope, z) may reveal opportunities for further analysis. It would also be recommended to explore a variety of other software solutions available in the marketplace. The problem is a difficult one where we can visually determine trail from non–trail, but pixel–based classification techniques alone remain inconsistent when applied to landscape solutions.

The ability to automate the analysis of LiDAR data to detect landscape changes between subsequent collections remains a significant capability for study, both for the value obtained from the information, and for the time–saving benefits that automation would provide.

LIST OF REFERENCES

Amzajerdian, F., Pierrottet, D. F., Petway, L. B., Hines, G. D., & Roback, V. E. (2011). *Lidar systems for precision navigation and safe landing on planetary bodies.* No. NF1676L–12532. Langley Research Center, Langley, VA. Retrieved from http://ntrs.nasa.gov/archive/nasa/casi.ntrs.nasa.gov/20110012163_2011012604.pdf

Andersen, H., McGaughey, R. J., & Reutebuch, S. E. (2005). Estimating forest canopy fuel parameters using LIDAR data. *Remote Sensing of Environment, 94*(4), 441–449. doi:DOI: 10.1016/j.rse.2004.10.013

Applied Imagery.*Quick terrain modeler application notes.* Retrieved 10 August 2011 from http://www.appliedimagery.com

Bates, K. T., Manning, P. L., Vila, B., & Hodgetts, D. (2008). Three–dimensional modelling and analysis of dinosaur trackways. *Palaeontology, 51*(4), 999–999–1010. doi:10.1111/j.1475–4983.2008.00789.x

BBC News. (2011). *California police arrest 100 over marijuana growing.* Retrieved July 29, 2011, from http://www.bbc.co.uk/news/world–us–canada–14351501

Contreras, M. A., & Chung, W. (2011). A modeling approach to estimating skidding costs of individual trees for thinning operations. *Western Journal of Applied Forestry*, *26*(3), 133–253. Retrieved from http://search.proquest.com/docview/880298911?accountid=12702

Coutermarsh, B. A. (Jul 2003). *Remote assessment of army tactical river crossing sites using LIDAR imagery.* (Technical Report Engineer Research and Development Center Hanover NH Cold Regions Research and Engineering Lab.

Devereux, B. J., Amable, G. S., Crow, P., & Cliff, A. D. (2005). The potential of airborne lidar for detection of archaeological features under woodland canopies. *Antiquity, 79*(305), 648–648–660. Retrieved from http://search.proquest.com/docview/217576229?accountid=12702

Diaz, J. C. F. (2011). Lifting the canopy veil, airborne LiDAR for archeology of forested areas. *Imaging Notes, 26*(2), 31.

ENVI (2003). *ENVI user's guide*. Research Systems Inc. (RSI)

Espinoza, F., & Owens, E. R. (2007). *Identifying roads and trails hidden under canopy using LIDAR* (M.S. thesis) Naval Postgraduate School, Monterey, CA.

Fleece, W. C. (2002). *Modeling the delivery of large wood to streams with light detection and ranging (LIDAR) data.* No. PSW–GTR–181).USDA Forest Service.

Gobakken, T., and Naesset, E. (2004). Estimation of diameter and basal area distributions in coniferous forest bymeans of airborne laser scanner data. *Scandinavian Journal of Forest Research, 19*(6), 529.

Harding, D., Dabney, P., Abshire, J., Huss, T., Jodor, G., Machan, R., and Zheng, Y. (June 22–24, 2010). *The slope imaging multi–polarization photon–counting lidar: An advanced technology airborne laser altimeter.* Arlington, VA: NASA Earth Science Technology Forum. Retrieved from http://esto.nasa.gov/conferences/estf2010/papers/Harding_David_ESTF2010.pdf

Harding, D. J., Dabney, P., & and Valett, S. (2011). *Polarimetric, two–color, photon–counting laser altimeter measurements of forest canopy structure.* NASA Goddard Space Flight Center, city and state. Retrieved from http://ntrs.nasa.gov/archive/nasa/casi.ntrs.nasa.gov/20110009937_2011009361.pdf

Heezin Lee, Slatton, K. C., & Hojin Jhee. (2005). Detecting forest trails occluded by dense canopies using ALSM data. *Proceedings IEEE 2005 International Geoscience and Remote Sensing Symposium, 2005.* (IGARSS), vol. 5, Jul., 2005, pp. 3587 – 3590.

Heritage, G. L., & Large, A. R. G. (2009). *Laser scanning for the environmental sciences*. Chichester, UK, Hoboken, NJ: Wiley–Blackwell.

IKG Research. *Automatic methods for the fusion, reduction and consistent combination of complex, heterogeneous geoinformation.* Retrieved 10 August 2011 from http://www.ikg.uni–hannover.de/index.php?id=312

Jensen, J. L. R., Humes, K. S., Vierling, L. A., & Hudak, A. T. (2008). Discrete return lidar–based prediction of leaf area index in two conifer forests. *Remote Sensing of Environment, 112*(10), 3947–3957. doi:DOI: 10.1016/j.rse.2008.07.001

Kim, S., McGaughey, R. J., Andersen, H., & Schreuder, G. (2009). Tree species differentiation using intensity data derived from leaf–on and leaf–off airborne laser scanner data. *Remote Sensing of Environment, 113*(8), 1575–1586. doi:DOI: 10.1016/j.rse.2009.03.017

Krogstad, F., & Schiess, P. (2004). *The allure and pitfalls of using LiDAR topography in harvest and road design.* Vancouver, B.C., Canada: Joint Conference of IUFRO 3.06 Forest Operations in Mountainous Conditions and the 12th International Mountain Logging Conference.

Leica Geosystems GIS & Mapping, LLC Product Information. (2011). *"ALS 70 airborne laser scanner"* Retrieved from http://www.leica–geosystems.com/downloads123/zz/airborne/ALS70/brochures/Leica_ALS70_6P_BRO_en.pdf

Macon, C., Wozencraft, J., Joong Yong Park, & Tuell, G. (2008). Seafloor and land cover classification through airborne lidar and hyperspectral data fusion. Paper presented at the *Geoscience and Remote Sensing Symposium, 2008. IGARSS 2008. IEEE International, , 2* II–77–II–80.

McGaughey, R. J., Andersen, H., & Reutebuch, S. E. (2006). Considerations for planning, acquiring, and processing LIDAR data for forestry applications. Paper presented at the *11th Biennial USDA Forest Service Remote Sensing Applications Conference,* Salt Lake City, UT.

McGirk, T. (2009). *Mexican drug cartels set up shop in California parks.* Retrieved, 2010, from http://www.time.com/time/nation/article/0,8599,1917547,00.html

A modeling approach to estimating skidding costs of individual trees for thinning operations. (2011). *Journal of Forestry*, *109*(5), 253–253. Retrieved from http://search.proquest.com/docview/880298911?accountid=12702; http://sfxhosted.exlibrisgroup.com/nps?genre=article&sid=ProQ:&atitle=A

National Aeronautics and Space Administration (NASA). (2011a). *"'CALIPSO' spacecraft aerosol and cloud measurements."* Retrieved from http://www–calipso.larc.nasa.gov/products/

National Aeronautics and Space Administration (NASA). (2011b). *Laser vegetation imaging sensor.* Retrieved 16 August 2011, from https://lvis.gsfc.nasa.gov/index.php?option=com_content&task=blogcategory&id=96&Itemid=93

National Aeronautics and Space Administration (NASA). (21 April 2011). *National space science data center.* Retrieved 18 August 2011, from http://nssdc.gsfc.nasa.gov/

NGA.*National geospatial intelligence agency homepage.* Retrieved 18 August 2011 from https://www1.nga.mil/Pages/Default.aspx

Olsen, R. C. (2007). *Remote sensing from air and space* Bellingham, Wash: SPIE Press.

Poullis, C. (2008). *A vision–based system for automatic detection and extraction of road networks*. Retrieved from http://doi.ieeecomputersociety.org/10.1109/WACV.2008.4543996

Reutebuch, S. E., Andersen, H., & Carson, W. W. (2003). Accuracy of a high–resolution LIDAR–based terrain model under a conifer forest canopy. *Canadian Journal of Remote Sensing*, *29*(5), 1.

Reutebuch, S. E., Andersen, H., & McGaughey, R. J. (2005). Light detection and ranging (LIDAR): An emerging tool for multiple resource inventory. *Journal of Forestry, 103*(6), 286–286–292. Retrieved from http://search.proquest.com/docview/220792372?accountid=12702

Richards, J. A., & Jia, X. (2006). *Remote sensing digital image analysis.* Berlin Heidelberg: Springer–Verlag.

Richardson, J. J., & Moskal, L. M. (2011). Strengths and limitations of assessing forest density and spatial configuration with aerial LiDAR. *Remote Sensing of Environment, 115*(10), 2640–2651. doi:10.1016/j.rse.2011.05.020

Richmond, R. D., & Cain, S. C. (2010). *Direct–detection LADAR systems*. Bellingham, WA: SPIE Press.

Sauber, J., Hofton, M., Bruhn, R., Lutchke, S., & Blair, B. (2011). *DESDynI lidar for solid earth applications.* No. GSFC.CPR.4516.2011).Goddard Space Flight Center. Retrieved from http://ntrs.nasa.gov/archive/nasa/casi.ntrs.nasa.gov/20110013379_2011013824.pdf

Shan, J., & Toth, C. K. (2009). *Topographic laser ranging and scanning: Principles and processing*. Boca Raton: CRC Press/Taylor & Francis Group.

Szeliski, R. (2010). *Computer vision: Algorithms and applications* (Draft ed.). Retrieved from http://szeliski.org/Book/

Tilley, B. K., Munn, I. A., Evans, D. L., Parker, R. C., Roberts, S. D. (2004). *Cost considerations of using LiDAR for timber inventory*. Retrieved 12 September 2011 from http://sofew.cfr.msstate.edu/papers/0504tilley.pdf

Toth, C. K. (2009). The state–of–the–art in airborne data collection systems—focused on LiDAR and optical imagery. *Photogrammetric Week '09,* 147.

TreeMetrics, Ltd (2011). *TreeMetrics method of timber measurement and optimization.* Retrieved 2 September 2011 from http://www.treemetrics.com/technology/index.html

Vosselman, G., & Maas, H. (2010). *Airborne and terrestrial laser scanning*. Dunbeath: Whittles Publishing.

Walsh, D. (2011). *Warfighters reap benefits of LIDAR mapping technology — defense systems* Retrieved 10 August 2011, from http://defensesystems.com/articles/2011/07/18/tech–watch–geoint–lidar.aspx

Wehr, A., & Lohr, U. (1999). Airborne laser scanning—an introduction and overview. *ISPRS Journal of Photogrammetry and Remote Sensing, 54*(2–3), 68–82. doi:DOI: 10.1016/S0924–2716(99)00011–8

White, R. A., Dietterick, B. C., Mastin, T., & Strohman, R. (2010). Forest roads mapped using LiDAR in steep forested terrain. *Remote Sensing, 2*(4), 1120.

Wulder, M. A., & Seemann, D. (2003). Forest inventory height update through the integration of lidar data with segmented landsat imagery. *Canadian Journal of Remote Sensing, 29*(5), 536–543. doi:10.5589/m03–032

THIS PAGE INTENTIONALLY LEFT BLANK

INITIAL DISTRIBUTION LIST

1. Defense Technical Information Center
   Ft. Belvoir, Virginia

2. Dudley Knox Library
   Naval Postgraduate School
   Monterey, California

3. Marine Corps Representative
   Naval Postgraduate School
   Monterey, California

4. Director, Training and Education, MCCDC, Code C46
   Quantico, Virginia

5. Director, Marine Corps Research Center, MCCDC, Code C40RC
   Quantico, Virginia

6. Marine Corps Tactical Systems Support Activity (Attn: Operations Officer)
   Camp Pendleton, California

7. Head, Information Operations and Space Integration Branch,
   PLI/PP&O/HQMC, Washington, DC

8. Richard C. Olsen, PhD
   Professor of Physics & Director, Remote Sensing Center
   Naval Postgraduate School
   Monterey, California

9. Cajun James, PhD
   Principal Research Scientist
   Research and Monitoring Manager
   Sierra Pacific Industries
   Anderson, California